Faculty of Science and Technology

Department of Geology

A structural, geomorphological and InSAR study of the unstable rock slope in Oksfjellet, Kåfjord, Troms

—

Marie Bredal

GEO-3900 Master's thesis in Geology

May 2016

Frontpage: photo from Oksfjellet by H.S.S. Bunkholt, NGU

Abstract

The main focus of this study has been to combine field observations of structural and geomorphological elements and interferometric synthetic aperture radar (InSAR) to investigate the unstable rock slope in Oksfjellet. The site is located along a NNE faced slope in a glacially eroded valley in Kåfjord, Troms. The Caledonian bedrock comprises mainly mica schists and display ductile (Caledonian) and brittle (post-Caledonian) structures. Brittle faults and fractures trending NE-SW and NW-SE and a ductile shear zone/thrust seem to have controlled the location of the unstable rock slope.

Displacements detected by InSAR correlated well to bedrock structures and morphological elements observed in the field. Satellite InSAR detected displacements, down to a rate of less than 1 mm/year, that is thought to reflect geological processes. It can be concluded that the combination of satellite InSAR and ground-based InSAR provided additional and important information that complemented field observations, and proved valuable in order to assess displacements patterns at different temporal and spatial scales.

Toppling and wedge failures along pre-existing post-Caledonian fractures are the main failure mechanisms in Oksfjellet, but sliding along foliation surfaces is also a viable failure mechanism. A deep-seated sliding surface is indicated along the thrust parallel foliation or along the intersection between foliation/thrust and fractures, producing an overall down to the NNE movement of the unstable area. The slope is classified as a complex field with similarities to deep-seated gravitational slope deformations.

Fractures and faults delimiting the unstable rock slope at Oksfjellet coincides with NNE-SSW to NE-SW and NW-SE trending regional Mesozoic brittle structures.

Acknowledgements

First of all, I want to thank my supervisor Lars Harald Blikra, at the University of Tromsø (UiT) and The Norwegian Water Resources and Energy Directorate (NVE), for valuable guidance and feedback. To Steffen Bergh, my co-supervisor at UiT. I am grateful for the amount of time and effort you have put into assisting me. Thanks to Tom Rune Lauknes my co-supervisor at Norut, for continuous support, patience and invaluable guidance when processing InSAR data. A special thanks to the handymen at NVE Seksjon for Fjellskred in Manndalen for hospitality, constant optimism and lots of humor, that made field work an ease. I want to thank Norut for letting me use their office, where I found peace, quiet and coffee. Martina Böhme at Geological Survey of Norway (NGU), your contribution to this master project have been invaluable and I appreciate all the knowledge and insight I learned from you. In addition, I want to thank Harald, for constant encouragement and optimism, and for always taking time to teach me new ArcGIS or GSAR tricks. Another special thanks goes to Line (Norut) for endless support and for always taking time for my questions (the most stupid ones were saved for you!). Thank you Ingrid (NVE), for enthusiastically sharing all your knowledge, for assisting when analyzing GB-InSAR data and for taking interest in my project. Marius, thank you for being such an excellent field assistant.

Vegard, thank you for housing, for making me food and for taking me skiing, but most of all, thank you for just being there. Now it’s on me to prepare you dinners and to take you to the mountains. And Astrid, for patiently letting me be the third wheel on all your dates with Vegard. Therese, Iris and Helene, thank you for always looking out for me. Åshild, we did it! Thank you for being such a happy face. Katrin, Halldis, Marte and Simon, the barracks wouldn’t have been the same without you.

Aunt Aid, Uncle Sverre, Vegard, Astrid, and Erlend, thank you for being you.
Julie, this wouldn’t have been possible without you. We wrote this thesis together! Thank you.

…pappa. I know you would have been proud.

Marie Bredal — May 2016, Tromsø.

Content

1 Introduction

1.1 Background for the study

Norway is known for its dramatic landscape with steep mountains and adjacent deep fjords. The alpine landscape is particularly susceptible to geohazards, where smaller rockslides and rockfalls are relatively common, having resulted in both losses of life and damage on infrastructure and settlements. However, some of the most severe natural disasters experienced in Norway have been caused by the more rare and larger rockslides that have resulted in tsunamis in narrow fjords (Blikra et al., 2006). Due to an increased awareness of geohazards and the necessity to adopt new land for homes and roads, the importance of mapping, monitoring and mitigation of geohazards is increasing.

The initiation and driving mechanisms present during rock slope failures are not well understood. Traditionally, mapping and monitoring of rock slope failures have been based on historical events, extensive field investigations, traditional in-field measurements of displacements and calculation of run-out distances. These techniques are expensive, time consuming, and can only cover small areas. For the last few years, new interests and new technologies have contributed to a better understanding of rock slope failures, and the study of rock slides consists in an interdisciplinary study, including structural geology, geomorphology, engineering geology and remote sensing (Jaboyedoff et al., 2011). Remote sensing techniques such as ground- and spaceborne Synthetic Aperture Radar Interferometry (GB-InSAR/InSAR) are making it possible to monitor greater areas over a larger time period, when compared to methods such as dGPS (differential Global Positioning System) and the above-mentioned traditional methods.

1.2 Objectives

The motivation of this thesis is obtain a better understanding of how the location and orientation of geological structures in Oksfjellet might have been advantageous for the evolution of the observed failures. The study is approached by combining structural geology, geomorphology and remote sensing. The main focus of this master's thesis is to map ductile and brittle geological structures and investigate how they may have contributed to the development of morpho-tectonic and geomorphological elements. Further, InSAR data is analyzed and verified against field observations of geological and geomorphological features, in order to examine how InSAR data may contribute to the understanding of deformations at different spatial and temporal scales. Initiation mechanisms and evolution factors that could have influenced to the detected displacement patterns and mapped deformations will be discussed, as well as the relation between the unstable rock slope at Oksfjellet and regional ductile and brittle structures.

1.3 Definitions

Apex: The highest point from which the fan radiates (Highland & Bobrowsky 2008).

Block toppling: Forward rotation and overturning of individual columns that are divided by steeply dipping fractures (Goodman & Bray, 1976).

Flexural toppling: Forward rotation and overturning of rock mass that is truncated by closely spaced and steeply dipping joints striking parallel to the slope (Goodman & Bray 1976).

Colluvium: Coarse grained and immature slope-waste material deposited in the lower part of mountain slopes or escarpments (Blikra & Nemec, 1998).

Conjugated fractures: Two fracture sets intersecting at a constant angle of 30 – 60°.

Counterscarp: Scarp dipping in opposite direction of the back scarp. An uphill faced scarp (Agliardi et al., 2001, Ambrosi & Crosta, 2006).

Crevasse: a deep open cleft or fracture.

Crown fracture: Fractures in material still in place adjacent to the highest parts of the main scarp (Varnes 1978)**.**

DEM: Digital Elevation Model.

dGPS: Differential Global Position System.

DSGSD: deep-seated gravitational slope deformation (Agliardi et al., 2012).

Fault: A discontinuity with a large offset (>10 cm), often linked by fractures.

Foliation: Planar structures formed during tectonism and metamorphism.

Fracture: A planar structure caused by stress. Extensional fractures are fractures showing evidence of movement perpendicular to the fracture plane. Shear fractures show movement parallel to the fracture plane (Fossen, 2010).

Graben: A depression delimited by two parallel, vertical or oppositely dipping faults (Fossen 2010).

Horst: An elevated area relative to the surrounding rock. The elevation is delimited by vertically to opposite dipping normal faults (Fossen, 2010).

InSAR: Interferometric Synthetic Aperture Radar.

LIDAR: Light Detection and Ranging.

Lineaments: Linear to sub-linear elements that can be detected on aerial photos, often representing geological structures and zones of weakness (Fossen, 2010).

Morpho-structures: Description of the morphological expression of a deformation structure with gravitational or tectonic origin (Agliardi et al., 2001).

Permafrost: The ground temperature must stay below 0°C for two or more consecutive years (Andersland & Ladanyi 2004).

Plane failure: Failure along a single plane that dips out of the slope (Wyllie & Mah 2005).

RADAR: Radio Detection And Ranging.

SBAS: Small baseline subset method.

Talus: Rock fragmented by rock failure, often angular and coarse grained and cumulated at the base of cliffs or steep slopes.

Talus fan deposits: features that are emplaced over time by surface mechanisms of different slope processes. Such processes are mainly rock falls, debris flows, and avalanches (Leeder, 2011).

Trench: Linear and deep cut relative to the surrounding rock. An expression of extensional opening of vertical of steeply dipping surfaces. Large scale trenches is referred to as graben structures (Agliardi et al., 2001).

Transfer zone: The zone between two parallel and adjacent faults, where the offset is transferred from one fault to the other. Structures in these zones might also be mentioned as transfer- or relay ramp structures (Twiss & Moores, 2009).

Toppling: rock failure involving forward rotation and overturning of rock columns, cut by well-defined and steeply dipping fractures(Goodman & Bray 1976, Hungr et al., 2014).

Unstable rock slope: An area that has moved from its geological original location, along weaker surface planes in the bedrock.

Wedge failure: Sliding of rock mass along two sliding planes with a downslope facing intersection line (Wyllie & Mah 2005, Hungr et al., 2014).

1.4 Geographic location and climate

Oksfjellet (1143 m a.s.l.) is located in Kåfjorddalen, 2 km southeast of the community Birtavarre (Fig. 1) and is defined by an approximately 4 km long, up to 400 – 500 m high, NW-SW trending, steep northeast facing cliff. The unstable area is roughly 500 m x 160 m at an elevation of 950 m a.s.l. display great deformation and extensive fracturing. A front block with a size of 30 m x 150 m and a southern back fracture with a height of 50 m delimits the area to the north and south. To the east and to the west the unstable is bounded by prominent fracture scarps striking NNE-SSW to NE-SW. Oksfjellet has a plateau-like morphology, where fracturing is less prominent and the surface consists of material weathered by repeated freezing and thawing and the hillside below the steep cliff face consists of deposits forming fan shaped deposit systems. Much focus regarding rock fall hazard has been directed to Holmen, a populated area a few km northwest of the unstable area because of the impending risk and consequence of rock falls.

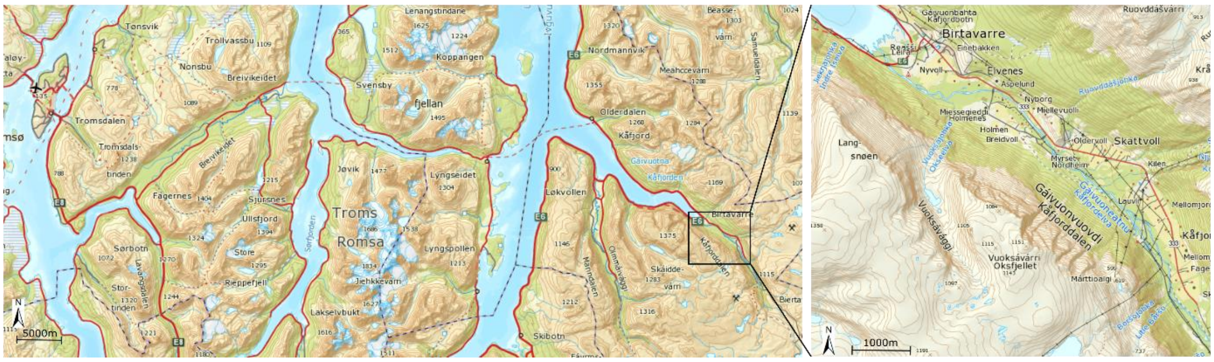

Fig. 1 Map showing the geographic location of Oksfjellet in Kåfjord in Troms. Modified after norges-kart.no.

The complex topography in Troms makes its mark on the subarctic climate, as there are distinct differences between the coastal region and the inland. The weather in Kåfjorddalen is characterized by relatively small amounts of precipitation. Discontinuous permafrost exists in the mountains in Norway and investigations in Troms suggest a lower permafrost limit at 990 m a.s.l. in the outermost coastal areas and a decreased limit at 550 m a.s.l. in the more continental inner fjords. Several of the detected unstable rock slopes in the area are within areas of warm permafrost (Christiansen et al., 2010). Permafrost might exist sporadically close to sea level, below the regional permafrost limit and in deep-seated rockslide terrain (Blikra & Christiansen, 2013).

1.5 Previous work

Troms county and the area adjacent to Lyngen peninsula is characterized by a high spatial density of unstable mountain slopes, first demonstrated by (Corner 1972). Through history several mountains in the region have suffered major rock slope failures, e.g., Hølen in Balsfjord (Bunkholt et al., 2013) and Pollfjellet in Lyngen (Blikra et al., 2006). Today, the most eminent threat is considered to be the rock slide at Nordnes, where a worst case scenario predicts a 11 million m^3 slide resulting in a tsunami with a maximum run-up height of 25 − 30 m (Glimsdal & Harbitz 2008).

The last ten years, research considering rock slope failures in the area has been done by e.g., Blikra et al., 2009, Braathen et al., 2004, Blikra & Christiansen, 2013 and Lauknes, 2010. Mapping of geohazards in Troms are done by Geological Survey of Norway (NGU)on behalf of The Norwegian Water Resources and Energy Directorate (NVE) during a national project with the objective to focus on large unstable mountain slopes. Related to the on-going project by NVE, several master theses have been written at UiT regarding geohazards

(Husby, 2011, Rasmussen, 2011, Hannus, 2012 Eriksen, 2013, Skrede, 2013, Hernes, 2014, Bakkhaug, 2015, Nopper, 2015), where the main objectives of these have been to correlate field investigations in different unstable areas to the regional geology. Foliation- and lineation measurements, deformed structures, drainage patterns and permafrost presence have all been analyzed, discussed and used as a basis for a suggestion for the controlling factors in the unstable areas.

Oksfjellet was first stated a potential unstable rock slope by NGU and dGPS measurements begun in 2003 (Blikra et al., 2006). In 2008 and 2009, ground based LIDAR scanning (TLS) was carried out, but errors in the data set made the result inconclusive. dGPS measurements have shown small displacements in the unstable area where the front block exhibits the highest displacements rates, of 3 – 4mm/year (Bunkholt et al., 2013). In 2011, a LiSALab (GB-InSAR) system was installed by NVE to monitor the displacements at Oksfjellet. The result showed that a small region was displaced 15 – 20 mm/week (Kristensen 2011). Following GB-InSAR campaigns in 2014 and 2015 showed displacement in several small areas, with the greatest displacement rate of up to 25 mm/week (Skrede & Kristensen 2014). In autumn 2015 the GB-InSAR was installed at Holmen to monitor reported rock fall activity at a time when NVE was building a retaining wall to protect a private house and its premises. Measurements in mid-September showed rapidly accelerating displacements of an area of 6000 – 12000 m^2 about 950 m a.s.l. above Holmen moving at a rate of 43 cm/24h at its peak (NVE 2015a, NVE 2015b).

1.6 Regional geology

The bedrock in the western and coastal regions of Troms comprises Precambrian basement rocks and Caledonian thrust nappes (Andresen, 1988). East of the Lyngen Peninsula the bedrock comprises mainly Caledonian thrust units, which are gently dipping to the northwest (Corfu et al., 2014), resulting in a smoother topography (Corner, 2005). The region consists of several fjords and associated arms of fjords that transitions to a strand flat in the outer and northern parts of the region. The NW-SE oriented Kåfjorden is a side fjord to the N-S oriented Lyngen fjord merging from the Lyngen peninsula, which is linked to Storfjorden farther southeast. Oksfjellet is located in the inner region of Kåfjorddalen where trace of the paleic surface is present as plateaus on top of mountains extending to 1100 – 1300 m a.s.l. The landscape was largely formed during glaciations, where glacial carving, erosion and deposition have resulted in the alpine high-relief topography seen today. U-shaped valleys are partly filled with glaciofluvial material above the upper marine limit, whereas marine sediments occur below this (Olsen et al., 2013). V-shaped hanging valleys commonly form the side valleys of the main drainage system.

1.6.1 The Caledonian nappes of Central Troms

The Caledonian geology of central Troms is characterized by four major Allochthons, from base and upwards; the Lower, Middle, Upper and Uppermost Allochthon (Fig. 2).

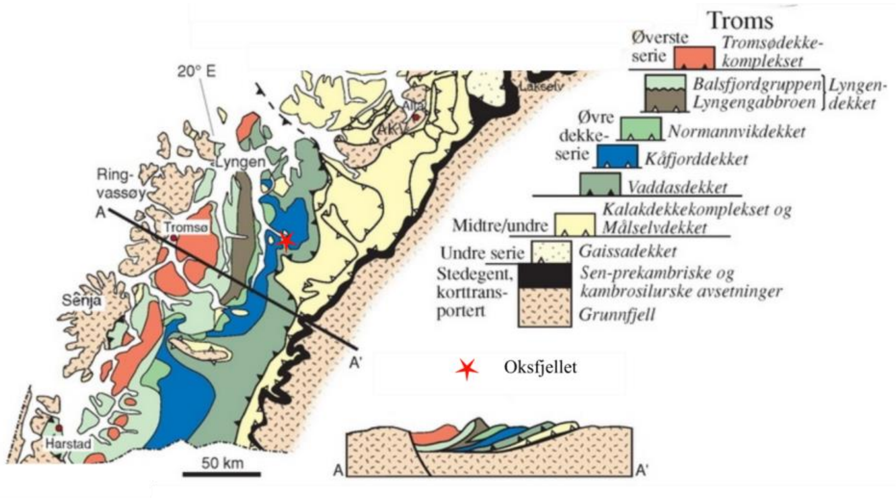

Fig. 2 Map showing the four major Allochthons in Troms. Profile AA' is located south of the studied area, marked by a red star. Modified after (Fossen et al., 2006)**.**

In the studied area the bedrock belongs to the Upper Allochton and the Reisa Nappe Complex (Quenardel & Zwaan 2008), which is further divided into, from bottom to top, the Vaddas Nappe, Kåfjord Nappe and Nordmannvik Nappe, with an increasing metamorphic grade upwards in the nappe stack. In Oksfjellet, Kåfjord- and Vaddas Nappe is present as sedimentary sequences originating from Late Ordovician to Early Silurian time, that have been folded and metamorphosed during east-southeastward emplacement of the nappes (Gee et al., 2008, Corfu et al., 2014). The Upper Allochthon, including the Kåfjord and Vaddas nappes, comprises rocks formed both in platformal and arc-related settings, which includes ophiolites, and rocks taht have been subject to multiple tectonic events and a complex history of deformation (Andresen, 1988). The Caledonian Nappes and corresponding folds and ductile fabrics in central Troms were formed during the closing of the Iapetus Ocean in Early to Mid-Paleozoic. During the following Caledonian orogenesis in Silur, different units were stacked and thrusted onto Baltica. The Lower and Middle allochthons are inferred to derive from Baltica, the Upper Allochthon is derived from the Iapetus Ocean, island arc-complexes and ophiolites and the Uppermost Allochthon includes exotic elements from Laurentia (Gee et al., 2008 and Andresen, 1988).

1.6.2 Post-Caledonian brittle structures

Previous work show that onshore and offshore fault systems in the coastal areas of northern Norway are dominated by NNE-SSW-, NE-SW-, and NW-SE trending faults and fractures, that formed during multiple stages of rifting and basin formation on the Norwegian continental rift-margin in the Paleozoic through Mesozoic-Cenozoic time periods (Bergh et al., 2007, Hansen & Bergh, 2012).

On the Lofoten and Vesterålen margin, brittle structures define a network of steep right stepping faults trending NE-SW and NNE-SSW (Bergh et al., 2007). The two dominant sets are a result of Triassic to Early Cretaceous WNW-ESE extension (Hansen 2009), whereas NW-SE trending faults are considered younger in age, formed in the Late Cretaceous due to transform opening of the North Atlantic Ocean (Faleide et al., 2008).

On the SW Barents Sea margin, post-Caledonian brittle faults display similar trends of NNE-SSW trending, moderately to steeply dipping brittle faults, and ENE-WSW trending, steeply to moderate dipping normal fault zones (Fig. 3). They define two major NE-SW trending fault complexes; the Troms-Finnmark and Vesfjorden-Vanna fault complexes. These faults bound major horsts onshore such as the West Troms Basement Complex, and basins offshore (Indrevær et al., 2013).

The central part of Troms county, onto the Lyngen peninsula and even farther east, dominated by Caledonian Nappes, is characterized by NE-SW trending lineaments, outlined as e.g., the Vestfjorden-Vanna Fault Complex and the Kvaløysletta-Straumbukta Fault (Olesen et al., 1997,Gabrielsen et al., 2002) Brittle faults are suggested to be a result from reactivation from ductile Precambrian or Caledonian structures (Indrevær et al., 2013). NE-SW to E-W transfer zones are linking the NNE-SSW striking faults described by (Gabrielsen et al., 2002). The transfer zones correspond to late Cretaceous to Paleogene NNW-SSW extension (Hansen, 2009).

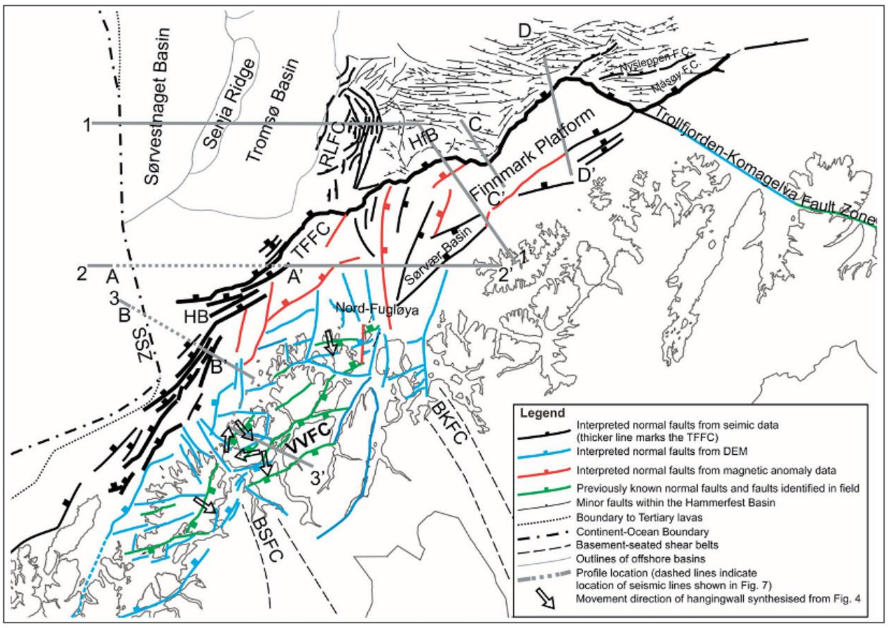

Fig. 3 Map showing brittle faults in SW Barents Sea margin. BKFC: Bothnian Kvænangen Fault Complex, BSFC: Bothnian-Senja Fault Complex, RLFC: Ringvassøy-Loppa Fault Complex, SSZ: Senja Shear Zone, TFFC: Troms-Finnmark Fault Complex, VVFC: Vestfjorden-Vanna Fault Complex. From (Indrevær et al., 2013)**.**

1.6.3 Quaternary geology and geomorphology

Glacial and interglacial periods, as well as the ongoing isostatic uplift, have influenced the topography in Troms. Valleys, cirques and fjords have been carved and the mountains have been scoured by the ice (Vorren & Mangerud 2007).

The quaternary period is characterized by great temperature shifts. Cold, glacial periods allowed large ice shields to build, and during warm, interglacial periods the temperatures could exceed the temperatures that we have today. After last glacial maximum (LGM) the warmer climate caused the ice shield to start retreating from Eggakanten about 18 000 – 20 000 C14 years ago. The retreat included several re-advances and halts, which are documented by moraines in today's landscape. One of the most prominent re-advances of the ice shield, the Skarpnes event in Younger Dryas, lasted from 11 000 B.P. to 10 000 B.P. from today (Vorren & Mangerud 2007, Olsen et al., 2013). This was followed by three local events of re-advances in Preboreal period, the Ørnes event (c. 9800 – 9900 ± 150 B.P.), the Skibotn event (9500-9600 ± 250 B.P.) and a younger event (c. 9400 ± 250 B.P.). The retreat of the ice in Kåfjorddalen is reconstructed by Corner (1980) based on marine limits and ice-front accumulations (Fig. 4). The weight of the ice caused the Earth's crust to deform and the retreat of the ice after LGM led to a slow and still ongoing rebound of the crust. The coastline in Troms has a yearly uplift of 1 – 1,5 mm (Dehls et al., 2000).

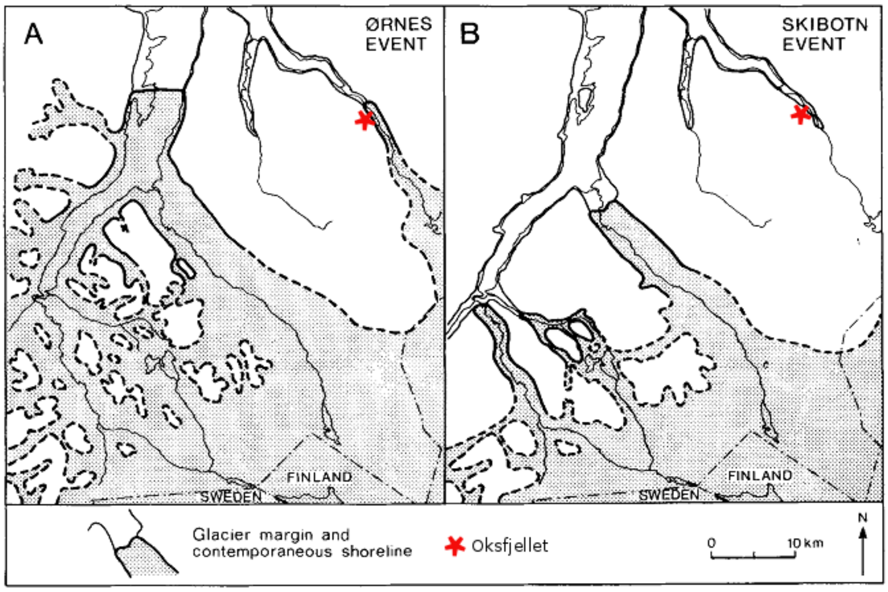

Fig. 4 Reconstruction of the extent of the position of ice- shield during the A) Ørnes and B) Skibotn event. Modified after Corner (1980)**.**

2 Methods

The chapter presents the methods used in the thesis. As mentioned, the motivation of this master project have been to gain a better understanding of the unstable rock slope in Oksfjellet, were the main focus has been to map geological structures and geomorphological features (section 2.1). Secondly, satellite InSAR data have been processed, analyzed and verified against geological features, therefore, an introduction to SAR interferometry (InSAR) and its possibilities and limitations is given in section 2.3 and 2.4, and a description of satellite InSAR datasets and the processing procedure used, is given in section 2.5.

In addition to GB-InSAR results analyzed by NVE, this master project will include further analysis and comparison of the extent of deformation detected by GB-InSAR, against mapped geological features and satellite InSAR datasets. GB-InSAR data are processed with the tools of LiSA Mobile software and analyzed by NVE (Kristensen 2011, Skrede & Kristensen 2014, Skrede in prep). A short introduction to GB-InSAR system and its possibilities and limitations is given in section 2.6.

2.1 Structural and geomorphological mapping

2.1.1 Regional map analysis

Structural and geomorphological features are mapped and geographically projected using ArcGIS (10.2.1) with applications such as ArcMap and ArcScene. The coordinate system used is WGS 1984 UTM Zone 33. Orthophotos originate from www.norgeibilder.no and the high resolution (1 m x 1 m) Digital Elevation Model (DEM) used was made available by NGU. The DEM, with a resolution of 10 m x 10 m used when processing InSAR data, originate from the Norwegian Mapping Authority (NMA). Geological map over Manndalen with scale 1:50 000 and digital geological- and quaternary maps used originate from NGU. The strike and dip of ductile foliation and brittle fractures were measured applying the right hand rule (RHR) and georeferenced. Structural orientation data has been analyzed as lower hemisphere stereographic projections using the software Stereonet9.

2.1.2 Field work

Fieldwork was conducted in August 2015. The unstable area and close surroundings were mapped, but due to steep and often inaccessible terrain, not all outcrops were visited. The exposed face at Oksfjellet and the surrounding areas were investigated and photographed by helicopter made available by NVE. Interpretations of these areas are largely based on aerial photos taken on the flight and high resolution DEM's.

NGU have contributed to the master project by making previous field work observations, photos and structural measurements available.

2.2 dGPS

NGU installed GPS points (Fig. 5) at Oksfjellet in 2003, and measurements have been done annually or with intervals of a few years, where presumed unstable points are measured relatively to defined fixed points. From the measurements, the mean annual displacement between the first and the last measurement is estimated.

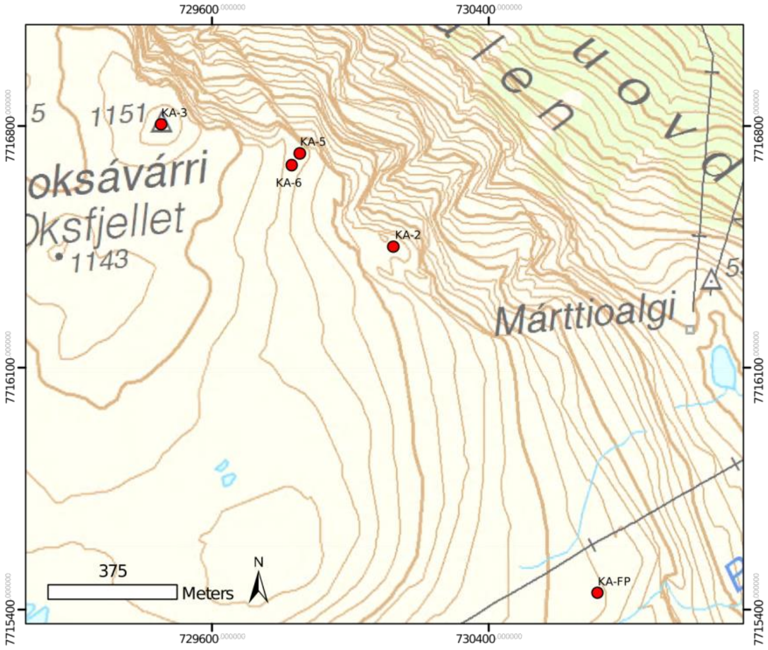

Fig. 5 Map showing the location of dGPS points at Oksfjellet. KA-FP is used as a fixed point.

2.3 Satellite InSAR

A Synthetic Aperture Radar (SAR) is an active air- or spaceborne instrument which images the Earth's surface, by transmitting radiated microwave pulses and measuring the echo (backscatter) of the reflected surfaces on the ground (ground swath) that is illuminated. A focused SAR image is organized in radar coordinates, range and azimuth, where range is the distance from the radar to the scatterer and azimuth is the distance along the flight path (Massonnet & Feigl 1998) (Fig. 6).

A moving instrument produces a Doppler shift as signals reflected from objects in front of the instrument is shifted relative to the signals reflected from behind. The range of the object is found by timing the return of the reflected signal. The side looking geometry causes distortions in the radar image and needs to be converted into map projected coordinates, a process called geocoding.

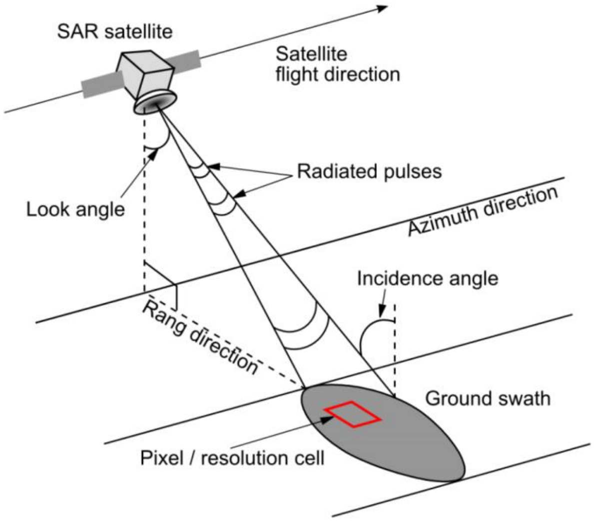

Fig. 6 Geometry of a Synthetic Aperture Radar (SAR) system. Modified by Eriksen (2013) **from** Lauknes (2010)**.**

Right-looking SAR satellites orbits the Earth from pole to pole, that when descending (north to south) looks westward and when ascending (south to north) looks eastward (Fig. 7). By combining the rotation of the Earth and the orbital path of the satellite, the entire surface of the Earth is imaged by two different satellite geometries (Ferretti, 2014).

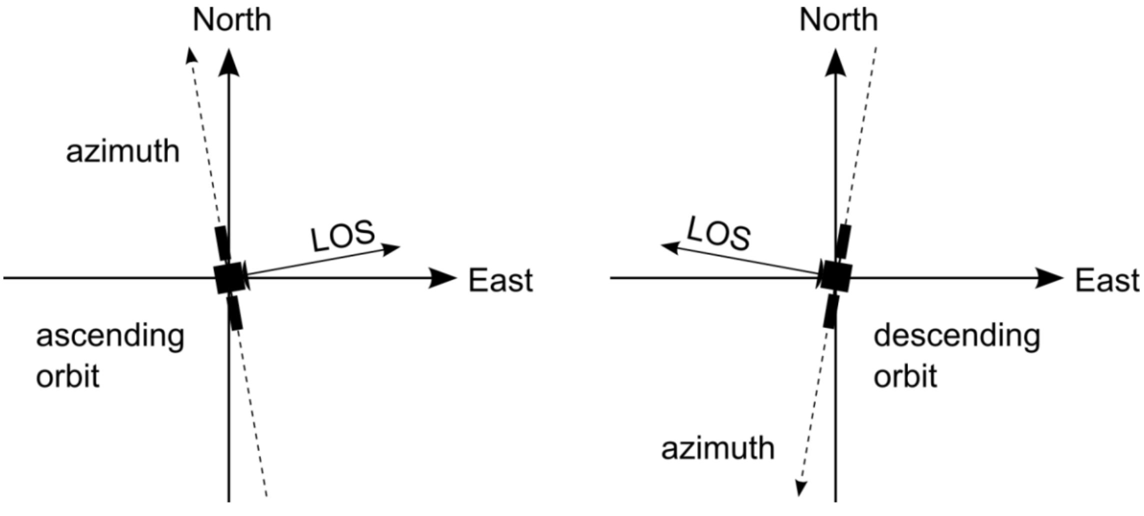

Fig. 7 The geometry of ascending and descending satellite orbits. From Eriksen (2013).

2.3.1 Phase and amplitude

Information about the location and property of a target is acquired by recording the backscattered signal, which is complex, containing both the amplitude and the phase of the received echo.

The *amplitude* depends on the amount of backscattered electromagnetic energy from the target, and contains information about the geometrical properties. The most important parameter for describing the reflectivity is the surface's roughness. A rough surface will *scatter* the signal in many directions, while a smooth surface that will *reflect* the signal based on simple geometrical effects, appear dark in radar images.

The *phase* (2-1) is a function of the propagation delay between the transmitted and received electromagnetic wave and is proportional to the target distance:

$$\phi = \frac{4\pi}{\lambda} R \qquad (2\text{-}1)$$

The phase depends on the transmitted phase and contains information about the distance from the sensor to the target. The distance from the target to the sensor is described as an integer of number of wavelengths (λ), plus a segment equal to a fraction of λ. The phase is a random parameter uniformly distributed between $-\pi$ and π, and from it the displacement is calculated.

2.3.2 Limitations

High relief terrain causes geometrical distortion due to the SAR acquisition geometry (Fig. 8). *Layover* can appear when the mountain top is closer to the radar than the foot of the mountain, resulting in reverse imaging of scatters and superimposed images. *Foreshortening* can appear on the front or the back of a mountain, resulting in compressed or expanded pixels on the ground and consequently loss of details. Radar *shadow* appear in the areas not being illuminated by the radar. The effects of layover and shadow are dependent of the incidence angle of the satellite and the topography (Fig. 6).

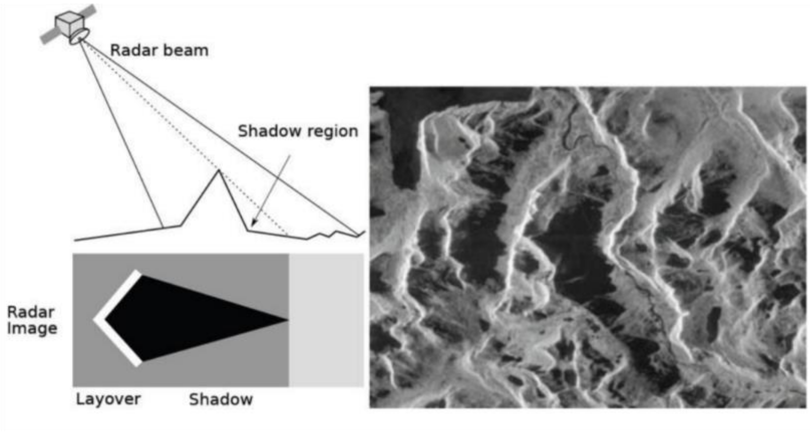

Fig. 8 Figure and image showing the effect of layover and shadow in mountainous areas. From (Lauknes et al., 2010)**.**

2.4 Interferometry

An interferogram is produced by combining two SAR-images and showing the phase difference between repeated acquisitions. The pixel values of an interferogram, are expressed in modulo-2π corresponding to λ/2 due to the two-way travel of the wave. The result is presented as cyclic phase differences that induce succession of patterns called “fringes” when deformation exceeds half the wavelength of the radar (Hanssen, 2001). If other contributors such as topography, atmospheric path delay and noise can be removed from the signal, the interferometric phase is a powerful tool to calculate variations due to surface displacement or acquisition geometry (Ferretti, 2014).

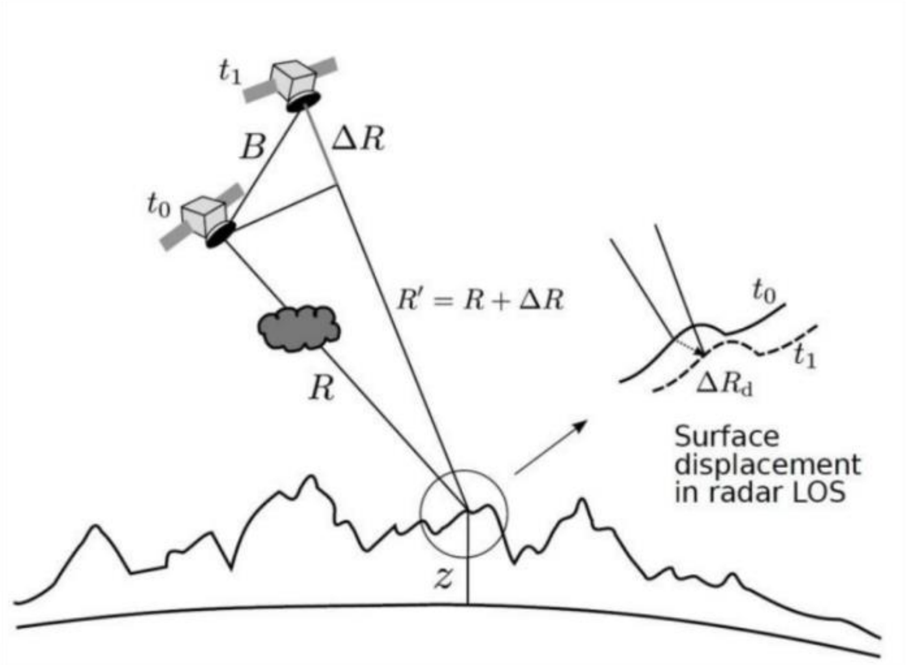

Fig. 9 Surface displacement between two SAR acquisitions, at times t_0 and t_1. The phase difference ΔR_d is recorded. The cloud introduces atmospheric delay $\Delta\varphi_{APS.}$ The altitude, z, introduces the contribution to the topography, $\Delta\varphi_{topo.}$ B is the baseline, the orbital distance difference between the two SAR acquisitions. From (Lauknes 2010)**.**

2.4.1 Calculating surface displacement

Interferometric phase $\Delta\varphi$ (2-2) is used to calculate the surface displacement $\Delta\varphi_{\mathrm{displ}}$. If there has been a displacement between two SAR image acquisitions this is introduced in the phase contribution, $\Delta\varphi_{\mathrm{displ}}$.

$$\Delta\varphi = \Delta\varphi_{topo} + \Delta\varphi_{displ} + \Delta\varphi_{APS} + \Delta\varphi_{decorr} \qquad (2\text{-}2)$$

The difference in position, B, (Fig. 9) of the SAR instrument between two acquisitions creates a phase *contribution from the topography,* $\Delta\varphi_{topo}$, that is removed by the use of DEM. The phase *contribution from atmospheric delay,* $\Delta\varphi_{APS}$, is caused by inhomogeneities in temperature, pressure, water content and electron density in the atmosphere. Because atmospheric conditions changes quickly with time, two SAR images can have completely different APS (Atmospheric Phase Screen). In high relief topography vertical stratification of the atmosphere into layers of different propagation velocities causes additional atmospheric delay (Ferretti 2014). The delay is strongly correlated to the local topography and can often be seen as fringes following topographic contour lines (Massonnet & Feigl 1998).

Phase decorrelation, $\Delta\varphi_{decorr}$, is due to changes in position of property of the individual scatters, arising from geometric effects or temporal changes of the backscatter (Zebker & Villasenor, 1992). The decorrelation sources contribute to the c*oherence,* γ, which is quality measure of the interferometric phase and has a value between 0 and 1. If a pixel in an interferogram has a coherence value of 1, the phase contribution is constant between the two images.

2.4.2 Phase unwrapping

The interferometric phase can only be measured within the interval $[-\pi, \pi]$. Phase unwrapping is the process of restoring the correct multiple of 2π to each point of the interferometric phase image (Lauknes, 2010). If the displacement rate between acquisitions for the SAR images used to create the interferogram is too great, the phase difference in the interferogram will be larger than 2π. The phase value will then start over again (wrap around), creating displacement ambiguities. According to the specificity of the site and the expected velocity of the target object, maximal temporal baseline (interval between scenes) and spatial baseline (distance between sensors) used to build interferograms, will be set differently to avoid decorrelation.

Sampling is only possible during snow free periods, causing irregularities in the sampling frequency, as there is no information about the displacement in winter. Linking interferograms between seasons may cause unwrapping errors, resulting in underestimation of displacement.

2.4.3 Time series

The use of InSAR to study surface displacement was fully demonstrated throughout the 1990’s and the extent of the different phase contributors to the final result was discovered. The challenge is to isolate the wanted signal (the surface displacement) from the rest of the phase contributors (see section 2.4.1). The use of single interferograms is vulnerable to errors related to the DEM and the different interferometric phase contributors. Throughout the years, several techniques have been developed to mitigate this. By moving from single interferograms to time series of interferograms one can study the temporal displacement pattern (Lauknes et al., 2010). *Stacking*, a technique of averaging many interferograms, was introduced by Zebker & Villasenor (1992) produces a mean displacement map with reduced noise from the atmosphere. *The small baseline methods (SB)* was first introduced by Berardino et al., (2002). The basics behind all SB methods are to combine interferograms with a short spatial baseline to minimize decorrelation caused by spatial effects and errors in the DEM. The SBAS algorithm estimates displacement in between each acquisition, making it possible to study the seasonable variations and the nature of displacement through time.

2.5 Characteristics and processing of InSAR dataset

2.5.1 Characteristics of InSAR datasets

The characteristics of the different sensors, TerraSAR-X (TSX) and RADARSAT-2 (RSAT-2), used in the thesis is summarized in Table 1. The RSAT-2 dataset includes scenes over 6 years between 2009 and 2014, except 2011 and TSX includes scenes over 7 years, between 2009 and 2015. The main differences to take into account between the two sensors are the *frequency band*, the corresponding *wavelength* (C: λ=5,55 cm for RSAT-2 and X: λ=3,1 cm for TSX) and the revisit time (24 days for RSAT-2 and 11 days for TSX). The two datasets also have different *spatial resolution*. The TSX geocoded resolution is better, with a pixel size of c. 10 m x 10 m. RSAT-2 have a pixel size of c. 19 m x 19 m. For both datasets, an ascending geometry has been used, where the satellite is moving from S-SE to N-NW looking toward E-NE. The LOS orientation for TSX is 78.5 °N with an incidence angle of 44.7°. LOS for RSAT-2 is 74°N with an incidence angle of 30.9°.

Table 1 Characteristics for the satellite data.

Parameters	**TSX**	**RSAT-2**
Orbit	Ascending	Ascending
Dataset mode	StripMap	Fine Mode
Time period	2009 – 2015	2009 – 2014
Band	X: λ=3,1 cm	C: λ=5, 55 cm
Revisit interval	11 days	24 days
Pixel size [range, azimuth]	5 x 5	2 x 4
LOS orientation	78.5 °N	74 °N
Incidence angle	44,7°	30,9°

2.5.2 Processing of InSAR datasets

Processing of satellite InSAR datasets was done using GSAR, a generic interferometric SAR processing system. It is an interactive data language (IDL) application developed at Norut (Larsen et al., 2005). Its inputs are SAR images, orbit data and a DEM. The output is geocoded InSAR displacement data. The main processing steps can be summarized as the following:

1. Setting of general parameters regarding the processing and selection of input data.
2. Based on the chosen temporal- and spatial baseline and the time of acquisition, interferograms are generated.
3. Goldstein filtering are done to reduce the noise in the images.
4. A manual quality check of the interferograms is performed to remove the images with low coherence and high level of noise.
5. The next steps are removal of atmospheric phase contribution, calculation of mean coherence and selection of pixels with high coherence.
6. Phase unwrapping is followed by reference point selection and displacement estimation using stacking- or SBAS algorithm.
7. Lastly, the estimated displacement is geocoded from radar geometry to a geographic coordinate system.

The coherence in the studied area is good due to the lack of vegetation and high amounts of solid bedrock. A common reference point was chosen for the two datasets separately, based on field investigations, study of orthophotos, slope angle maps and coherence data. They are both placed in the same area, low slope angle, solid bedrock, high coherence and where no displacement is assumed. The distance from the unstable area to the calibration points is reasonably short (c. 1 km), so that atmospheric noise is assumed to have little influence over that distance.

The revisit interval and the sensor wavelength affect the detection capability, depending on the displacement rate of the unstable area (described in Chapter 2.4). LOS does also affect the detection capability. One-dimensional (1D) displacement along LOS is measured and any displacement with a direction moving perpendicular to that is missed. The ascending geometry and the local topography causes geometrical distortions, such as layover effects that affect the west-facing slopes, and shadowing that affects the east-facing slopes. The steeper incidence angle in the RSAT-2 dataset makes is more sensitive to vertical displacements.

dGPS measurements (Bunkholt et al., 2013) and GB-InSAR results (Skrede & Kristensen, 2014, Kristensen, 2011) show that the front block in the unstable area (further described in section 3.4.1) is presumed to move at a rate of 3 – 4 mm/year. Early satellite InSAR results revealed a small displacement change (± 0,5 mm/year) over the curved scarp in the back of Oksfjellet. Based on these results, different temporal baselines (maximum time between acquisition) were chosen when setting the processing parameters, in order to compare the results, evaluate the effects and find out which are best. Long temporal baselines are favorable for detecting slow displacement rates, therefore, a maximal temporal baseline of 720 days were chosen for both TSX and RSAT-2. The long baselines connect interferograms through seasons, resulting in a high number of interferograms. To detect the slower displacements and reduce the signal-to-noise ratio, only long temporal baselines were chosen, and to reduce DEM error, short spatial baselines were used. A maximum temporal baseline of 5000 days and a minimum temporal baseline of 1460 days were implemented in the processing of TSX and RSAT-2 data. Any result showing movement faster than half a wavelength (16 mm for TSX and 28 mm for RSAT-2) in the time intervals 720 days and 1460 days will be affected by underestimation. Stacking of the interferograms was used to calculate the mean annual displacement. The SBAS algorithm was used for TSX (720 days) in order to access time series for comparison with GB-InSAR data. The main processing characteristics are summarized in Table 2.

Table 2 Processing characteristics

Dataset	Maximum temporal baseline [days]	Minimum temporal baseline [days]	Spatial baseline [m]
TSX-asc	5000	1460	10
	720	-	40
RSAT-2 asc	5000	1460	300
	720	-	600

2.6 Ground-based InSAR

Ground-based Synthetic Aperture Interferometry (GB-InSAR) is based on the same physical principles as satellite InSAR, but differs in some aspects, related to the characteristics of the devices and their location.

The terrestrial systems are portable devices, which use the movement along a linear rail of a few meters to synthesize radar images. It is located at the exact same position for all acquisitions, hence there is no spatial baseline between acquisitions. It is also located mush closer to the target, allowing for better resolution, better accuracy and allows for capturing targets at a distance up to 4000 m (see Fig. 10). It is also more easily installed with a line-of-sight sub-parallel to the moving target. Finally, GB-InSAR has a high temporal resolution which reduces temporal decorrelation that easily detects fast movements (Luzi, 2010).

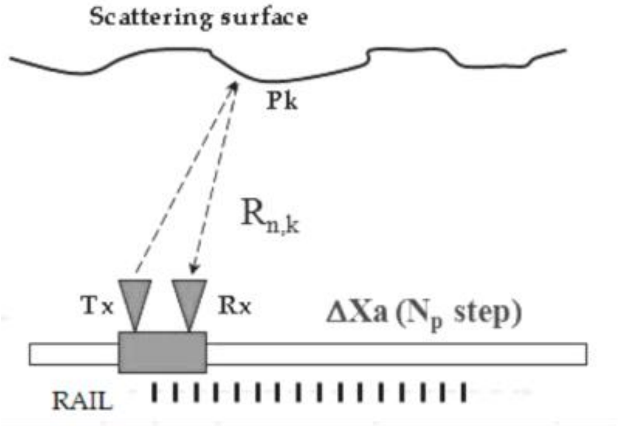

Fig. 10 GB-InSAR acquisition setup through linear movement, including transmitting antenna (Tx) and receiving antenna (Rx). From Luzi (2010)**.**

A higher frequency than satellites lead to higher resolution and higher accuracy, but on the other hand penetration capability is reduced, making the system more sensitive to the disturbing effects of vegetation and atmosphere.

2.6.1 Advantages and limitations

GB-InSAR has been used in numerous case studies monitoring slope instabilities, mostly related to the detection of movement on large areas in order to say something about spatial and temporal variations compared to conventional monitoring devices (Herrera et al., 2009, Barla et al., 2010, Agliardi et al., 2013). From these studies and other studies in Norway (Kristensen 2013a, Kristensen 2013b, Rouyet 2013, Skrede & Kristensen 2014) one can state some of the limitations and the potential of GB-InSAR for monitoring slope instabilities, some of which are common with satellite InSAR.

Unlike the use of in situ instrumentation, radar remote sensing techniques allow obtaining information in inaccessible and hazardous areas and monitoring can proceed throughout night and day and in almost all meteorological conditions. Also, unlike in situ instrumentation, which acquires information in single points, remote sensing techniques acquire information in several adjacent pixels and therefore exhibits good coverage allowing for identification of the spatial distribution of movement measurements. The high sampling frequency allow for continuous and near real-time monitoring and identification of fast slope movements. A high sampling frequency increases the statistical reliability of the measurements. As for satellite InSAR there are problems related to phase wrap and require a displacement between acquisitions to be smaller than half a wavelength ($\lambda/2$) to avoid phase ambiguities.

3 Results

The chapter describes the bedrock in Oksfjellet, including Caledonian ductile structures (foliation, folds and related structures) and post-Caledonian brittle structures (faults and fractures). Secondly, the geomorphological elements in the unstable areas are described. Lastly, the displacement documented by GB-InSAR and satellite InSAR will be described and related to geological structures and geomorphological elements. An overview of the investigated area is shown in Fig. 11 and Fig. 12.

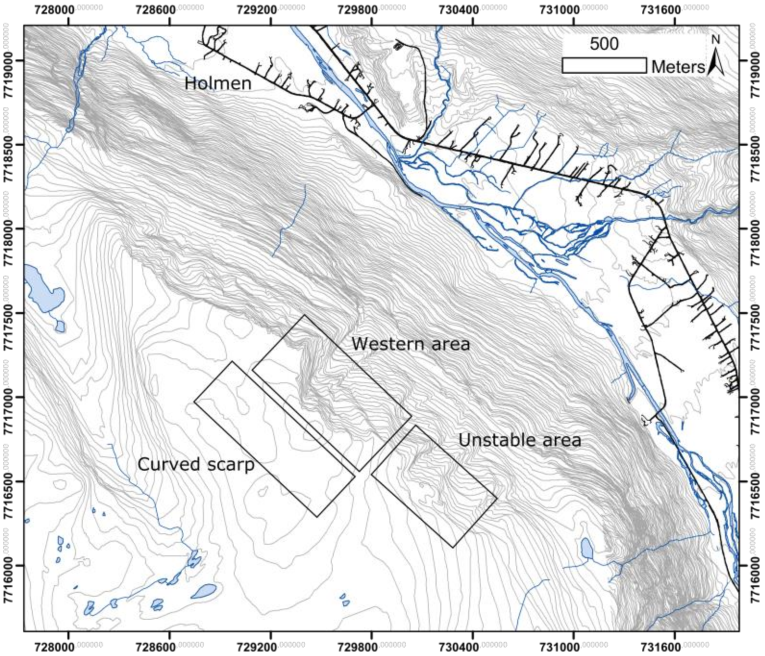

Fig. 11 Overview of Oksfjellet and the surrounding area. The different areas will be referred to. 5 m contour lines.

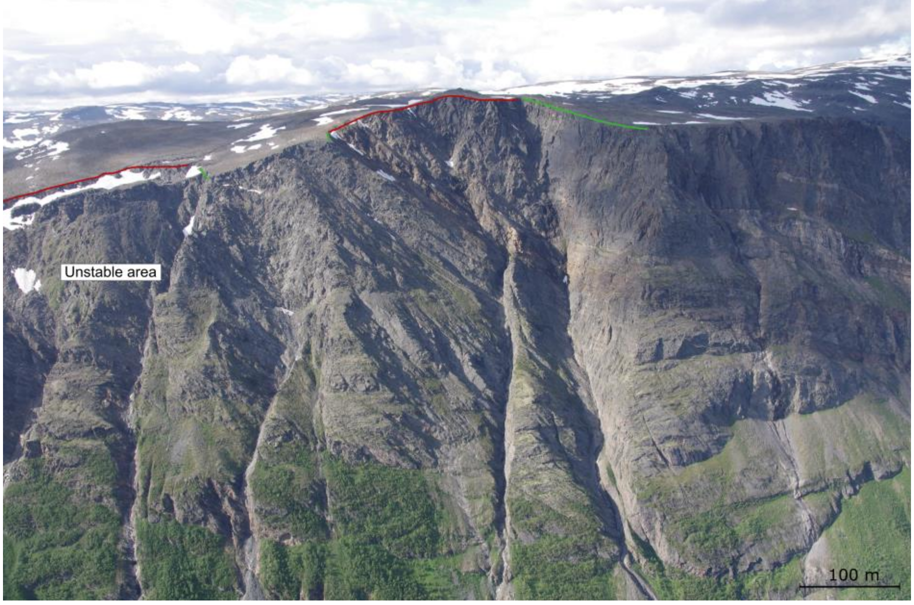

Fig. 12 Overview photo of the face of Oksfjellet, including the unstable area and the western area. Red and green lines show the back scarps. Photo by Böhme (NGU).

3.1 Bedrock composition

In Oksfjellet, rocks of the Vaddas Nappe and Kåfjord Nappe make up the bedrock, that comprises foliated mica schists with varying content of biotite, muscovite, garnet, quartzite and feldspar (Fig. 13).

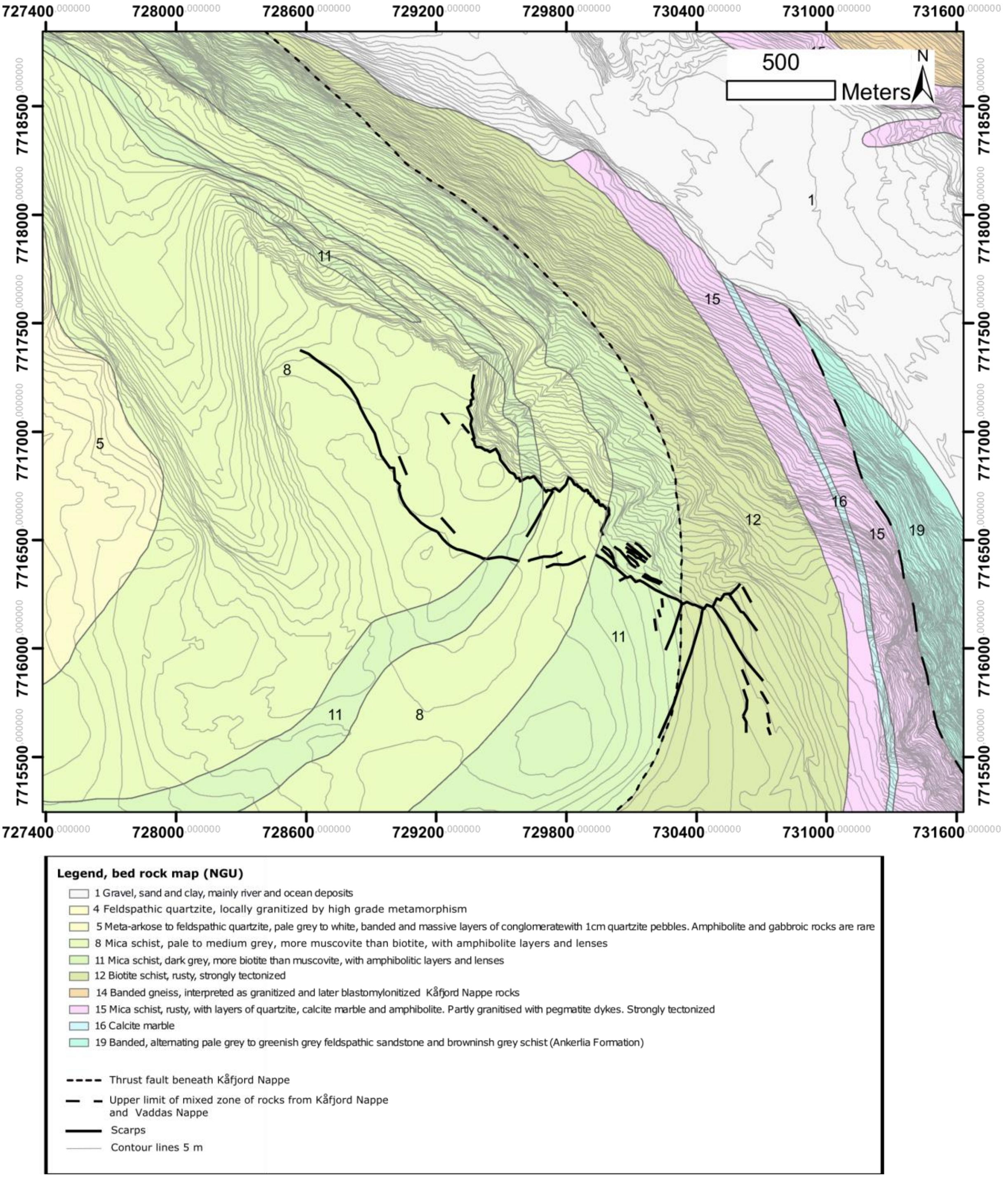

Fig. 13. Geological map over Oksfjellet retrieved and modified after NGU (www.geo.ngu.no/kart/berggrunn) draped over topographical map with 5 m contour lines, showing the most prominent scarps.

The lowermost parts of the mountain slope are covered by muscovite and garnet-rich colluvium, and is replaced at higher elevations by rusty biotite schists. The rusty biotite schists are located in a mixed zone of rocks from both the Vaddas Nappe and the Kåfjord Nappe, where amphibolite lenses and lenses of calcite marble are observed. Oksfjellet comprises alternating well-foliated lithologies of muscovite rich and biotite rich mica-schists, that also include a high amount of garnets above 900 m a.s.l. Within the muscovite-dominated lithology amphibolite lenses are found, varying in size from a few centimeters to half a meter within the foliated strata (Fig. 14).

Fig. 14 Photos of lens-shaped boudins in bedrock schist. Left: Calcite veins forming lens-shaped boudins. Right: Lens-shaped amphibolite boudins.

The foliation is parallel to lithological contacts and easily distinguished due to the competence contrast between the lithological units. The schistose mica-rich units are more easily weathered than the massive, and likely more competent, quartz-rich lithologies. The indicated lithologies in Fig. 15 are based on a combination of field observations and an interpretation of photos taken from helicopter, that overall, coincides well with the bedrock map.

Fig. 15 Photo showing the main characteristics of the different foliated lithologies in Oksfjellet. Photo by Böhme (NGU)

3.2 Caledonian ductile structures

The Caledonian structures observed at the face of Oksfjellet and the surrounding area form the basis of the description of foliation, folds and related structures in section 3.2.

3.2.1 Regional Caledonian structures

The area is dominated by flat-lying Caledonian structures, evident as alternating lithological contacts (S0) (Fig. 13 and Fig. 15) parallel to well-developed ductile foliation (S1) striking NE-SW. The macroscale folds (Fig. 16) are isoclinal, intrafolial folds with an axial surface parallel to the main foliation. They fold layers of alternating lithologies (S0), and thus they are interpreted to be F1 folds. Local areas display macroscale up-right folding of the foliation into antiforms and synforms, interpreted to be F2-folds. The exposed face at Oksfjellet show a pronounced bend-up (20 – 40°) of the foliation and the foliated strata obliquely, and with low angle (< 30°) truncate the more flat-lying strata farther southeast defining a structural disconformity with a ramp flat geometry (Fig. 16).

Fig. 16 Photograph showing large-scale monocline folding (bend-up) of the main foliation, and isoclinal intrafolial folding at the steep face of Oksfjellet. Photo by Böhme (NGU).

3.2.2 Folds and ductile shear zones (thrusts)

The bedrock schists at Oksfjellet show a well-developed ductile foliation (S1) striking NE-SW to NNE-SSW and dipping from gently to steeply (15 – 40°) to the WNW-NNW (Fig. 17). The foliation (S1) is parallel to the indicated contacts (S0) between the alternating lithologies seen in Fig. 13 and Fig. 15, suggesting that S1 formed axial-planar to major shear folds during nappe emplacement (Lindahl et al., 2005).

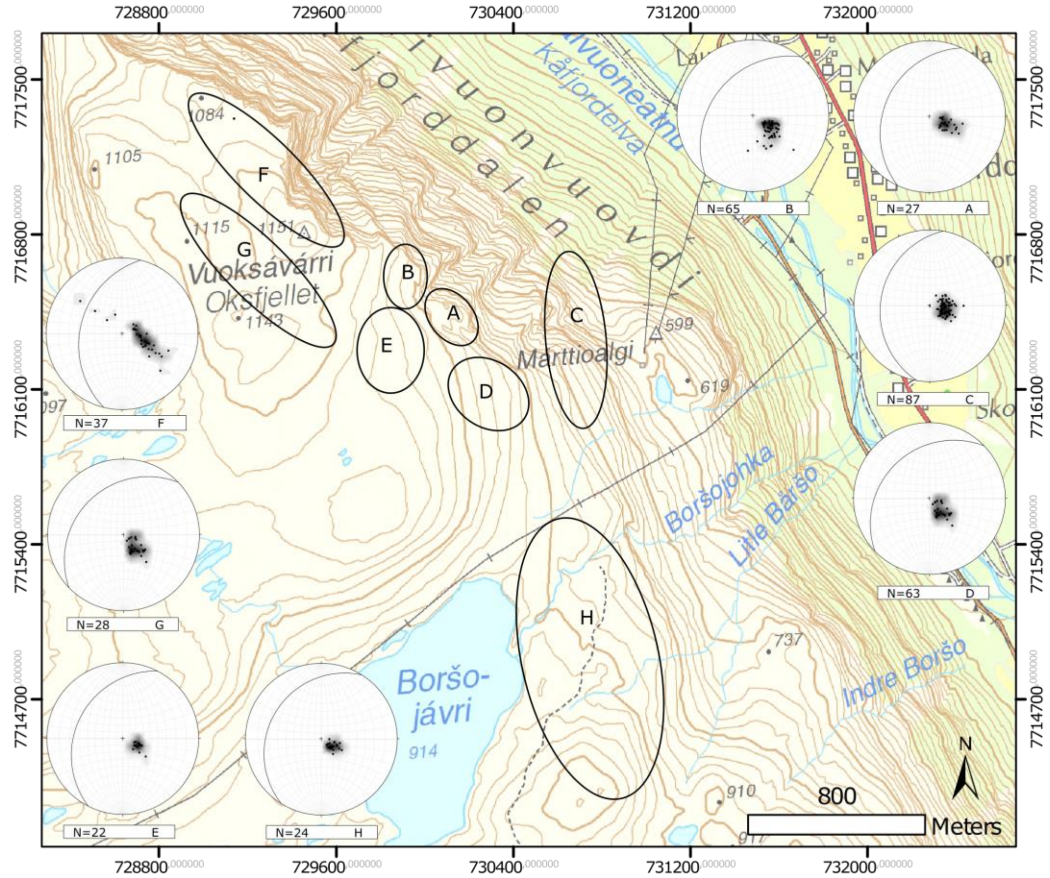

Fig. 17 Map showing the strike and dip of the foliation as contoured poles and the mean foliation as great circle at different areas in Oksfjellet.

Such a large scale monocline-like synformal fold is exposed at the steep NNE face of Oksfjellet (Fig. 16). The internal strata of the nappe section cut up section at a low angle, producing a structural disconformity. This truncating portion is interpreted as a ductile shear zone, likely a thrust, emplacing lower strata on top of younger in an imbricated thrust stack (Fossen & Hurich 2005). Related upright folds (F2- folds) refold the main foliation (S1).

The foliated bedrocks at Oksfjellet are not always continuous due to differences in lithology and competence. Lenses of various size, composed of massive quartz-units and amphibolites enclosed by the host rock schists, are observed at several localities in Oksfjellet. Lens-shaped structures of amphibolite and calcite marble with sizes varying from centimeters to 50 cm, found in the upper lithologies at Oksfjellet cause local variations in strike and dip of the foliation. Some of the more aligned lenses comprise internal isoclinal F1-fold hinges that are truncated by the surrounding foliation (Fig. 14, right) The intrafolial lenses observed in Oksfjellet resembles boudins, and thus may have a similar origin (Goscombe et al., 2004).

3.3 Post-Caledonian brittle structures

The foliated bedrock in the studied area is cut by numerous brittle structures such as joints, fractures and faults (Fig. 18). An outline of fractures with corresponding strike and dip of fracture planes observed in the unstable area in Oksfjellet is given in Fig. 19.

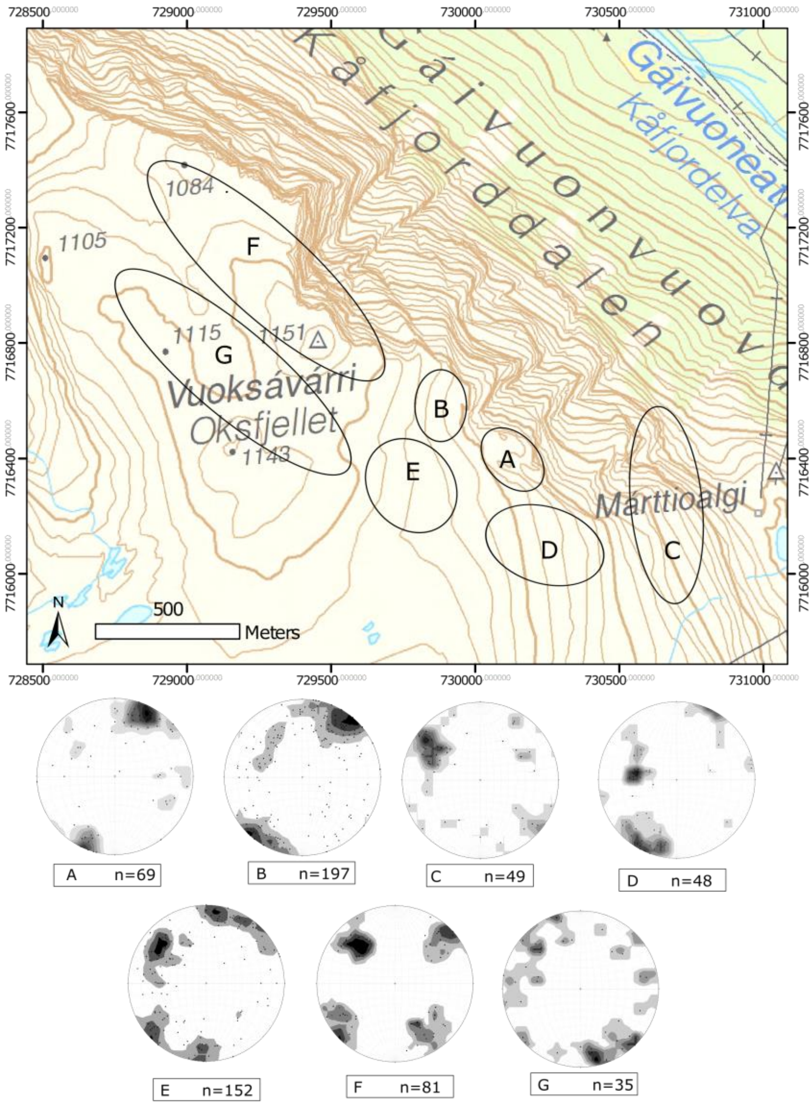

Fig. 18 Topographical map showing the strike and dip of fractures as contoured poles at different areas in Oksfjellet.

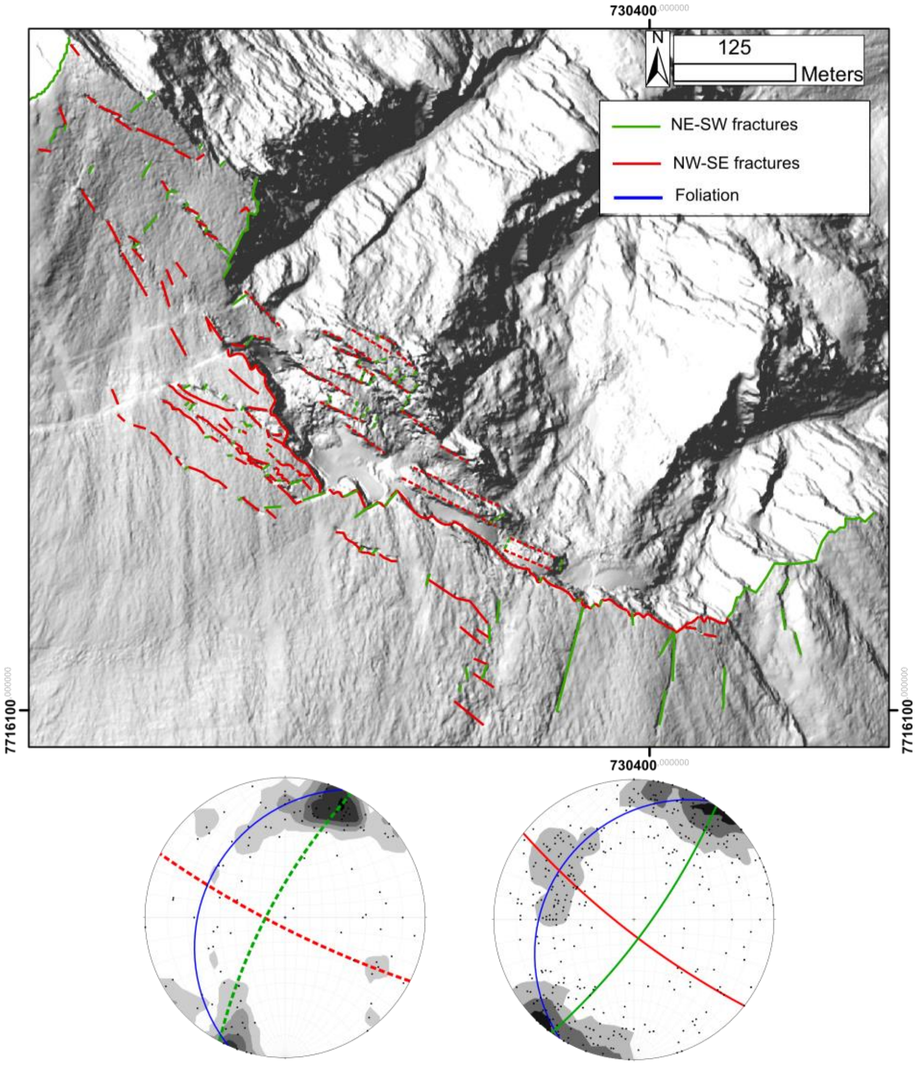

Fractures and foliation
in the main unstable area

Fractures and foliation
outside the main unstable area

Fig. 19 Shaded DEM showing the main fracture sets in to the unstable area. Fractures within the deformed area are marked by dashed lines.

The analysis of fractures at Oksfjellet and the surrounding area show that the main orientations for the fractures are striking NW-SE to NNW-SSE and NNE-SSW to NE-SW, and subordinate orientations of fractures are striking E-W and N-S. NW-SE and NE-SW striking fracture sets are observed throughout the studied area, whereas the E-W striking fractures are mainly found in the innermost areas of Oksfjellet. In the lowermost parts of Oksfjellet, below the unstable area, NW-SE and NE-SW striking fracture sets are most dominant. The observed fractures are steep to sub-vertical, with dominant dip direction toward NE and SW. Most of the mapped fracture sets, both along, behind and in front of the main back fracture scarp (see below) of the unstable area in Oksfjellet, are open fractures, i.e. they show evidence of separation perpendicular to the fracture surface. Both the NE-SW and the NW-SE striking fracture set is observed with oppositely dipping variations commonly intersecting at a constant dihedral angle of approximately 50-60°, hence they may represent conjugate sets. Different fractures observed in Oksfjellet are displayed in Fig. 20, from more than 1 m wide crevasses to cm wide joints width the step-wise geometry often observed as a result of the interacting NW-SE and NE-SW striking fracture sets.

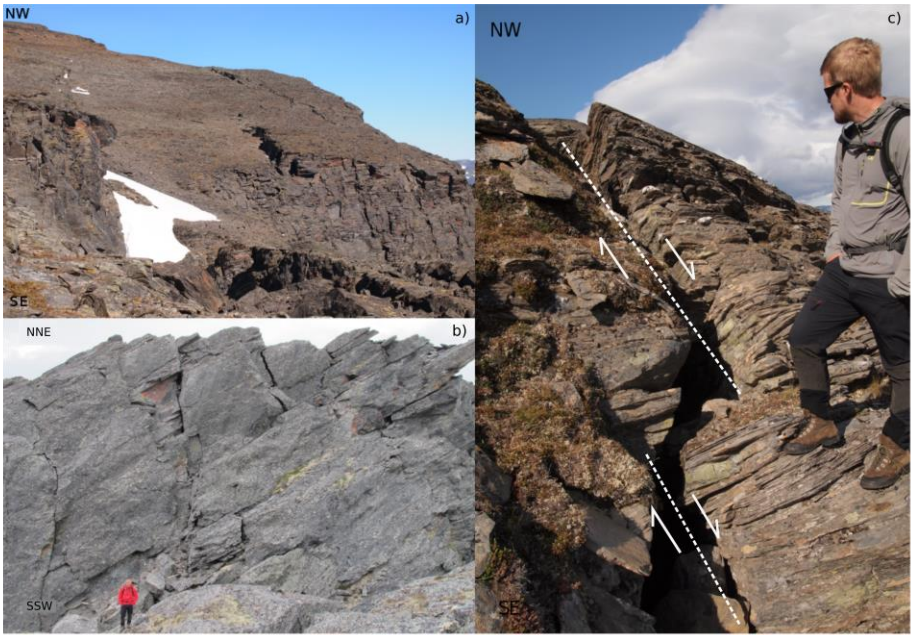

Fig. 20 Photos showing various fractures and crevasses in the studied area. a) Crevasses striking NW-SE, parallel to the slope and the back fracture scarp. b) NE-SW striking vertical and sub vertical fractures in the unstable area showing displacement along the foliation to the NW c) Step-wise fracture striking NW-SE with a sub vertical dip.

3.3.1 Back fracture

The back fracture scarp bounding the unstable area at Oksfjellet is defined by longitudinal fractures parallel to the valley, i.e. striking NNW-SEE to WNW-ESE and dipping steeply (70-85°) N to NNE (Fig. 21).

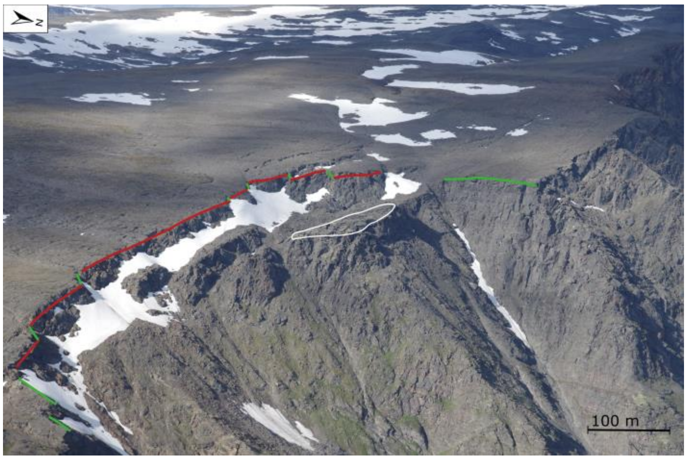

Fig. 21 Overview phot of the delimiting back fractures (red lines) and cross-fractures (green lines) and the proposed graben structure between the back fracture and the front block (white lines). Photo by Böhme (NGU).

The height of the back fracture is about 50 m in the middle part of the unstable area and show a successively decreasing height towards NW and SE making up a step-wise and apparently, down-faulted block geometry. The back fracture scarp cuts the gently dipping foliation at a high angle. The back fracture scarp itself is segmented along strike by alternating NW-SE and NE-SW striking cross-fractures, with steep dip towards NNE seen in Fig. 27. Because of the loose material and continuous snow coverage in the trench there are uncertainties of how deep the fractures are propagating downwards. In front of the back fracture scarp there is a deep trench and a large counter scarp in relation to it, filled by loose blocks. The width of the trench is c. 110 m from the back fracture scarp to the counterscarp and the height of the counterscarp is 10 – 15 m. The vertical displacement of the counter scarps location today, relative to the location of the back fracture scarp is about 15 m. The horizontal displacement over the trench is approximately 40 m (Fig. 22). These are the cumulated values estimated using aerial photos and high resolution DEM (1 x 1 m) in ArcGIS using 3D analysis, hence these values should be seen as interpretative.

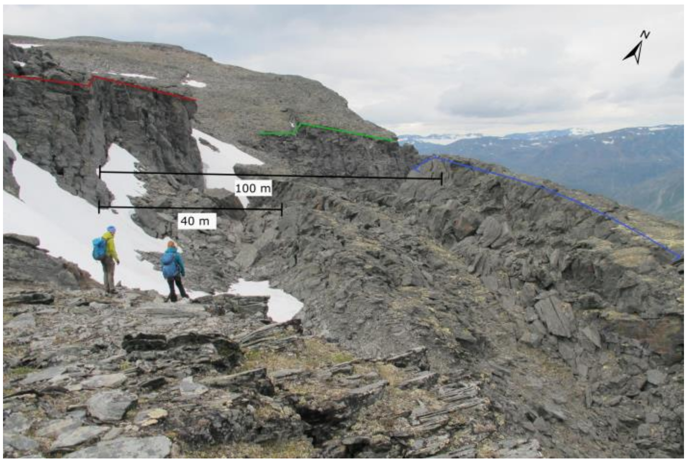

Fig. 22 Photograph showing the width, 100m, between the back fracture scarp (red lines) and the front block (blue lines), an accumulated displacement of c. 40 m in association to the cross-fracture scarp (green lines).

At an elevation of c 800 m a.s.l. a NNW-SSE striking fracture dipping sub-vertical to SW cuts the face of Oksfjellet (Fig. 23).

Fig. 23 Photo showing antithetic NNW-SSE striking fractures cutting the front of Oksfjellet. Photo by Böhme (NGU).

3.3.2 Cross-fractures

The unstable area is bounded to the east and to the west by NNE-SSW striking steeply dipping (c. 75°) cross-fractures that are at high angle to the back fracture scarp (Fig. 21). The stepped geometry of the eastern delimitation of the back fracture scarp (Fig. 24) is a result of alternating NW-SE back-fracture and NE-SW steeply dipping (c. 75°) cross-fractures. Due to NW-SE and NE-SW striking fractures, foliation surfaces striking NE-SW with a gentle dip of c. 30° to the NW are exposed at the eastern delimitation (Fig. 25).

Fig. 24 Photo showing the eastern delimitation of the unstable area. Red lines: NW-SE back fractures. Blue lines: NE-SW cross-fractures. Photo by Böhme (NGU).

Fig. 25 Photo showing the eastern delimitation of the unstable area and exposed foliation surfaces striking NE with a gentle dip (30°) to NW. Photo by Böhme (NGU).

The western delimitation of the unstable area (Fig. 21) is defined by a major NNW-SSE striking and steeply (70 – 85°) ESE-dipping fracture scarp, that can be traced for c. 100 m. The western scarp is cut by numerous steeply dipping NW-SE striking fractures that are persistent in and can be traced towards northwest. These fractures are dipping parallel to the slope, but some examples of oppositely dipping fractures are seen in NNE-SSW section view in Fig. 26.

Fig. 26 Photo showing the western delimiting scarp in NNE-SSW cross-section view cut by back fracture scarp parallel fractures. Photo by Böhme (NGU).

Northwest of the unstable area, see Fig. 12 the stepped geometry of the WNW-ESE striking scarp is formed by alternating NW-SE and NE-SW striking fractures steeply dipping (c. 70°) (Fig. 27). The western delimitating scarp in the western part of Oksfjellet is striking N-S with a sub-vertical dip to SE, traceable for c. 350 m. The NW-SE striking scarp is delimited to the east by NW-SE and NE-SW steeply dipping (c. 75°) fractures, exposing foliation surfaces striking NE-SW, dipping 40° to NW (Fig. 28).

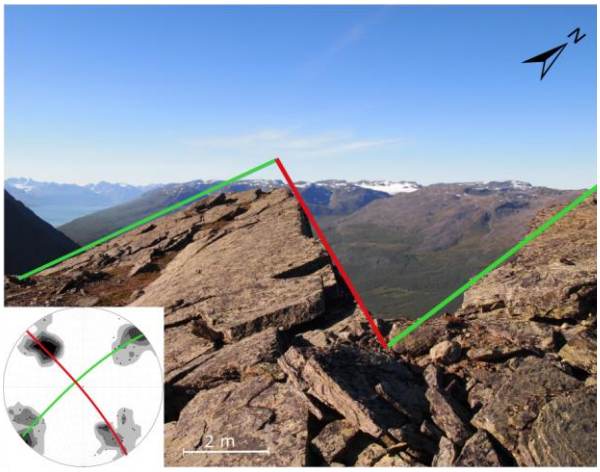

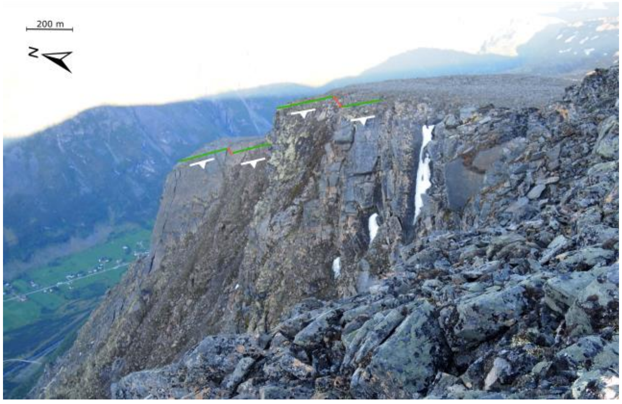

Fig. 27 Picture showing how the back fracture scarp coincides with the obtained fracture sets for the area.

Fig. 28 Picture showing alternating NW-SE and NNE-SSW striking fractures and exposed foliation surfaces at the eastern delimitation of the NW-SE striking scarp in the western part of Oksfjellet.

A structural map of Oksfjellet is presented in Fig. 29 based on field observation of geological and morpho-tectonic elements.

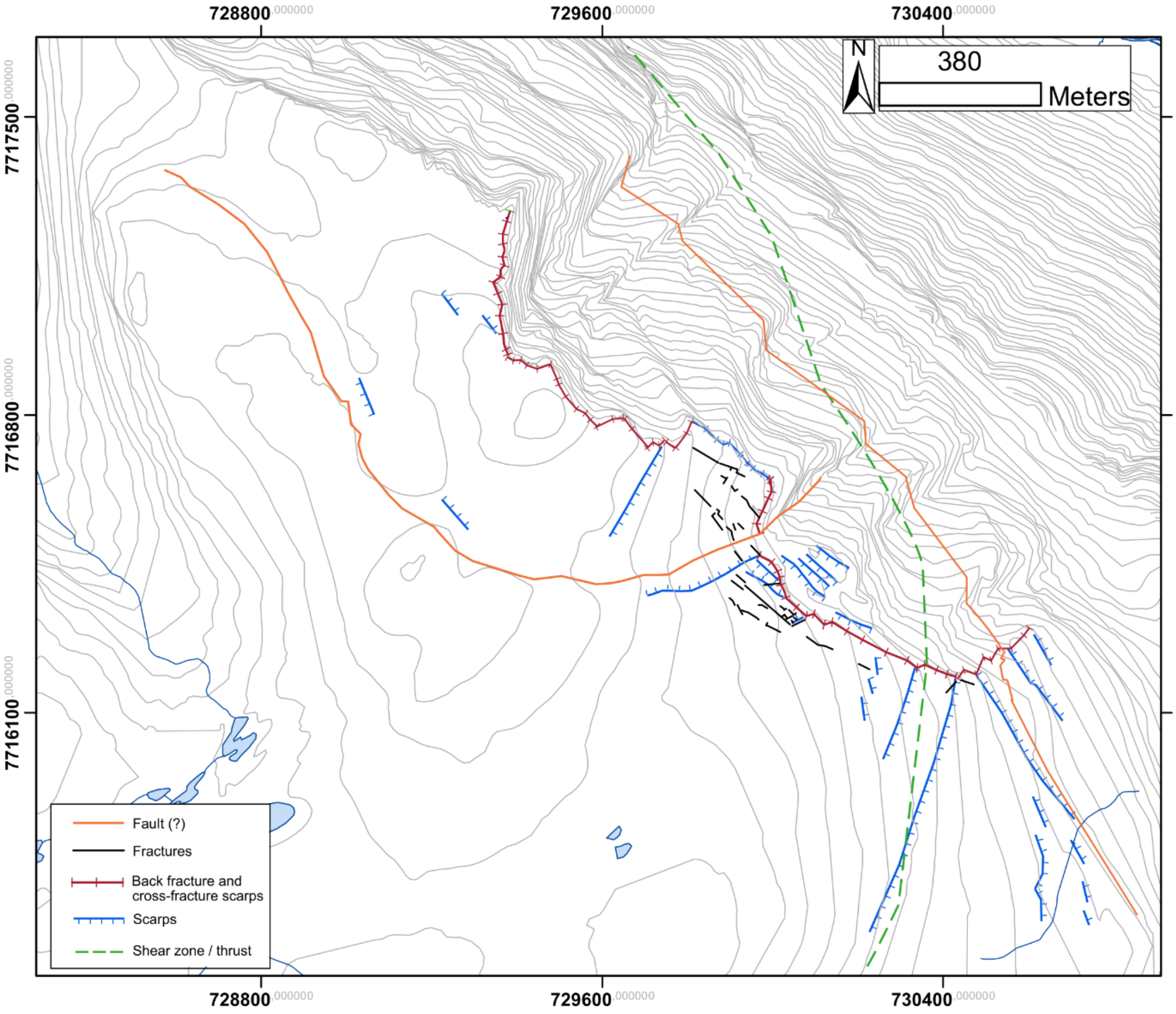

Fig. 29 Structural map of Oksfjellet based on field observations. 5m contour lines.

3.4 Morphological elements

The section describes morpho-tectonic elements (e.g., scarps, ridges and trenches) and surficial morphological elements, such as drainage and colluvium in the investigated area. A morphological map based on field observations, analysis of orthophotos and high resolution DEM, is presented in Fig. 30.

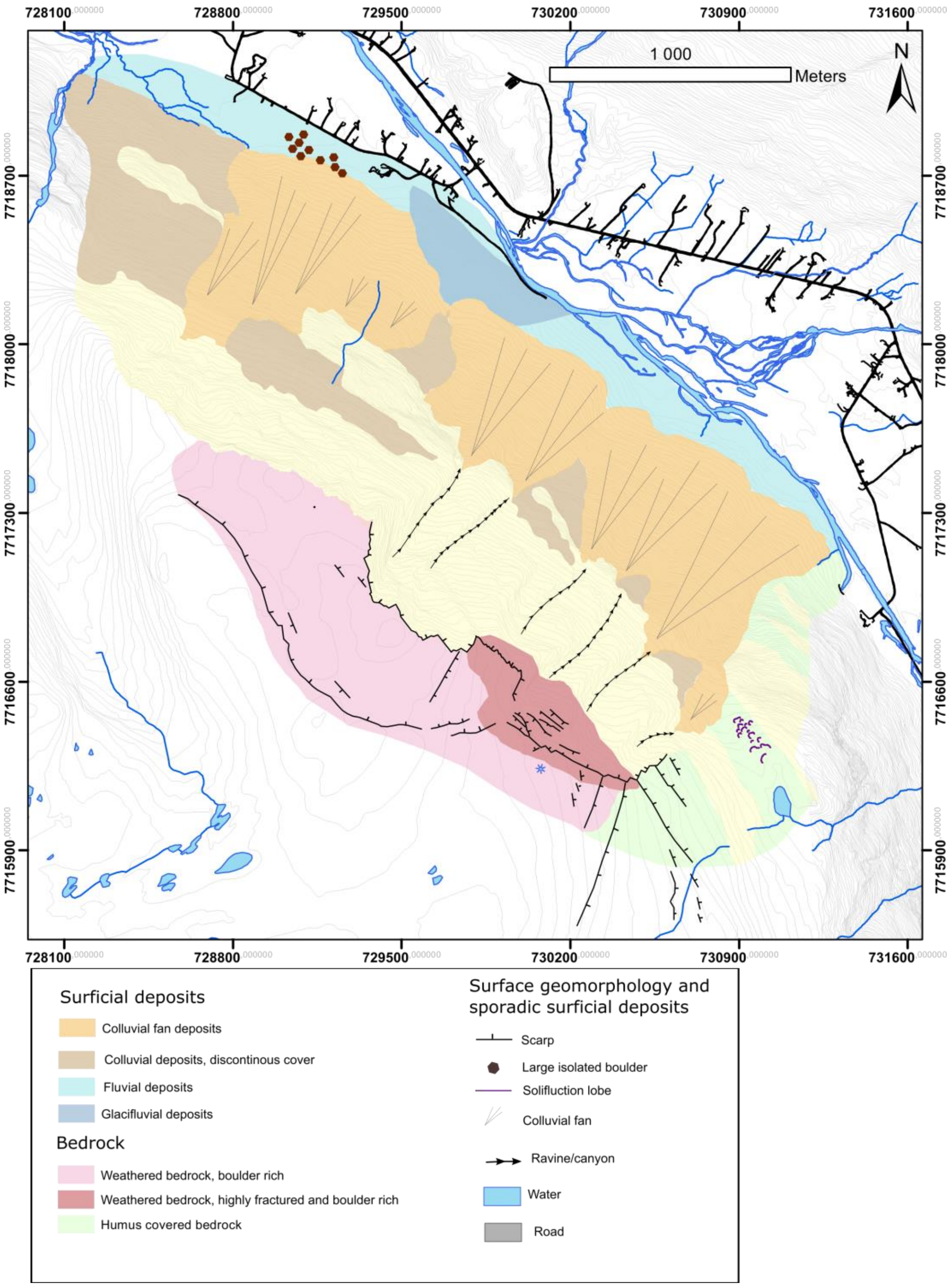

Fig. 30 Geomorphological map over Oksfjellet, based on field observations, aerial photos and high resolution DEM.

3.4.1 Scarps and trenches

Scarps are observed throughout the investigated area (Fig. 29), both in relation to the deformation, such as the scarps within and in proximity close to the unstable area, and in still intact bedrock.

In connection the to the back fracture scarp, a large counterscarp (15 m high, 30 m wide and 130 m long) is bounded by NW-SE and NE-SW striking sub-vertical fractures and on top shaped by the gently dipping foliation (c. 25° to NW) (Fig. 31). The is counter scarp /frontal block is truncated by fractures striking NW-SE and NE-SW with a sub-vertical dip. The alternating fractures defines columns that in the northeastern parts of the block that are overturned and show an increasing downslope rotation to NE (Fig. 31, right). Overall, the geometry of the block resembles a horst.

Fig. 31 Left: The counterscarp the unstable area, looking to northeast. Right: Overturning an outward rotation of blocks at the counterscarp.

The back fracture scarp and the counterscarp is linked by three overstepping ramps (Fig. 32), with a height of 6 – 8m, a length of approximately 80 – 100 m, and a width of 10 – 15 m and formed by the foliation on top. Contrary to the back fracture, they are striking NW-SE (Fig. 32).

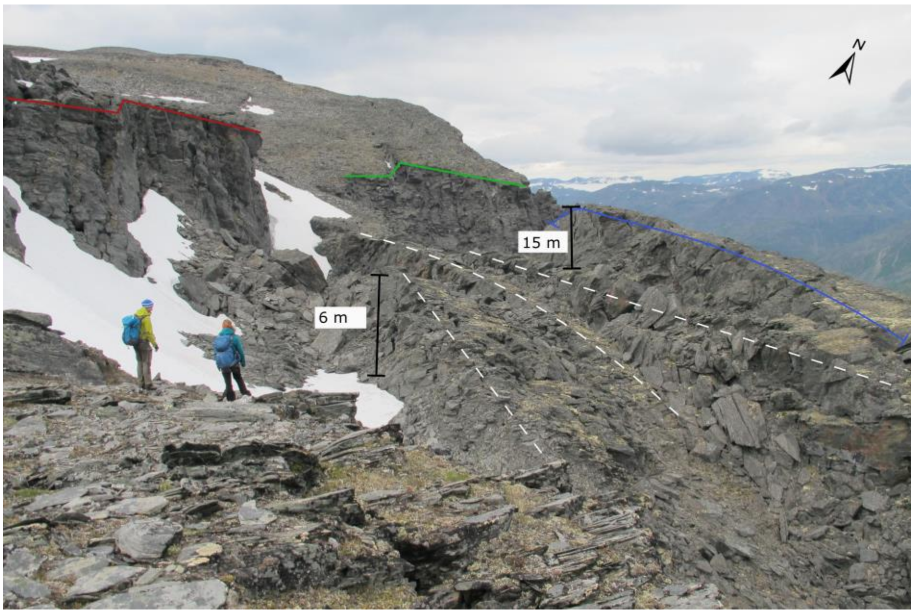

Fig. 32 Photo showing ramps/counterscarps (marked by dashed white lines) between the back fracture scarp and the front block.

Outside the unstable area, scarps are striking NNE-SSW and NW-SE with a vertical drop from 1 m to several meters, generally with an increasing drop towards the back fracture and the delimiting cross-fracture (Fig. 29).

In the inner parts of Oksfjellet a scarp displays a curved geometry (Fig. 11), with a strike varying from NNW-SSE dipping towards ENE in the western parts, to NW-SE striking in the middle, dipping steeply (c. 70°) to NE and bending in to the NE-SW striking cross-fracture, which dips steeply to SE bounding the unstable area to the west (Fig. 29). The curved scarp is defined by a combination of NW-SE and NE-SW striking sub vertical fractures. The vertical drop varies from c. 3 m in the middle of the scarp in the middle, to 1 – 2 m at the eastern and western part. The scarp is associated with deformation (Fig. 33) where fractures parallel to the scarps opens perpendicular to it, and counter-clockwise rotation of the foliation is documented. The curved scarp is interpreted to be a fault.

Fig. 33 Photo showing deformation related to the curved scarp, a vertical drop of c. 3 m and inward rotation of the foliation. Photo by Bunkholt (NGU).

3.4.2 Colluvium

Colluvial fans have formed beneath several channels located at the front of Oksfjellet (Fig. 23 and Fig. 30). The channels confine the path of debris derived from the upper parts of the mountain. The colluvial fans consist of by material that have been emplaced and accumulated over time, show a fan-like geometry with a thick and wide front and can be traced nearly to the apex zone where they are narrower and thinner. The fans are increasing in width, run-out length and cover depth, and display more frequent ongoing slope processes from Holmen toward the unstable area. Overall, a downslope coarsening of the colluvial fans are observed.

The fans display incised tracks with levees at the upper and middle part, consisting of angular and slightly downslope aligned boulders accumulated near the apex zone, whereas farther downslope, the material is replaced by smaller boulders and cobble. The fans are steep, with slope inclinations varying from 40 – 45° at the fan apex to 20 – 25° at the toes. With decreasing slope inclination, the confined channels spread out, and the depositional pattern becomes more complex. Both lobate shaped paths, stacked upon one another in an imbricated and overstepping manner and smoother areas with more scattered boulder-rich deposits are found. The largest boulders are scattered around at Holmen, with sizes up 5 m x 5 m.

No large scale rock failure deposits have been documented in the valley.

3.4.3 Drainage

Oksfjellet does not comprise any major stream, wet mark or lakes, however water was observed streaming into several fractures and holes outside the unstable area (Fig. 30). The streams were associated with ice- filled fractures. Water was also heard streaming deep within fracture systems in the area between the unstable area and the western area. The trench located in front of the curved scarp was is snow- and ice covered throughout the season and during melt snow melting, partially filled with water.

3.5 dGPS results

GPS point KA-2 is located on the front block in the unstable area (Fig. 5) Showing a horizontal displacement rate is estimated to c. 3 mm/year, whereas the vertical displacement in the same point is considered as not significant due the noise (Table 3).

Table 3 dGPS measurements at Oksfjellet. From NGU.

dGPS	Observation time		Movement [mm/year]			Direction[deg]		Significance	
	Start	End	Horizontal	Vertical	Total	Trend	Plunge	Horizontal	Vertical
KA-2	09.06.2003	07.08.2012	2,9	1,75	3,39	41,7	31,1	Yes	No
KA-3	09.06.2003	07.08.2012	0,19	1,77	1,78	61,3	83,7	No	No
KA-5	05.09.2006	07.08.2012	0,62	-1,87	1,97	28,1	-71,6	No	No
KA-6	05.09.2006	10.08.2010	1,25	-1,14	1,69	44,3	-42,2	No	No

3.6 GB-InSAR results

The main results, focusing on the largest areas and the highest displacement rates detected by GB-InSAR in 2011 (see Appendix 1), 2014 and 2015 are based on Kristensen(2011), Skrede & Kristensen (2014) and Skrede (in prep.) and summarized in Table 4. The areas associated with the labels in Table 4 are shown in Fig. 34.

Area A is located beneath the unstable area and is identified as the lobe shaped deposit seen in Fig. 34, area B is the large area from the top of the front block and c. 200 m downslope of c. 50 000 m^2 and area C consists of mostly large boulders just beneath the WNW striking back fracture.

Table 4 Main results from GB-InSAR monitoring campaign in 2011, 2014 and 2015.

Year	Time interval	Area [m^2]	Total displacement [mm]	Displacement rate [mm/day]	Areas in Fig. 34
2011	15.08 – 23.08	4500	18	2,6	A
		3500	4		C
2014	02.06 – 16.06	4200	45	3,3	A
		3600	25		C
	04.06 – 07.06	50 000	4	1	B
	18.08 – 29.09	6000	130	3	A
		3600	50		C
2016	29.05 – 07.09	4500	80	1,8	A
		3600			C
	22.06 – 26.06	50 000	4	1	B

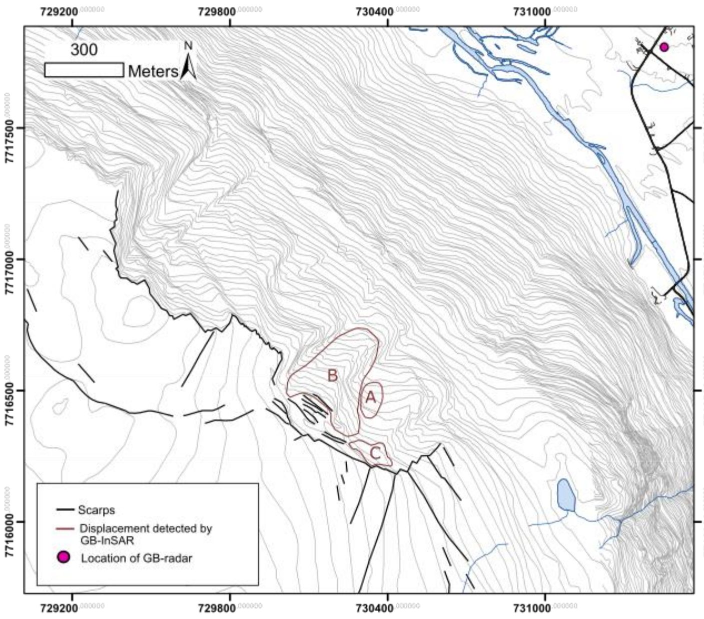

Fig. 34 Map showing the largest area (B) associated with displacement, and the areas associated with the highest displacement rates (A and C).

Cumulated displacements for the monitoring two campaigns in 2014 are presented in Fig. 35 and Fig. 36, where both campaign show displacements in the same areas, with a total displacement of 45 mm in June and 130 mm in August. The first campaign in 2014 (June 2 – June 16) was characterized by temperatures increasing from a few degrees to 10°C at June 8, followed by decreasing temperatures until June 16, when temperatures dropped to below 0°C and was accompanied by snowfall registered at the weather station at Nordnesfjellet, located an elevation of 700 m a.s.l., 20 km to the northwest of Oksfjellet. During the second campaign, temperatures were decreasing from c. 10°C, on August 18 to snowfall and temperatures below 0°C on September 18.

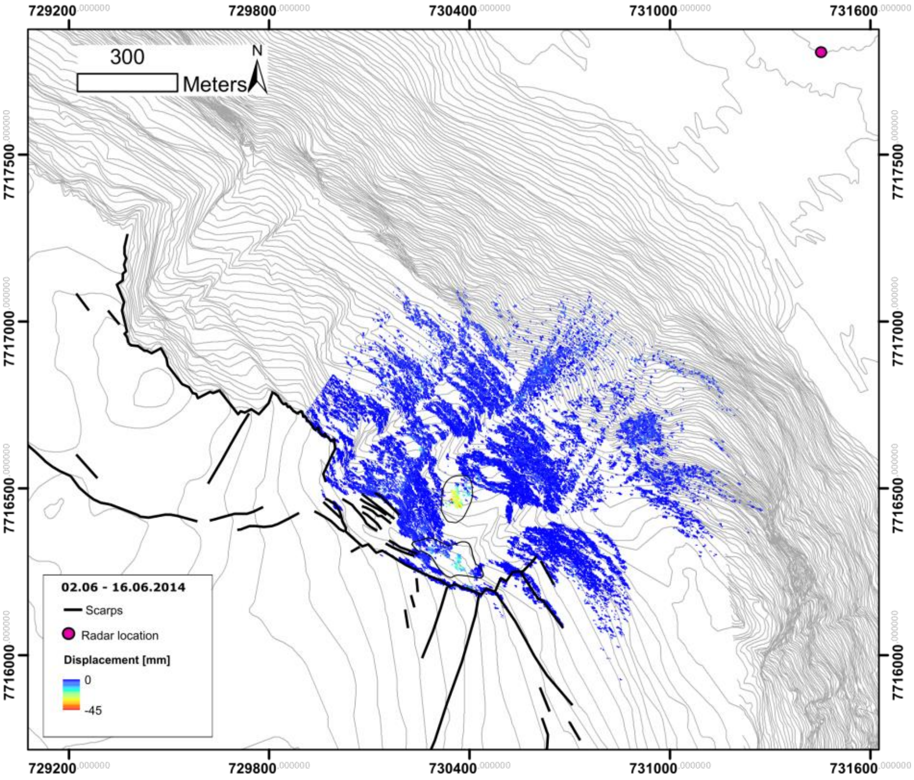

Fig. 35 Map showing the cumulated displacement for GB-InSAR monitoring campaigns in June 2014. Displaced areas are outlined.

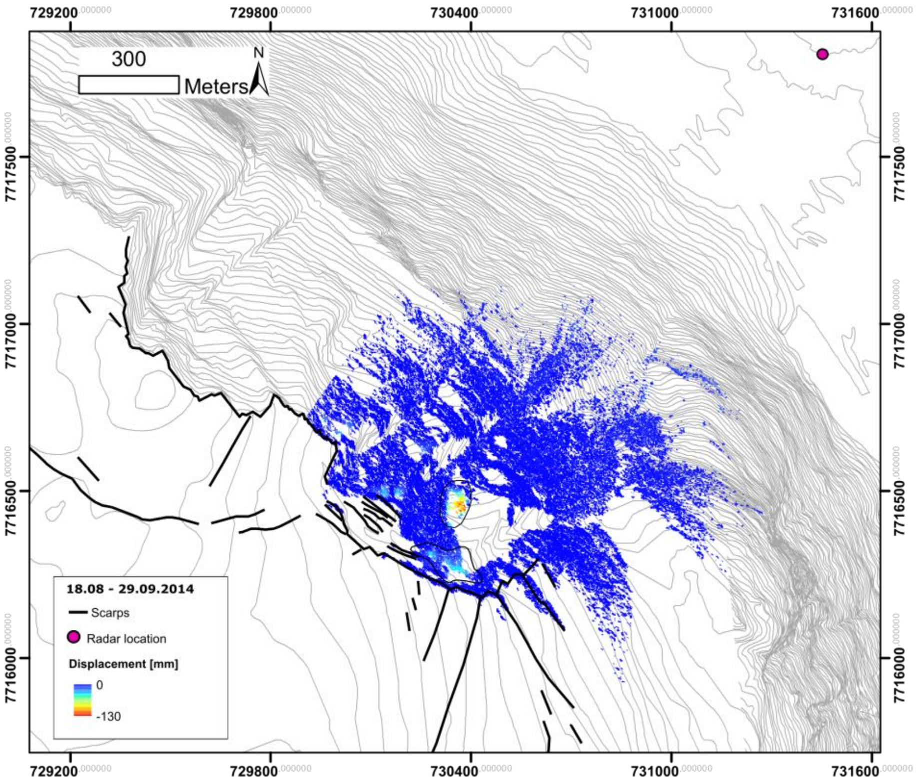

Fig. 36 Map showing the cumulated displacement for GB-InSAR monitoring campaigns in August 2015. Displaced areas are outlined.

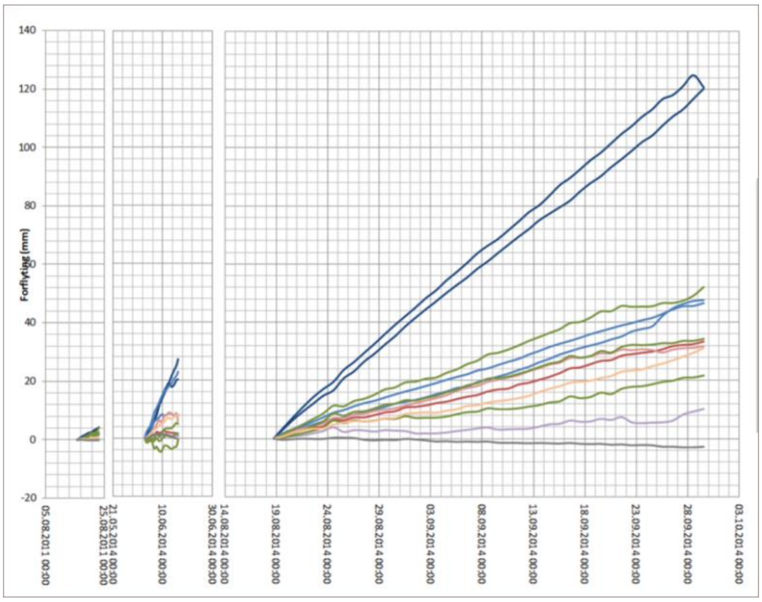

Fig. 37 Graph showing time series for different points in 2014. The equally colored lines segments correspond to the labeled areas in Fig. 34. Dark blue: A, light blue: C, red and orange: B.

Area B (Fig. 34) shows a displacement rate of 13 mm/week in June compared to a rate of 7 mm/week in August (Fig. 37). The displacement corresponds to area B in Fig. 34, which is displaced 3 – 4 mm over the period June 4 and June 7 seen in Fig. 38.

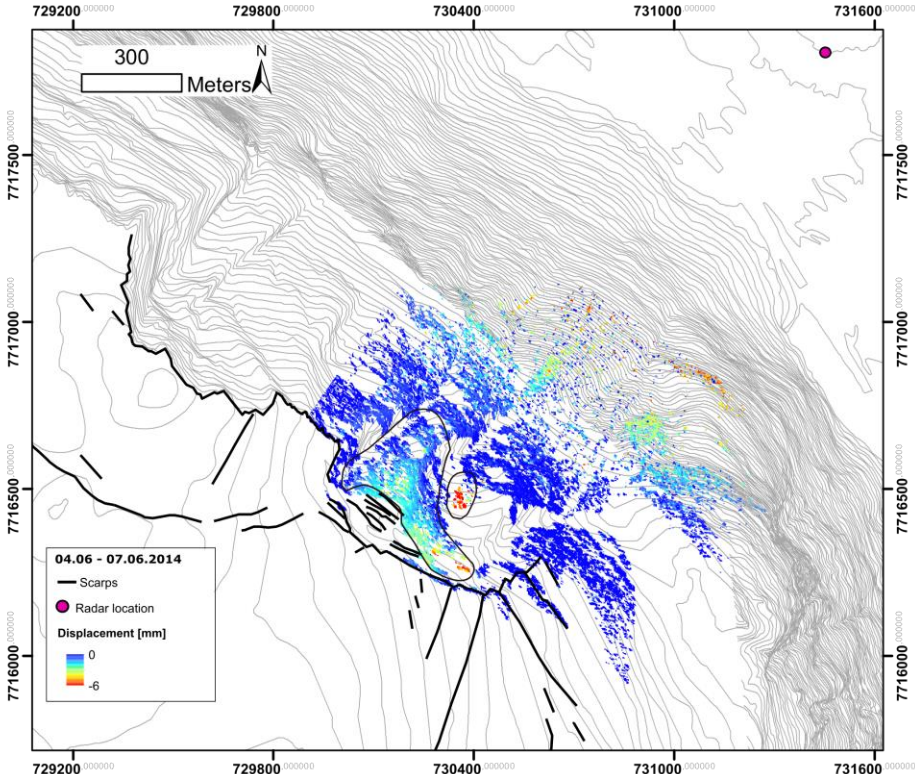

Fig. 38 Map showing displacement of 3 – 4 mm over three days in June 2014. Areas associated with displacement are outlined.

The monitoring campaign in 2015, from 29.05 to 07.09, detected displacements in the same areas, seen in Fig. 39, as the campaign in 2014. The total displacement of area A, which is identified as loose deposits beneath the unstable area (Fig. 34) was up to 80 mm (Fig. 40). A 4 mm displacement of a larger area (c. 50 000 m2) detected in the period from June 22 to June 26 (Fig. 42) may be correlated to increasing temperatures (Fig. 41) during the preceding days of the event. The total displacement during the monitoring campaign of the largest area (area B) is c. 25 mm.

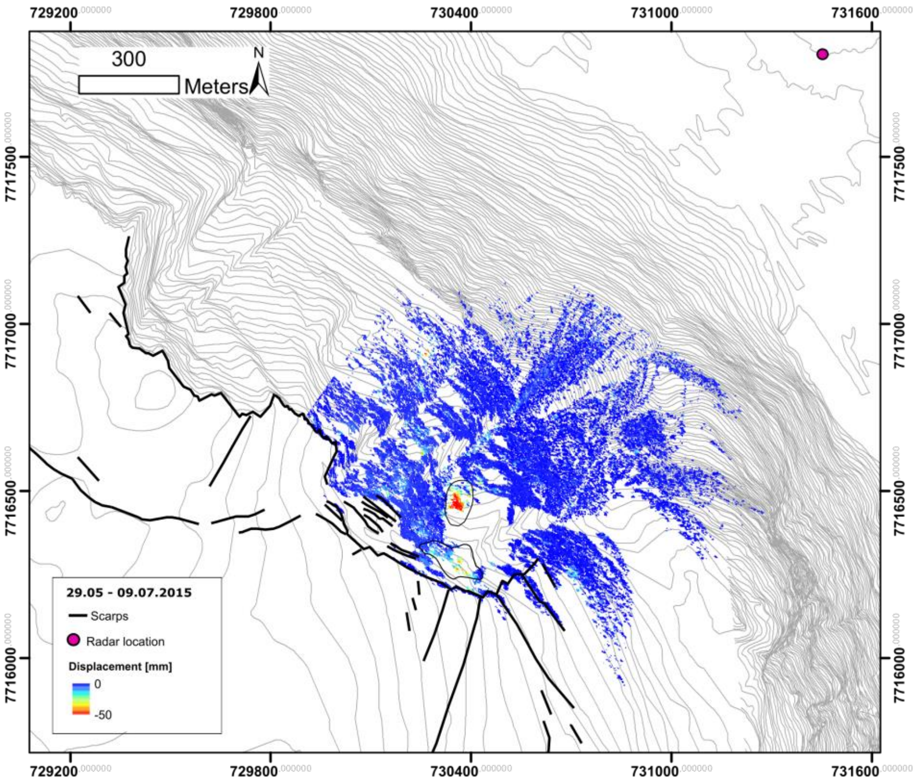

Fig. 39 Map showing the cumulated displacement during GB-InSAR monitoring campaign in 2015. Areas associated with displacement are outlined.

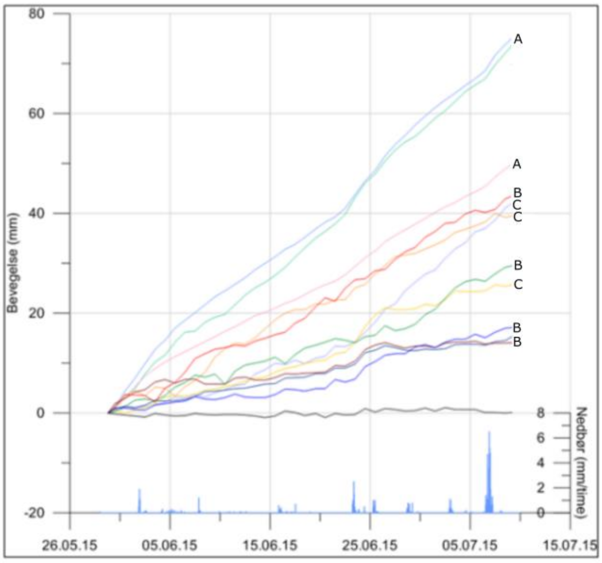

Fig. 40 Graph showing time series of the displacement and precipitation. The labels refer to Fig. 34. Modified from Skrede (in prep.)**.**

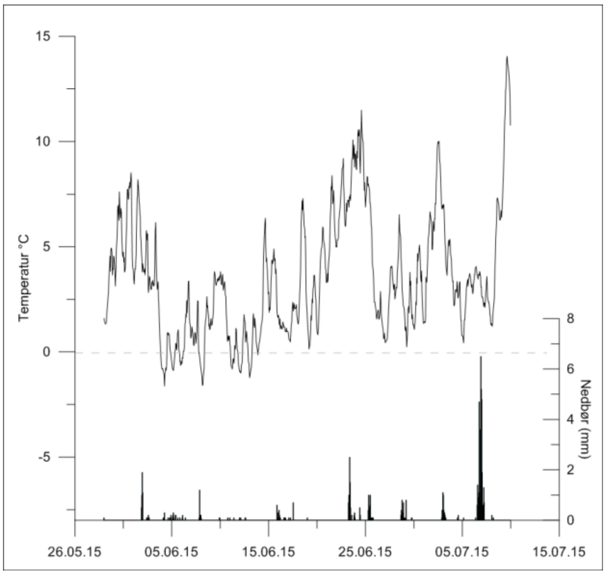

Fig. 41 Graph showing mean daily temperature and daily precipitation, from the weather station at Nordnesfjellet, during the monitoring campaign in 2015. From Skrede (in prep.)**.**

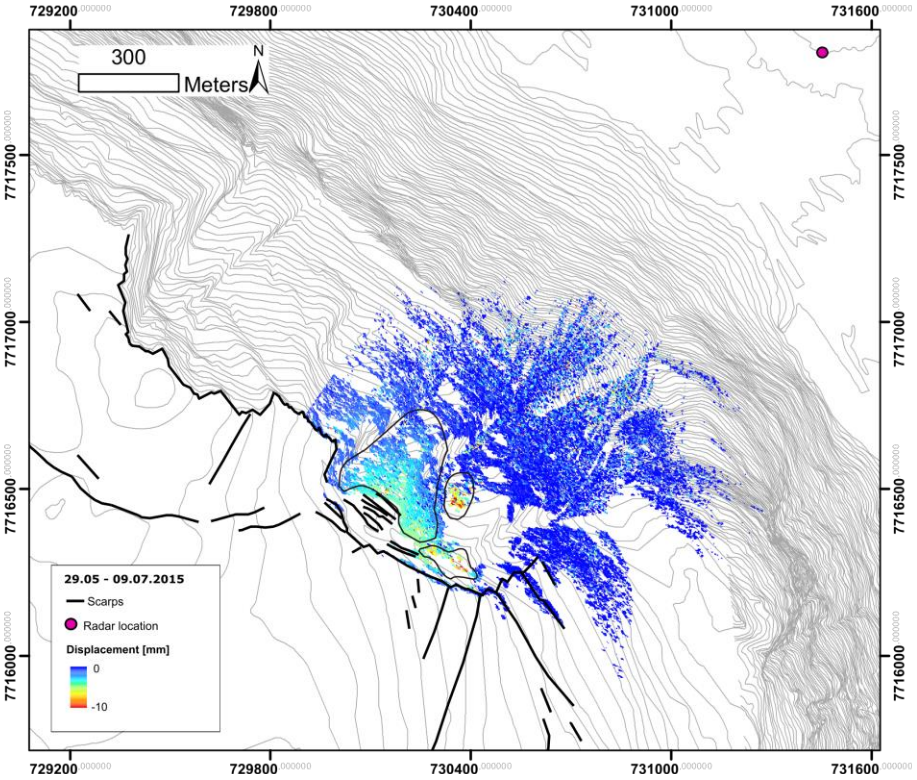

Fig. 42 Map showing the cumulated displacement during the time interval 22.06 – 26.06.2015. Areas associated with displacement are outlined.

3.7 Satellite InSAR results

This section describes stacking processed satellite InSAR results from the two sensors RADARSAT-2 (RSAT-2) and TerraSAR-X (TSX) presented in maps displaying displacement in terms of mm/year. Displacements are described in combination of field observations in order to relate the displacement patterns and magnitudes to geological features. Further, the displacements have been projected into the vertical plane, to better compare the datasets quantitatively. Negative values correspond to displacement downward and positive values correspond to upward displacement.

From the detected displacements, that show variable rates of vertical displacements depending on location and closeness to mapped fractures and scarps (Fig. 29), two main features can be emphasized:

- The fastest displacement rates (- 4 mm/year) are detected in the unstable area, where the displacements pattern is clearly controlled by the delimiting fractures and scarps described in chapter 3.
- A faster displacement rate by c. 1 mm/year is associated with the curved scarp in the inner parts of Oksfjellet.

Frost-weathered boulders and blocks characterize the morphology at the plateau at Oksfjellet. Displacements detected in these areas, in all datasets, can be explained by seasonal variation due to frost heave and thawing.

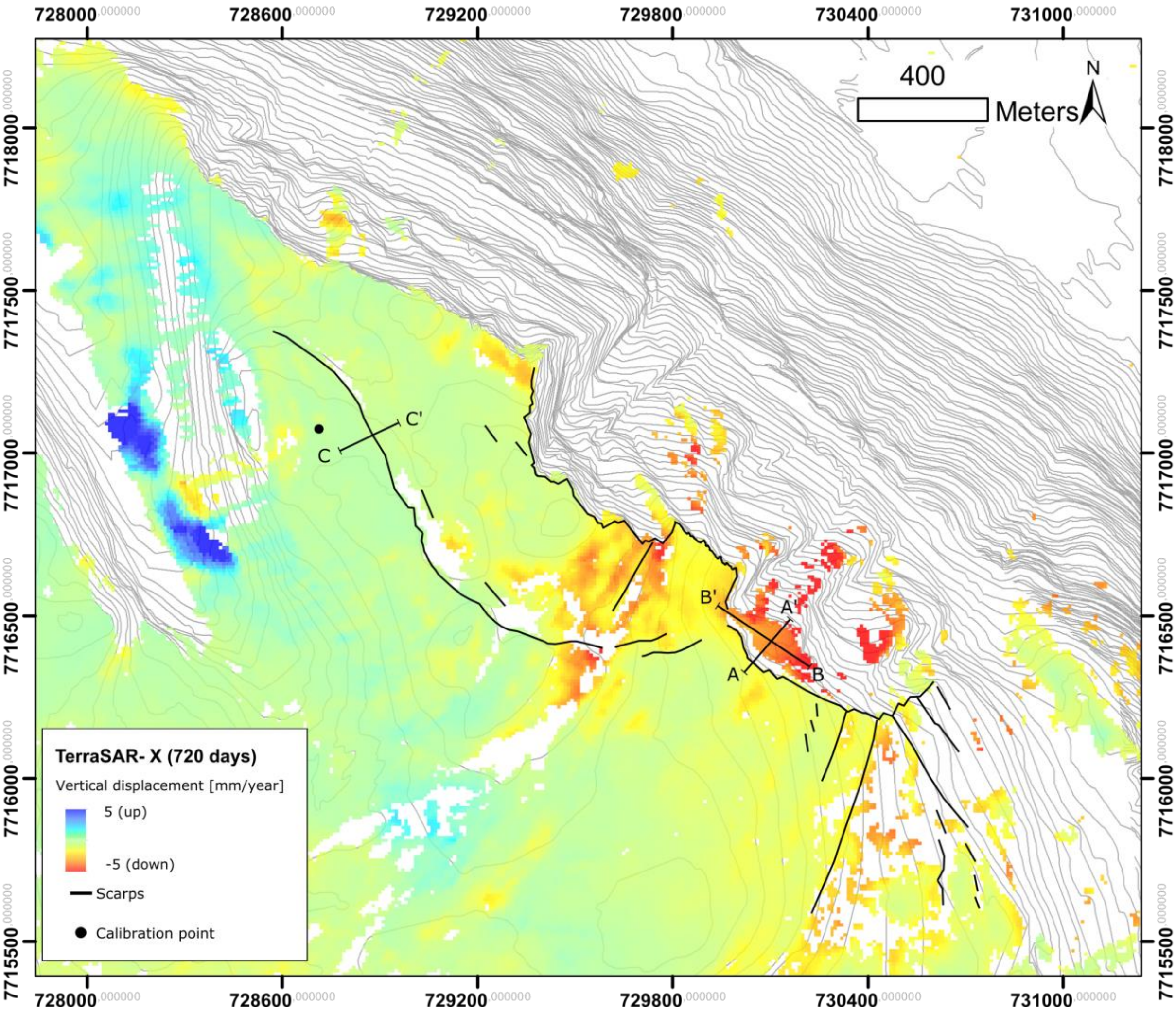

Fig. 43 Displacement based on TSX ascending data with a temporal baseline of maximum 720 days. Profiles AA', BB' and CC' are marked with solid lines.

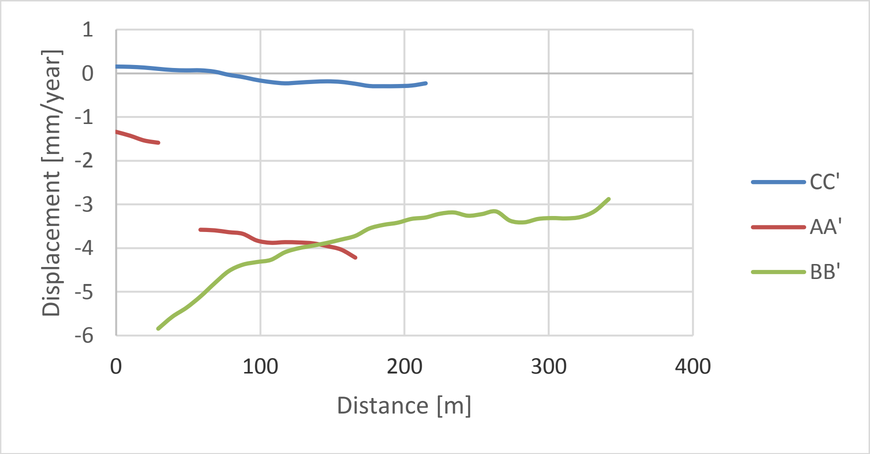

Fig. 44 Detailed profiles through TSX (720 days) data.

Results from TSX InSAR data, processed with a maximum threshold for temporal baseline of 720 days, are seen in Fig. 43, where red colored areas are displaced upwards and blue areas are displaced downwards. Displacement data extracted from profiles AA’, BB’ and CC’ is plotted in Fig. 44. Profile AA’ is slope parallel intersecting the back fracture scarp, profile BB’ is slope perpendicular intersecting the western bounding fracture scarp and profile CC’ is located at the plateau intersecting the curved scarp.

Profile AA’ intersects the back fracture scarp, which coincides with the lack of data in Fig. 44, and show subsidence of the unstable area. The displacement rate is increasing over the back fracture, from -1.5 mm/year behind the back fracture scarp and c. -4 mm/year in the unstable area. In profile BB’ the displacement rate is decreasing from c. -6mm/year at B to c. -4 – 3 mm/year at BB’, indicating the area to west of the cross-fracture scarp is subsiding. Profile CC’ shows variations in displacement rate over the curved scarp, where the northern side of the curved scarp is subsiding at a rate of c. 0.5 mm/year relative to the southern side of the curved scarp. The change in displacement rate in the plot coincides well with the mapped location of the curved scarp.

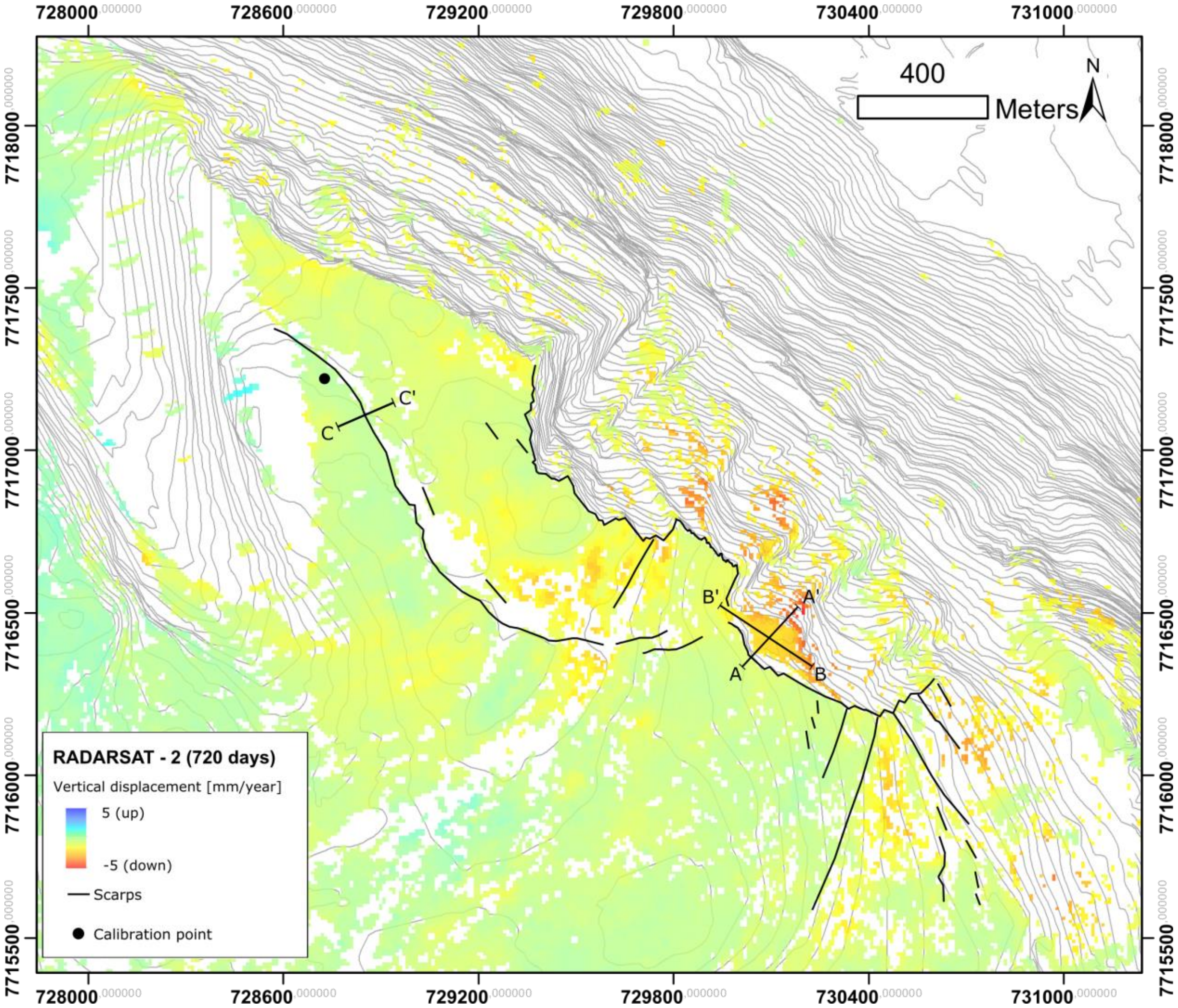

Fig. 45 Displacement based on RSAT-2 ascending data with a temporal baseline of maximum 720 days. Profiles AA', BB' and CC' are marked with solid lines.

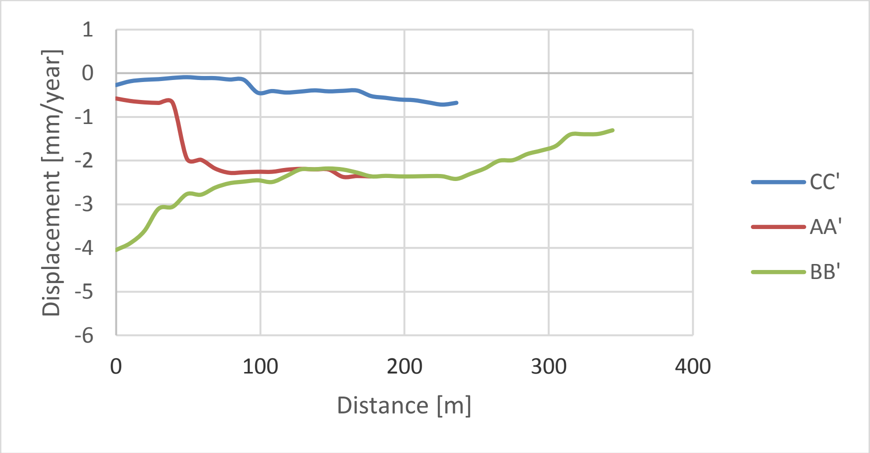

Fig. 46 Detailed profiles through RSAT-2 (720 days) data.

The results from RSAT-2, data processed with a temporal baseline of maximum 720 days, are seen in Fig. 45, with the associated displacement rates extracted from profiles AA', BB' and CC' plotted in Fig. 46. The overall trend for the data extracted from RSAT-2 is quite similar to TSX data. The displacement rates are 3 – 4 mm/year within the unstable area, seen in both AA’ and BB’ profiles, and a displacement of the northern side of the curved scarp of 0,5 mm/year relative to the southern side.

To focus on the small displacement detected over the curved scarp, RSAT-2 and TSX datasets were processed with a lower threshold for temporal baseline of 1460 days. The longer baseline causes ambiguous results in the unstable area due to decorrelation and phase wrapping and therefore only results on the plateau in relation to the curved scarp are analyzed.

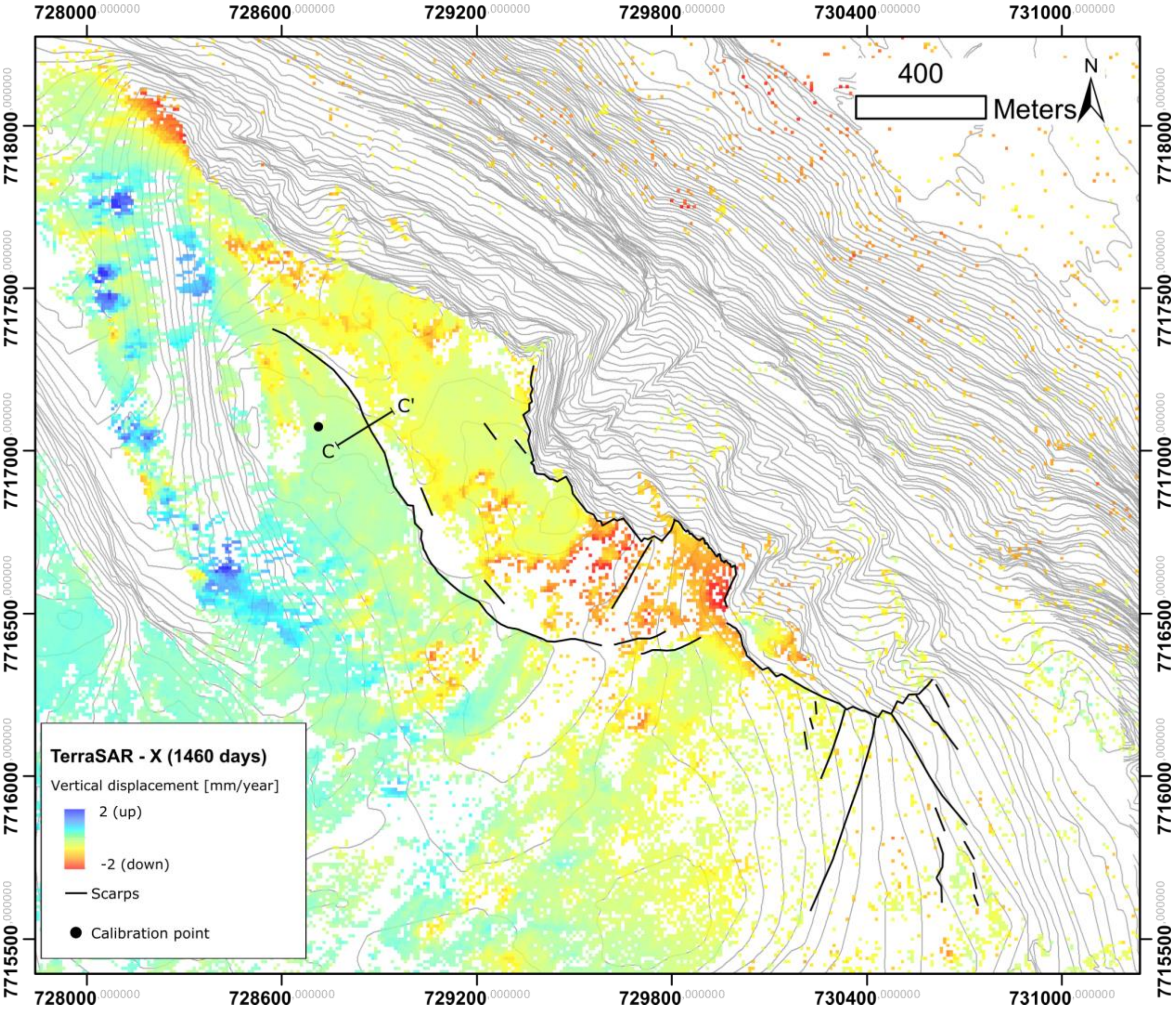

Fig. 47 Displacement based on TSX ascending data with a temporal baseline of minimum 1460 days. Profile CC’ is marked with solid lines.

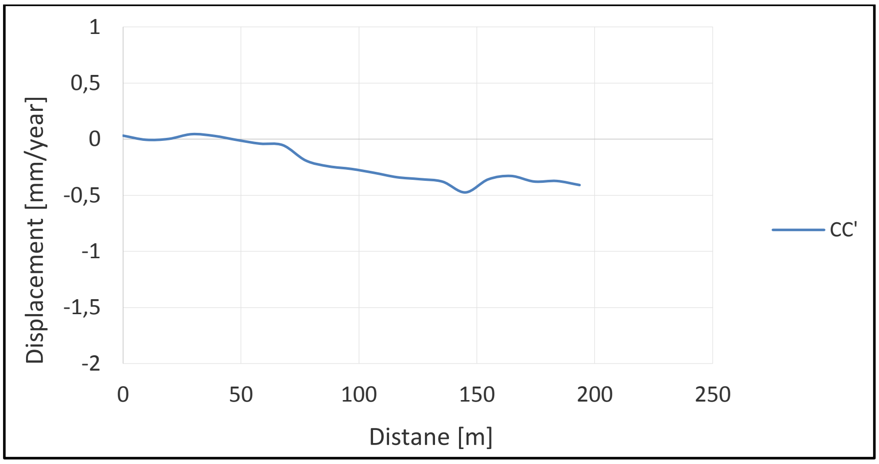

Fig. 48 Profile CC' through TSX (1460 days) data.

Results from processing TSX data with a minimum temporal baseline of 1460 days (Fig. 47) shows a small change in displacement over the curved scarp, seen as more yellow colors at the northern side of the scarp. Displacement values extracted from profile CC', plotted in Fig. 48, show a change in vertical displacement, from c. 0 mm/year at the southern side to c. -0,5 mm/year at the northern side that correlates well to the location of the scarp.

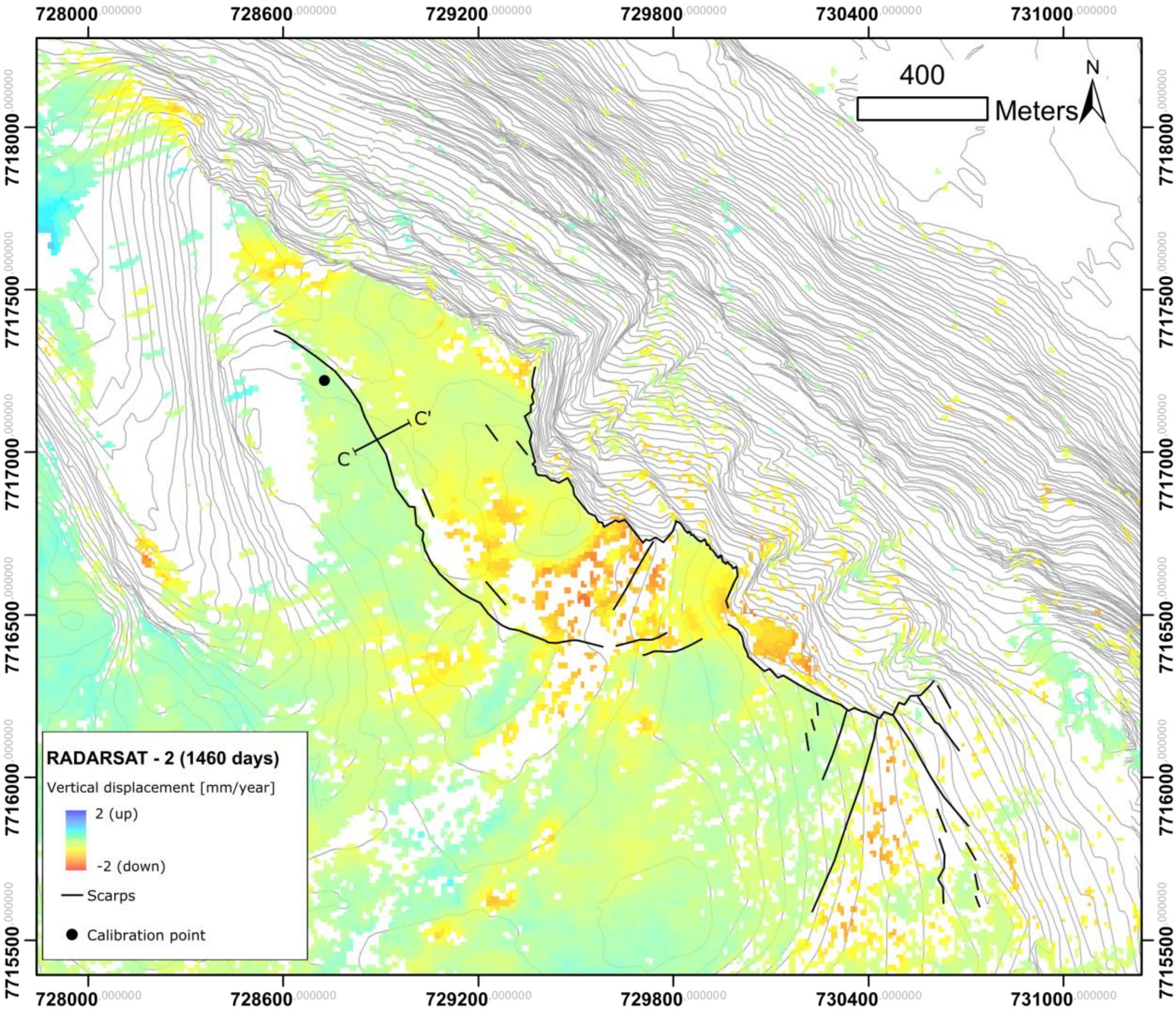

Fig. 49 Displacement based on RSAT-2 ascending data with a temporal baseline of minimum 1460 days. CC' are marked with solid lines.

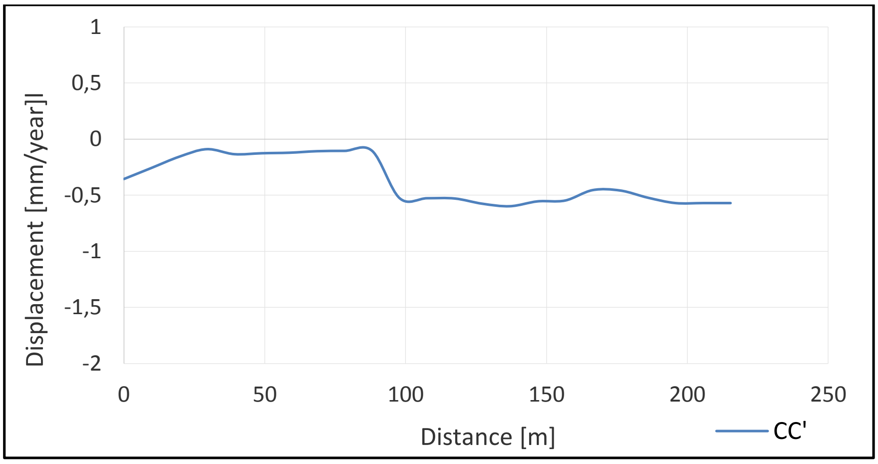

Fig. 50 Profile CC' through RSAT-2 (1460 days) data.

Results from processing RSAT-2 data with minimum temporal baseline of 1460 days are similar to TSX data with the same temporal baseline. The change in displacement of the northern side relative to the southern side of the scarp are visually in Fig. 49 and the extracted displacement values from profile CC' are plotted in Fig. 50. The estimated change in displacement rate of c. 0.5 mm/year, coincides with the location of the mapped scarp in both the map and the plot.

To further examine and support the small change of displacement rate, the mean displacement in areas of c. 15 000 m^2 at both sides of curved scarp, revealed an increased vertical displacement of 0.5 mm/year of the northern side relative to the southern side

3.7.1 Time series

In addition to the spatial distribution of ground displacement, the temporal evolution of displacement is assessed by SBAS processing of InSAR data. For each selected pixel, time series displayed as a displacement over time can be extracted.

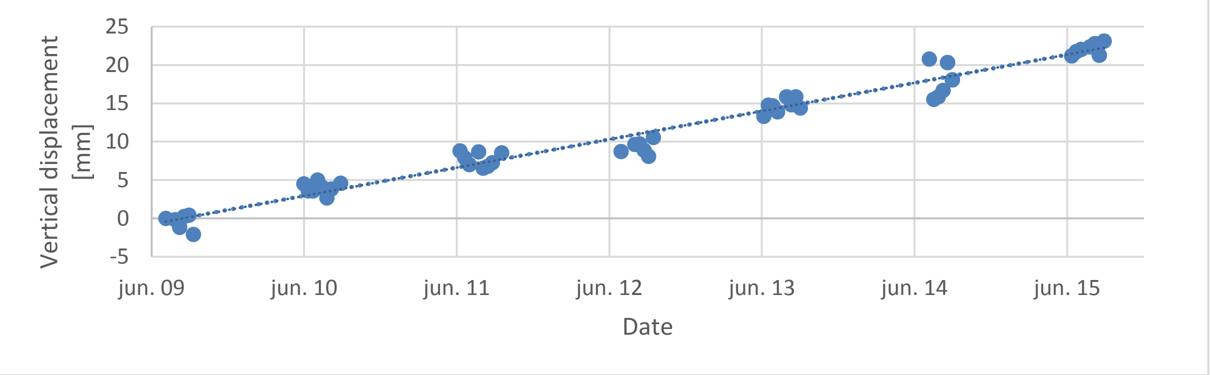

Fig. 51 Time series from 2009 through 2015 extracted from within the unstable area

TSX InSAR data was SBAS processed with a threshold of maximum 720 days for temporal baseline and time series from 2009 through 2015 was extracted from several points exhibiting high coherence in close proximity to GPS point KA-2 (Fig. 5) within the unstable area. The mean displacement values plotted over time in Fig. 45 show a constant rate of displacement away from the sensor.

4 Discussion

The chapter discusses how the bedrock in Oksfjellet, Caledonian ductile structures and post-Caledonian brittle structures, may have influenced on the origin of morphological features and displacements detected by InSAR. InSAR data and its relation to mapped geological features is discussed. The estimated displacement pattern two sensors (GB-InSAR/ satellite InSAR) are shortly compared to examine how they have contributed to the understanding of the detected displacement with different temporal and spatial scales. Different failure mechanisms are discussed based on analysis of the mapped brittle and ductile structures and their orientation, that are presented in stereonets. However, the different failure mechanisms involved, are not described in detail. Based on e.g., Agliardi et al., 2001, Braathen et al., 2004 and Wyllie & Mah, 2005, a classification of the unstable area is proposed. Lastly, different controlling factors, which may have initiated and driven the deformations is discussed. And whether the deformations are controlled by pre-existing regional brittle fractures and faults, are discussed. The discussion is based on the interpreted geological profiles (Fig. 52), one that is slope parallel and intersects the back fracture scarp (Fig. 53) and one parallel to the valley (Fig. 54), showing the geological structures in Oksfjellet.

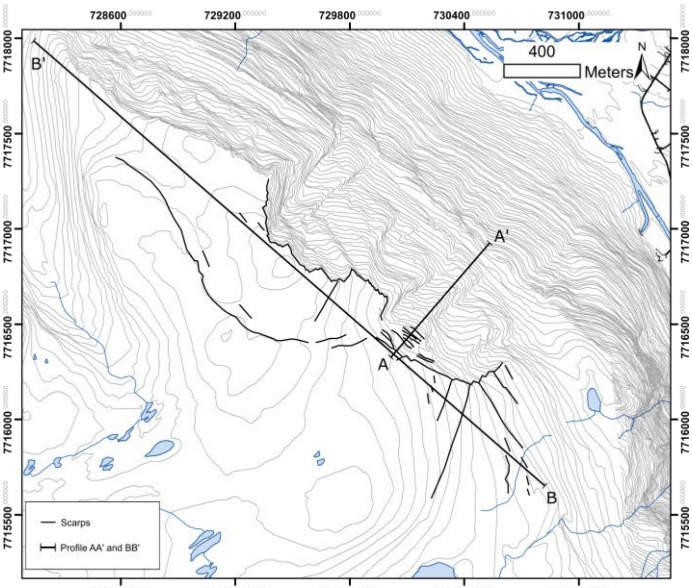

Fig. 52 Map showing the location of profiles discussed in this chapter.

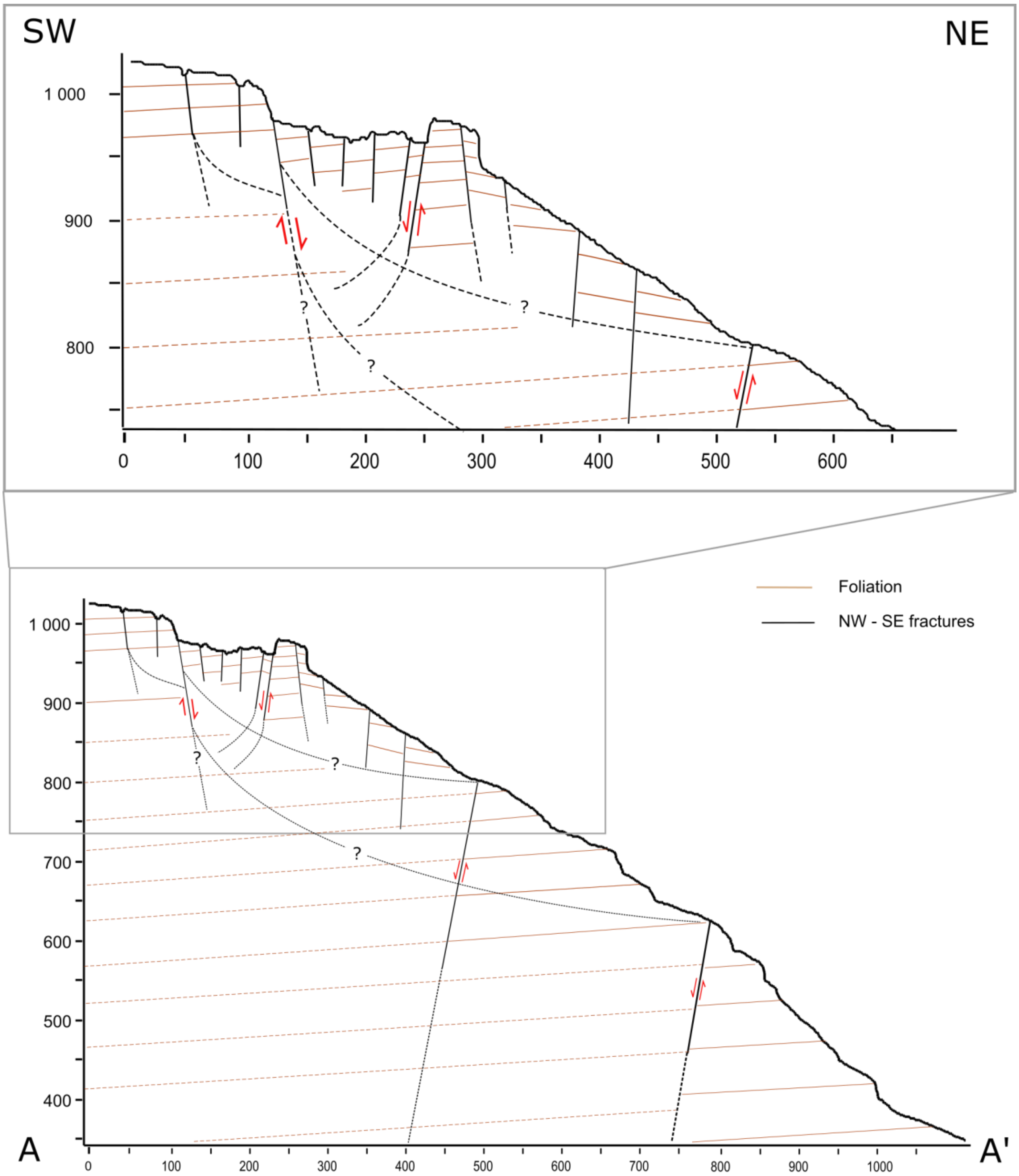

Fig. 53 Geological profile AA‘, intersecting the back fractures scarp. Note that this is a schematic profile, and many more NW-SE striking fractures were mapped in the field than those pictured.

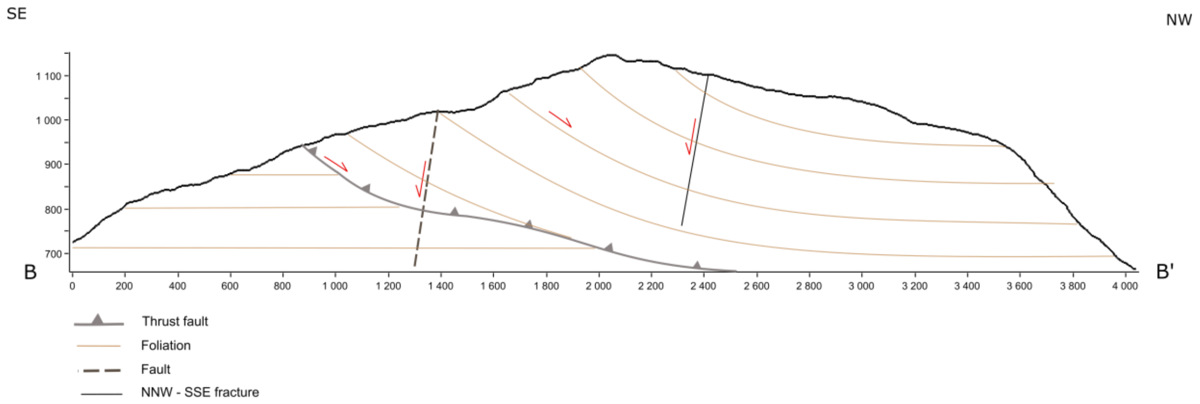

Fig. 54 Geological profile BB‘, parallel with the valley. The red arrows indicate movement in the unstable area.

4.1 Bedrock composition and geological structures

4.1.1 Caledonian ductile structures

This section discusses the origin of ductile Caledonian structures in Oksfjellet, and its locations and orientations that might be important for the understanding of the unstable area.

These ductile structures are all superimposed in primary bedding and lithological contacts (S0) in metasedimentary rocks. For example, the dominant ductile foliation (S1) of bed rocks is mostly parallel to bedding. This metamorphic foliation (S1) displays intrafolial folds (F1) and foliation-parallel thrust zones (S1) suggesting it formed by concentration and shearing during the Caledonian nappe emplacement. Up-right macroscale folds (F2) later deformed this foliation (S1). The oldest folds (F1) were formed during an early deformation event that locally folded the lithological contacts (S0) and also formed the foliation (S1). Re-folding of the main foliation (S1) is a result of the emplacement of younger strata on top of older strata in an imbricated thrust stack, seen as large scale synformal and monocline -like folds.

The lithological contacts between mica schists and rusty biotite schists are foliation parallel and sub horizontal in the northwestern part of Oksfjellet. In the unstable area, the location of the exposed foliation surfaces (Fig. 16) coincides with the contact between a Caledonian thrust ramp emplacing hanging wall strata on top of more flat-lying strata in the footwall in the easternmost parts of Oksfjellet (Fig. 54). These foliation surfaces, parallel to the lithological contact, dip 25 – 30° to northwest, perpendicular to the slope (Fig. 54), and may therefore be favorable oriented relative to the cross-fractures and thus may be reactivated to form a potential failure plane. Even though the lithological contrast between the two lithologies is considered small, the contact might have influenced the development of the failure. Such an observation is consistent with observation from other localities (Saintot et al., 2011) indicating that lithological contacts may be an important controlling factor for unstable rock masses.

The rusty mica schists associated with the indicated shear zone/thrust in Fig. 54, may indicate decomposition due to weathering by oxidation, a feature that weakens the rock. The weakened rock strength may have contributed to the location and extent failure at Oksfjellet. Pre-existing ductile fault zones are documented to conduit fluid flow, affecting the composition of fault rocks that influences failure due to chemical altering that leads to weakening of the rocks (Goddard & Evans 1995).

The bedrock in Oksfjellet comprises a well-developed foliation, parallel to the above mentioned lithological contacts (Fig. 53and Fig. 54). The steep dip (25 – 30°) of the foliation associated with the unstable area (Fig. 54) might have been a controlling factor for the observed failure at Oksfjellet, as well-foliated rocks are well documented by e.g., Braathen et al., 2004, Blikra et al., 2006, Henderson & Saintot 2011 and Saintot et al., 2011, to influence rock slope failures, as foliation may form potential reactivation planes

The geometry of the exposed foliation surfaces (Fig. 16) is largely defined by the large-scale monocline- like and upright fold described in section 3.2.2 and shown in Fig. 54. Since the foliation surfaces are dipping c. 30° to the NNW, perpendicular to the slope (Fig. 54) and may be favorably oriented relative to the cross-fractures, the increased dip in the fold limb might increase the likelihood of reactivation of weak zones, allowing for sliding along the fold limb to the NNW. A correlation between the occurrence of ductile folding and decreased slope stability is proposed by Saintot et al., 2011, due to shearing of foliation surfaces. Also, the exposed foliation surfaces are located at the contact between folded and unfolded units, where the rheology contrast between the units may guide the development of failure surfaces, supported by Saintot et al., 2011.

The dip of the foliation (S1) in the unstable area and close to where the eastern delimiting fracture is located, is between 25 – 30° to the NW (Fig. 54). The dip angle is within the friction angle range, 20 – 27° for planar discontinuities of mica schists (Barton, 1973), indicating that the foliation (S1) surfaces are favorable for a slope-perpendicular reactivation.

Exposed foliation surfaces, dipping c. 35° to the NW in the western area (Fig. 28), are comparable to similarly oriented foliation surfaces in the unstable area (Fig. 25). It is suggested that ravines in the west might originate from an earlier failure resembling the present failure farther east.

4.1.2 Post-Caledonian brittle structures

The following discussion is based on descriptions in section 3.3, and focuses on how brittle structures may have controlled and delimited the extent of failure and internal deformation of the unstable area. The bedrock in Oksfjellet and its surrounding area is truncated by brittle structures, such as faults and fractures, which intersects ductile structures, and are interpreted to have formed after the Caledonian orogeny, most likely during deformation in Mesozoic and Cenozoic (Indrevær et al., 2013). The mapped area shows a dominance of fractures striking NW-SE to NNW-SSE and steeply dipping towards SW and NW, and fractures striking NNE-SSW with steep dips variable to the NNW and SSE. These fractures are also documented to be present in intact bedrock and in the bounding structures of the unstable area, indicating that pre-existing fractures may have controlled the extent of the deformations.

4.1.2.1 Back fracture

The back scarp is trending WNW-ESE and is parallel to the slope of Oksfjellet (Fig. 21). In small scale, the back scarp defines a zigzag geometry made up of fractures striking both NW-SE and NE-SW with overall steep dip. These fractures are documented in intact bedrock as well, indicating that the back of the unstable area is defined by pre-existing fractures that have been reactivated by e.g., down-faulting and widening/opening in the unstable area. Fractures located behind the back scarp (Fig. 19 and Fig. 53) are striking equal to the ones defining the back scarp, supporting that they, and the main back scarp of the unstable area, are affected by gravitational subsidence with a downslope movement direction, that have resulted from opening of tensile fractures due to the development of the back fracture. Alternatively, they may be a result of new fractures propagating inward from the unstable area, due to movement along a sliding surface that intersects both ductile and brittle structures in the unstable area at depth. Slope-parallel opening of fractures may be favorable for the development of a deep-seated rock slope failure, as well as smaller portions of the bed rock such as toppling.

The stepped geometry of the WNW-ESE striking scarp formed by alternations of NW-SE and NE-SW striking steeply dipping fractures, in the western part of Oksfjellet is suggested to have formed due to the same above mentioned mechanisms and may be of gravitational origin due to an earlier failure event.

Parallel and antithetic to the back fracture scarp, a WNW-ESE fracture dipping c. 70° to the SE (Fig. 53) can be traced from the eastern boundary of the unstable area to the western bounding fracture scarp in the western area (Fig. 23). Downward rotation of the foliation in the area below the front block and the unstable area is most likely a result of, downslope movement and overturning of blocks due to NNE-NE directed expansion of the NW-SE striking sub vertical fractures. The lowermost parts of Oksfjellet show fewer fractures and no evidence of bulging or rotation of the foliation, indicating that the bedrock schists have not been deformed, and thus support restraining of this fracture set and sliding along a possible deep detachment or thrust boundary (further described in section 4.4.2).

4.1.2.2 Cross-fractures

The northwestern boundary of the unstable area is defined by a NNE-SSW striking fracture scarp dipping steeply to the SE (Fig. 26 and Fig. 54). This orientation and alignment of the scarp indicates that the extent of the unstable area to the northwest is controlled by re-activation of similar, pre-existing NNE-SSW striking fractures.

Contrary to the western bounding NNE-SSW striking fracture scarp (Fig. 54), cut by numerous NW-SE and NE-SW striking fractures in the unstable area, the western area is delimited by a persistent NNW striking sub vertical fracture to the ESE. In both areas, the development of the back fracture scarps is interpreted to have been controlled by the existence of these fractures and the eastern boundaries have been controlled by the location of the foliation surface mainly. Therefore, the persistent NNE-SSW striking fracture in the western area is suggested to have been formed by an earlier failure, similar to the present failure.

Overall, pre-existing brittle fractures might have been re-activated due to gravitational and extensional opening, related to deformation of the unstable area. Such observations are consistent with many other field studies, indicating that rock slope failures are linked to pre-existing structures (Braathen et al., 2004, Agliardi et al., 2009, Henderson & Saintot 2011, Saintot et al., 2011).

4.2 Relation between morphological elements and bedrock structures

4.2.1 Scarps

The unstable area displays a horst and graben-like structure (Gibbs, 1984), defined by the back fracture scarp and the antithetic fracture defining the frontal block to the SW (Fig. 53). The down to the NNE separation/movement across the structure is c. 40 m and the downthrow of the front block is approximately 15 m, caused by, most likely, movement on pre-existing extensional fractures combined with gravitational down-faulting. The area between the front block and the back fracture scarp is segmented by three, oblique to the back fracture, NW-SE striking and left-stepping counterscarps that resemble relay ramps (Gibbs, 1984), which may indicate that it is an accommodation zone (Larsen, 1988, Colletta et al., 1988). Such structures are commonly found in extensional regimes, connecting the hanging wall and footwall blocks by obliquely or en échelon arranged symmetrical structures (Larsen, 1988). The suggested relay ramps are connected to the intersection between the back fracture scarp and the western delimiting cross-fracture scarp (Fig. 33), resulting in only partial segmentation of the unstable area at the western boundary, whereas the back southern and eastern delimitation completely parts the unstable area from intact bedrock schists.

The curved scarp in the inner parts of Oksfjellet, defined by NNE-SSW and NW-SE sub vertical fractures, shows a horizontal displacement of 0,5 m and vertical displacement of 4 – 5 m at most, indicating that the northwestern part of Oksfjellet has been down-faulted (Fig. 33) to the NNE. Inward rotation of the foliation (Fig. 33) is interpreted to be due to expansion and movement perpendicular to the fractures. Alternatively, the movement might have occurred along a deep-seated detachment or sliding surface, similar to the interpretation in Fig. 54.

Other scarps, located outside the unstable area, strike mainly NNE-SSW and NW-SE (Fig. 29), parallel to the strike of the foliation or sub-parallel to the back fracture scarp. The foliation-parallel scarps may have formed along strike of pre-existing post-Caledonian ductile thrusts and further disintegrated by surficial frost weathering. NW-SE striking scarps are most likely related to the back scarp and the antithetic upslope dipping fractures (Fig. 54). Alternatively, their origin may relate to reactivation of foliation surfaces aling the shear zone/thrust. Both sets of scarps striking NNE-SSW and NW-SE display increasing vertical throw towards the unstable area, that may correlate to the increased density of fractures closer to the deformed area.

4.2.2 Colluvium

The colluvial fans (Fig. 30), which define the slope beneath Oksfjellet, display a complex pattern of confined channels, generations of lobate shaped paths and smoother areas with more scattered deposits, indicating formation by a combination of different slope processes, such as rock falls, debris flows and snow avalanches.

The high density of fractures in Oksfjellet results in easier fragmentation of the bedrock, that allows blocks to move independently. Rock falls are interpreted to impact and mobilize colluvial deposits (Hungr & Evans, 2004; Hsü,1975) causing debris flows and entrainment of material, seen as confined tracks which spread out to a more complex, lobate-shaped pattern as the slope angle decreases. The over-stepping appearance of the lobes indicates that there have been numerous debris flow events.

During winter, the plateau at Oksfjellet is a tremendous source area, where snow is being transported, distributed and accumulated. Due to the shady northwest face of Oksfjellet, snowflows are feasible slope process for large periods of time, from low density dry snow avalanches and cornice breakage in winter to water rich high density snow flows in spring. Dependent on the density, snowflow avalanches are capable of transporting varying amounts of rock debris that has accumulated on the slope due to rockfalls and related debris flows at Oksfjellet. In between these lobes, smoother areas with more scattered deposits are found, deposited by different snow flow processes, supported by Blikra & Nemec 1998, that suggests that snowflows leave behind scattered deposits with no distinct boundaries between events.

The colluvial fans display greater widths and run-out lengths below the unstable area, indicating more frequent slope processes due to the high density of fractures and rock fragmentation. Holmen, on the other hand display the largest isolated boulders, which are interpreted to be deposited by rock fall events. The steepness, the angular and immature deposits as well as the downslope coarsening of the colluvial fans are consistent with rock falls being the dominant process at Oksfjellet. Larger blocks and boulders that move faster and outpaces smaller ones, may have resulted in an overall downslope increase of surface roughness of the colluvial fans.

4.3 Relation between displacement data, bedrock structures and morphological elements

The section discusses the relation between displacement data, bedrock structures and morphological structures. Displacement data from the different sensors, GB-InSAR and InSAR, are compared in terms of spatial and temporal pattern.

4.3.1 dGPS

dGPS data provided by NGU shows that KA-2 is the only point showing any significant movement. KA-2 is displaced at a rate of 3 – 4 mm/year with a horizontal movement direction to the northeast (Table 3). The front block is highly fractured and one can assume that the movement pattern detected on the block is equally segmented. Therefore, the measured movement of point KA-2 is difficult to interpret and relate to bedrock structures observed in the field.

4.3.2 GB-InSAR

Analysis of GB-InSAR data show a complex displacement pattern, where different isolated areas are displaced at different rates, varying from less than 1 mm/day to 3,5 mm/day (Table 4). The fastest displacements are detected in the tongue shaped rock deposits below the unstable area (Fig. 34, area A), that during all campaigns have shown steady rates of assumed downslope displacement. The deposits are moving as a single body, and the high and steady velocity throughout the season indicates that the deposits might be ice-rich. Assumed constant accumulation of rock debris derived by disintegration of bedrock schists, and location at high altitude in a shadowy NNE faced slope, supports that the debris could be ice-rich and termed a rock glacier Haeberli (1983).

During monitoring campaigns in June 2014 and 2015, area B (Fig. 34) is displaced 3 – 4 mm during a period of 3 – 4 days. The leap in displacement could correspond to ice and snow melting, due to increased temperatures and precipitation during the preceding days of both events. Water could possibly have infiltrated and frozen in the fracture system causing local frost weathering. Alternatively, and consistent with the unstable rock slope in Nordnesfjellet, studied by Blikra & Christiansen (2013) the deformation of large unstable areas might be a result of variations in ice temperatures and water infiltration, which controls and might reduce the shear strength along deeper detachment surfaces.

The lower limit of the detected displacements seen in Fig. 38 and Fig. 42, might coincide with the back fracture scarp parallel antithetic fractures observed in the field (Fig. 53).

4.3.3 Satellite InSAR

Displacements detected by InSAR correlates well to the mapped bedrock structures. Both datasets, TSX and RSAT-2 with a maximum temporal baseline of 720 days, reveal a displacement pattern showing distinct subsidence of an area well-defined by mapped geological structures (Fig. 43 and Fig. 45). The subsiding area is bounded by the back fracture scarp (section 3.3.1) and cross-fracture scarps (section 3.3.2).

Profiles AA’, BB’ and CC’ (Fig. 44 and Fig. 46) show a similar trend but with varying magnitude of displacement rates, indicating that a comparison of the relative displacement values is valid. Profiles AA’, parallel to the slope and intersecting the back scarp, both show maximum displacement rates in the middle of the unstable area, that could correspond to increased vertical displacement associated with the graben structure. This is also documented in the slope perpendicular profiles BB’, that intersects the western cross-fracture scarp, where the magnitude of displacement rates in the middle of the block are equal to those in profile AA’. Profiles BB’, which are parallel to the NE-SW striking foliation that dips c. 30° to the northwest, show a decrease in displacement rates towards the cross-fracture scarp. The cross- fracture scarp may be functioning as a restricting structure, with the effect of decreasing the rates of displacement close to the scarp. Profiles BB’ show the greatest displacement rates at B’, which corresponds to area C in Fig. 34. The high displacement rates in this area coincide well with displacements detected by GB-InSAR during all campaigns. Profile CC’, for all data sets (TSX (720 days), RSAT-2 (720 days), TSX (1460 days), RSAT-2 (1460 days)), intersects the curved scarp (section 3.4.1) and show a consistent increase in displacement over the profiles (Fig. 44, Fig. 46, Fig. 48 and Fig. 50). Surface creep is thought to not produce the consistent change in displacement rate observed at the northern side of the curved scarp, and the scarp is interpreted to be a normal fault, where the detected displacement documents subsidence of the hanging-wall. InSAR- data appear to document active normal (down-) faulting. Osmundsen et al., 2010, interpreted the Lyngen peninsula as bounded by tectonic active faults. Indications of other active faults in the area might support the detected displacements along the scarp.

The curved fault coincides with the western bounding cross-fracture scarp in the unstable area, which is defined by alternating NW-SE and NE-SW striking sub vertical fractures. The cross-fracture scarp is therefore interpreted to have formed as a result of reactivation of pre-existing fractures due to a combination of active normal faulting detected over the curved scarp and down-faulting of the unstable area. The high fracture density and related disintegration might have created space, allowing for sliding along the foliation planes to the NW. The relation between faults, increased fracture density, poor rock stability and increased fluid flow are well documented by e.g., (Hoek & Bray 1981, Blindheim & Øvstedal 2002). Time series extracted from the front block show a constant rate of displacement of the front block in the unstable area. The displacements detected within each season are affected by noise, but the overall trend shows consistent downward displacement of the northern side of the scarp.

It can be concluded that the detected displacement patterns show a clear relationship between mapped geological structures. Displacements at a magnitude of less than 1 mm/year up to several mm/year coincided with the present geological process in Oksfjellet. It should be noted that 1 mm/year is close to the lower detection limit for long time series, but due to the consistent documentation by several InSAR datasets, the displacements are thought to reflect a real geological process.

4.3.4 Relation between GB-InSAR and InSAR

In order to compare GB-InSAR and InSAR results, the data sets were made similar in terms of line-of-sight and were projected into the vertical plane. The real displacement of the unstable area is assumed to be moving in a downslope direction, on average c. 30° from the vertical. If the displacement is directed purely downslope, the vertical displacement might be underestimated due to the differences between the real displacements and the vertical direction. The chosen datasets for comparison are TSX (720 days) (Fig. 43) and GB-InSAR data acquired from 22.06 – 26.06.2015 (Fig. 42), which both presumably reveal displacement of the unstable area. Few areas are illuminated by both sensors, as GB-InSAR data covers the lower parts of the NNE faced slope and the front of the unstable area, and satellite data covers the top and upper part of the unstable area (Fig. 55 and Fig. 56). The spatial pattern of both sensors combined, correlates well to the mapped geological structures, such as the bounding scarps of the unstable area and the graben, covered by satellite InSAR data and back fracture scarp parallel antithetic fractures and debris covered by GB-InSAR. The antithetic fractures (Fig. 23) coincides with the lowermost limit of displacements detected by GB-InSAR (Fig. 38 and Fig. 56). Considering of displacement rate, the sensors reveal a different pattern, where GB-InSAR results focus on displacement rates in terms of mm/day and satellite InSAR data are processed in order to reveal displacement at a scale of mm/year. Hence, GB-InSAR identifies faster slope processes, whereas satellite InSAR reveals slower displacements. Satellite InSAR reveal the fastest displacements in the middle of the unstable area (Fig. 44 and Fig. 46), that might correspond to increased vertical displacement in the interpreted graben structure. A similar pattern is observed in GB-InSAR data, were the fastest displacements are detected in the uppermost slope (Fig. 56).

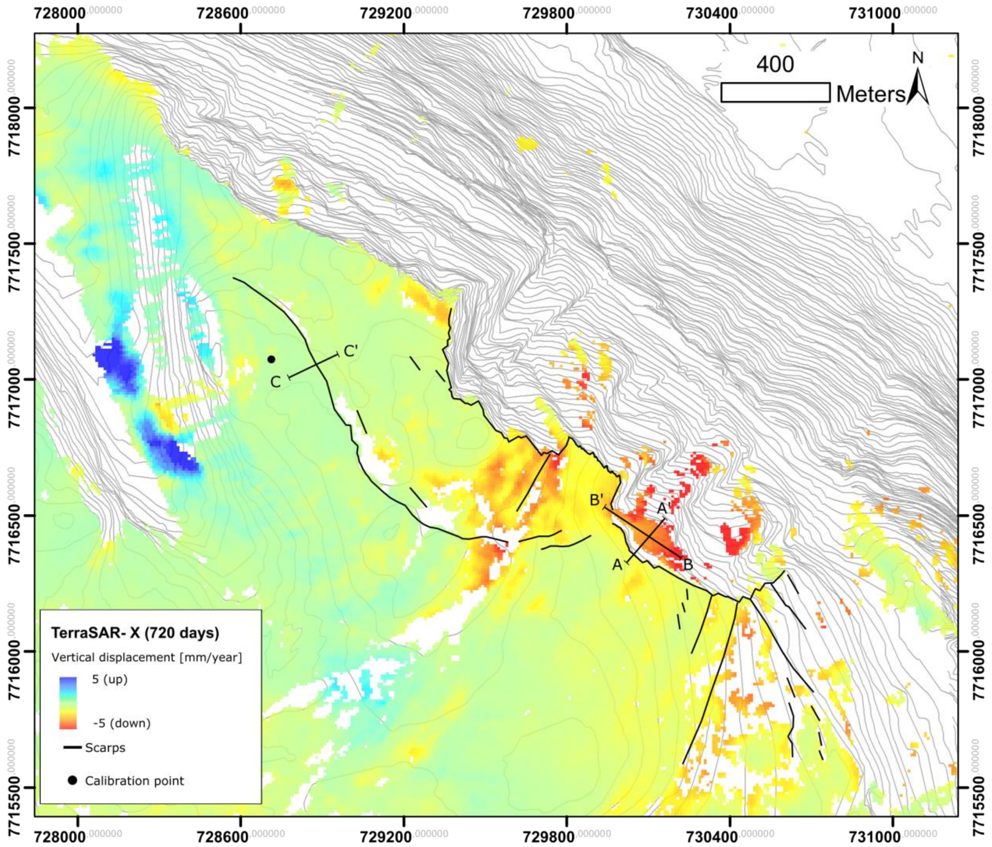

Fig. 55 Vertical displacement detected by TSX (720 days)

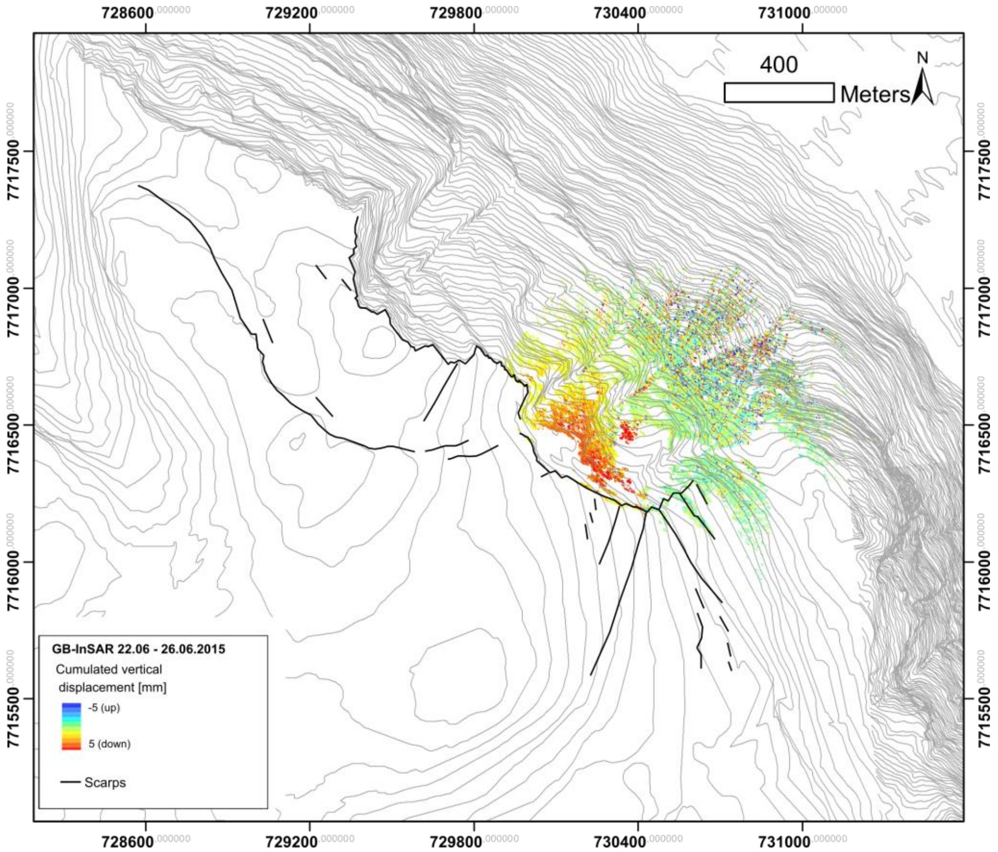

Fig. 56 Cumulated vertical displacement detected between 22.06 – 26.06.2015

4.4 Failure mechanisms and classification

Based on the documented ductile Caledonian structures, brittle post-Caledonian structures and morphological elements in the study area at Oksfjellet, different failure mechanisms for the unstable area are discussed according to Hoek & Bray 1981 and Wyllie & Mah 2005. Based on the structural geology, deformation characteristics, involved volume, a classification of the unstable area will be proposed, based on Agliardi et al., 2001, Braathen et al., 2004 and Agliardi et al., 2012.

4.4.1 Kinematic data

Structural data from presumed intact bedrock surrounding the unstable area, and from the front block within the unstable area (Fig. 57), was analyzed in order to evaluate the different failure mechanisms that might have influenced failure, based on stereographical kinematic analysis. The analysis considers the strike and dip of fractures relative to the slope and assesses the movement direction along fractures by differentiating between simple modes of failure, toppling, plane- and wedge failure (Hoek & Bray 1981, Wyllie & Mah 2005). These failures are associated with different geological structures and their typical pole plots demonstrate whether the theoretical and geometrical conditions for failure are met.

A restriction of the dip direction of the fractures away from the slope is set to 30° for toppling and plane failures, and the frictional angle, which is the typical frictional angle of mica schists, corresponds to 20 – 27° (Wyllie & Mah 2005).

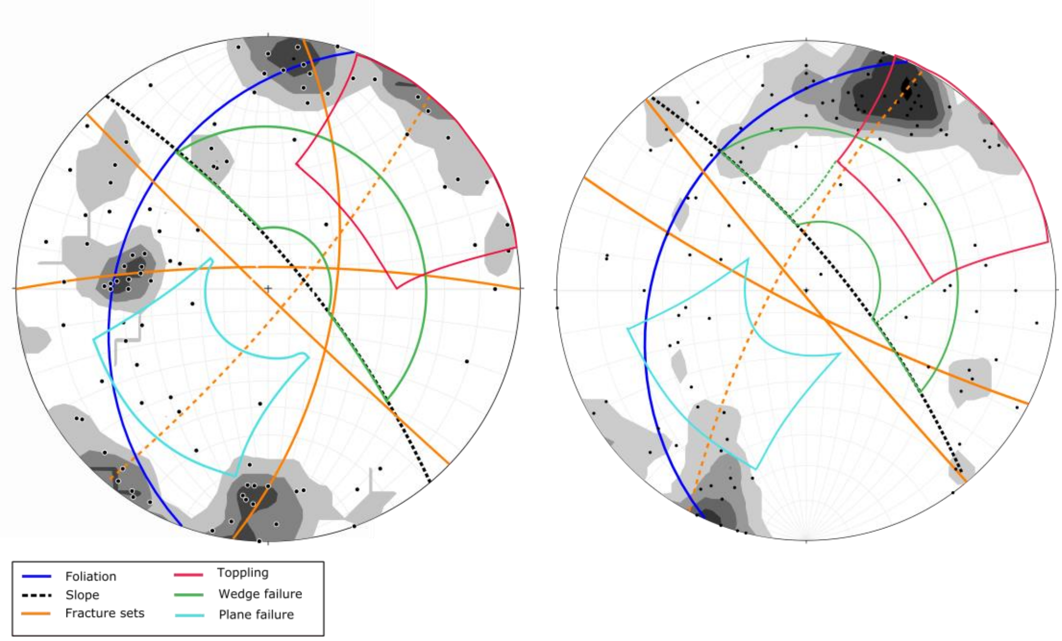

Fig. 57 Kinematic analysis of the fractures in intact bedrock (left) and in the deformed area (right) in Oksfjellet. Dashed yellow great circle indicate a less prominent fracture set.

Poles of fractures in intact bedrock surrounding the main unstable in Fig. 57 show that pre-existing and subvertical NE-SW striking fractures open to the SE or NW, making toppling a theoretical feasible failure mechanism along these fractures. Blocks are defined by variations of the NW-SE, N-S and E-W striking subvertical fractures, making them comparable to block toppling, that is bounded downward by the foliation described by Goodman & Bray (1976). According to the stereoplots, sliding is feasible along the foliation surface (c. 30°), indicating that a combination of block toppling and plane failure is possible.

The great circles of N-S, NE-SW and E-W fractures are within the field of wedge failure (Fig. 57, left), making wedge-failure a possible failure mechanism along these fractures. The different variations of fracture sets will possibly result in different wedge geometries.

The front block is truncated by NW-SE and WNW-ESE striking and subordinate NNE-SSW subvertical dipping fractures (Fig. 57 (right)). Field observations supports that the main failure mechanism along NNE-SSW fractures is possibly block toppling.

However, the kinematic analysis does only consider whether the geometrical conditions along each fracture set are met in order for failure to happen. The method does not consider shear strength of rocks determined by e.g., lithology, fracture persistence and fracture density (Stead & Wolter 2015).

4.4.2 Development of detachment

The section discusses the different indicators of movement along a potential deep-seated sliding surface and suggests a potential total failure mechanisms of the unstable area.

The graben structure in Oksfjellet (Fig. 53) shows a horizontal displacement of c. 40 m and down-faulting of c. 15 m, supporting a gravitational origin of the structure. A presumed listric back fracture and a slight inward rotation of the foliation in the graben structure, to a more stable position closer to the back scarp, may indicate movement along a deep detachment. These observations are consistent with other localities (Braathen et al., 2004, Ambrosi & Crosta 2006), indicating that movement might be guided by deep-seated detachments.

InSAR data shows consistent and slow displacement of the entire unstable area at a rate of 3 – 4 mm/year (Fig. 51), and little segmentation of the displacement that indicates that the unstable area behaves as continua. The rock mass strength and response to deformation is then determined by both intact rock properties and the individual fractures (Hoek et al., 2002), due to the high density of fractures, which also indicates that the displacement might be related to a deep-seated detachment or sliding surface.

A common, deep-seated sliding surface may exist in the subsurface slope at Oksfjellet, along (1) the moderately dipping foliation along the thrust ramp, or (2) along the intersection between the thrust/foliation and the main cross-fracture sets, the latter producing a wedge failure (Wyllie & Mah 2005). The overall controlling features for this kind of wedge failure may be interaction of the main foliation/shear zone/thrust and the NE-SW and NW-SE striking sub-vertical fractures. The total movement vector, down to the NNE, is visualized in Fig. 58. Interaction of these elements that lead to different stages of failure from the west to the east can be inferred. In this scenario, the western area is considered the most evolved, and the curved scarp the least evolved. Thus, the western area is proposed to have failed at an earlier stage, as suggested in section 4.1.1 and 4.1.2.

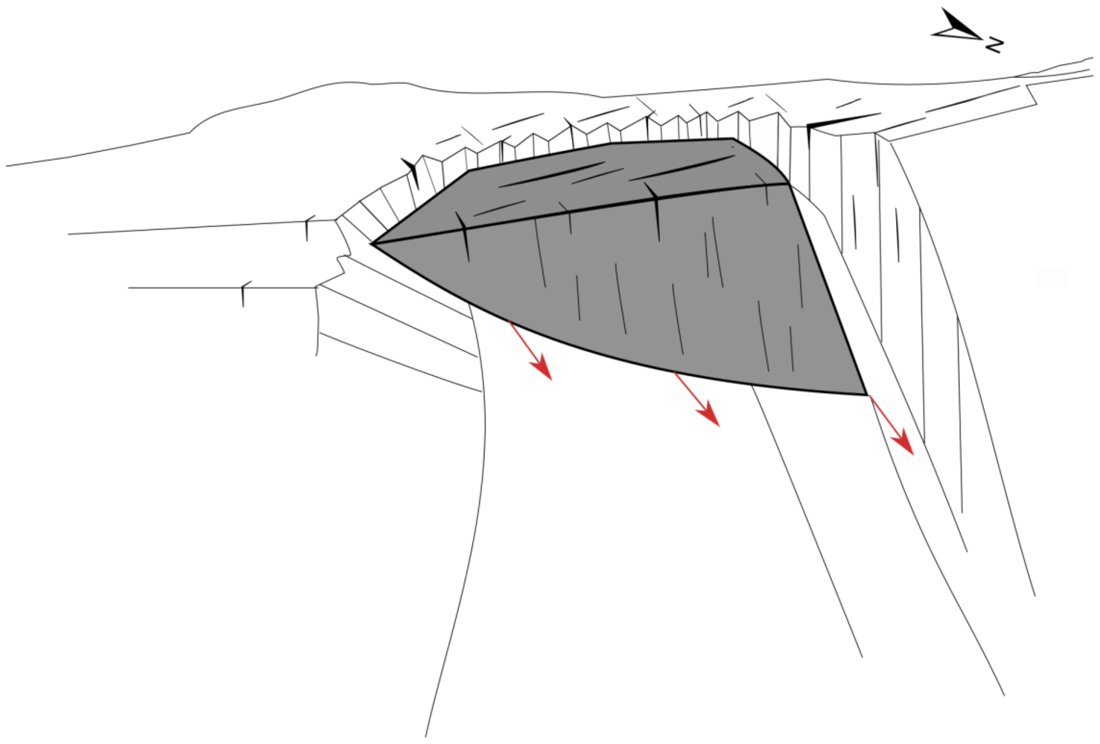

Fig. 58 Schematic drawing of the suggested failure mechanism at Oksfjellet. The suggested total movement vector, down to the NNE, is illustrated by red arrows.

4.4.3 Classification

The intricate interaction of failure types and mapped deformations in Oksfjellet is characteristic for complex fields (Braathen et al., 2004). The volume of roughly c. 35 Mm^3, which is a worst case estimation based on the geological profiles (Fig. 53 and Fig. 54), is consistent with the volumes of complex fields that commonly exceeds 20 Mm^3 (Braathen et al., 2004). Based on the large volume, the chaotic surface morphology, graben structures, segmented fault blocks and complex deformation mechanisms, the unstable rock slope at Oksfjellet is classified as a complex field.

Several of the deformational features in Oksfjellet may be of gravitational origin and often they seem to coincide with inherited tectonic lineaments. These are the most common indicators of a deep-seated gravitational slope deformation (DSGSD) (Agliardi et al., 2012). Hence, Oksfjellet can possibly be compared to DSGSDs due to e.g., the graben structure. Indications of an earlier failure event in the western part of Oksfjellet (see section 4.1.1 and 4.1.2), is supported by several studies regarding DSGSDs in the Alps, where some DSGSDs are interpreted to consist of two or more clustered unstable rock slopes sharing parts of the same boundary (Ambrosi & Crosta 2006), while other DSGSDs includes failures of different ages, that could span over several glacial cycles (Agliardi et al., 2012). The presence of a Caledonian thrust ramp exactly beneath the unstable area at Oksfjellet, confirms that pre-existing tectonic features (i.e. ductile fabrics) controlled and might have influenced on the localization of the unstable area. Similar interpretations were made by Ambrosi & Crosta 2006 and Agliardi et al., 2009, who related large DSGSDs to major pre-existing tectonic features in the Alps.

4.5 Controlling factors

The unstable rock slope at Oksfjellet is influenced by several internal and external factors, such as water, freezing and thawing, permafrost, glaciations and seismic activity, that may control the stability of the slope. Several of these factors have been mentioned when discussing the origin of the different features and deformations seen at Oksfjellet. This section will shortly summarize potential controlling factors.

4.5.1 Water and permafrost

No major rivers, creeks or lakes occur in Oksfjellet, indicating that precipitation and melt water from snow and ice during spring and summer, is the main source of the water infiltrating the fracture system. Effects that may relate to water are seen as seasonal changes in the displacement pattern detected by GB-InSAR. Both campaigns showed a leap in the movement of a large area over a few days in spring 2014 and 2015 (Fig. 42 and Fig. 38), and an overall trend of increased displacements in spring compared to displacements in autumn. This can be explained by deformation due to variations in ice temperature and water infiltration, which could reduce the shear strength and maybe control movement along deeper detachment surfaces. These factors are described by e.g., Braathen et al., 2004, who infers that water will increase the pore pressure, resulting in reduced effective normal stress and shear resistance of a potential slide surfaces. Water could also increase the driving forces by adding weight and an outward pressure to rock columns and/or function as a lubricant, which decreases frictional forces along slide surfaces or cause weathering, resulting in weakened bedrock (Goddard & Evans 1995). Increased water pressure due to snow melting and heavy rainfall may build up along the shear zone/thrust, resulting in local destabilization of the slope and further opening of pre-existing fractures, also indicated by e.g., Crosta & Agliardi 2003.

The displacement pattern described above is consistent with nearby localities (Blikra & Christiansen 2013) suggesting that there is a seasonal control of displacement rates, that might be related to permafrost. Findings of ice in several large fractures supports that the upper parts of Oksfjellet are most likely located within areas of altitudinal permafrost. A warmer climate, resulting in thawing of permafrost may increase the frequency of rock failures in the future (Gruber & Haeberli 2007).

4.5.2 Glacial processes and rebound

The topography in Oksfjellet and Kåfjorddalen are influenced by glacial activity, and glacial deposits are found in the valley (Corner 1980) (Fig. 30). Glacial erosion could have been a controlling factor for several large rock slope failures in Norway, due to steepening and increased susceptibility of weak layers to form. Release of tensile strain energy, which supported rock mass during glaciation, may have resulted in propagation of fractures and increased the likelihood of rock slope failures to take place (Braathen et al., 2004). Pre-existing fractures observed in Oksfjellet, might have formed or been re-activated due to ice deloading.

4.5.3 Seismic activity

Seismic activity possibly represents an additional factor controlling the deformations at Oksfjellet, since neotectonic activity has been documented, along Stouragurra fault in Finnmark and Nordmannvik fault in Troms, identified by (Dehls et al., 2000). 6,6 M is regarded as a minimum magnitude for earthquakes to trigger a rock slope failure (Keefer 1984), however, earthquakes of a magnitude larger than 5.5 M are rare in Norway (Dehls et al., 2000). Even though the NW-SE striking Nordmannvik fault is located in an area with a high density of unstable rock slopes (Corner, 1972), its influence on the stability of those slopes is uncertain.

4.6 Inheritance of regional brittle structures

The back fracture scarp and the cross-fracture scarp bounding the unstable area, the western area, as well as the curved fault is defined by alternations of NW-SE and NE-SW striking and steeply dipping fractures (Fig. 19).

Hence, brittle structures controlling the deformations at Oksfjellet might be related to pre-existing regional fault-fracture (lineament) patterns documented both onshore in the coastal areas of northern Norway and on the offshore rifted margin (see chapter 1.6.2, Fig. 3). These regional lineaments are dominated by NNE-SSW to NE-SW and NW-SE striking Mesozoic brittle faults and fractures (Bergh et al., 2007, Hansen & Bergh 2012, Indrevær et al., 2013).

4.7 Hazard evaluation

Movement detected by satellite InSAR show a homogeneous movement of the unstable area down to the NNE (Fig. 58), presumably along one or several deep-seated sliding surfaces (Fig. 53). The consequences of a worst-case scenario failure of Oksfjellet are great, crossing the valley, damming the river and affecting both private and public properties (Bunkholt et al., 2011).

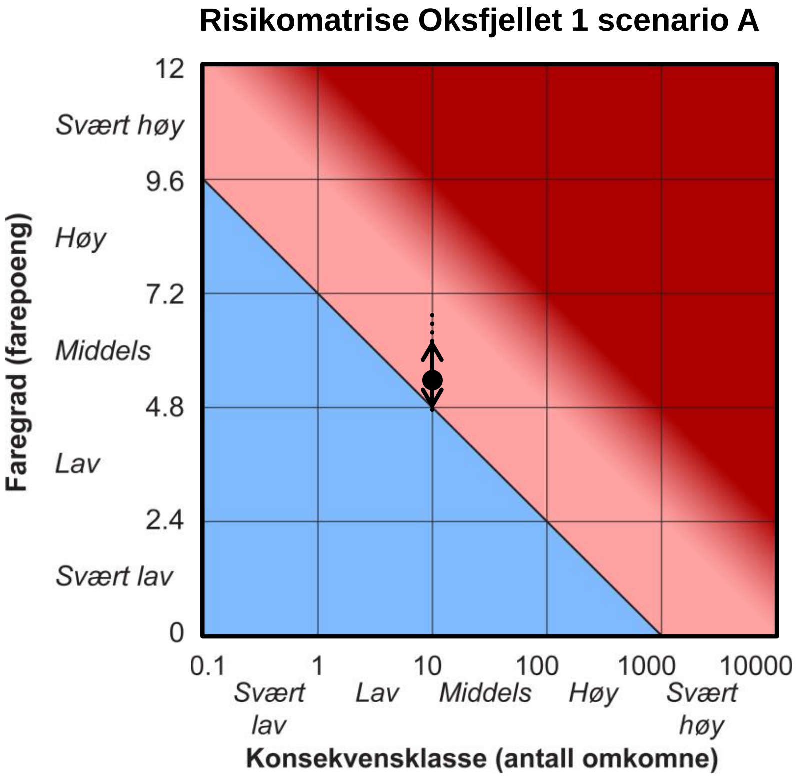

Fig. 59 Risk classification matrix for Oksfjellet. Blue: low risk. Pink: moderate risk. Dark red: high risk. The risk is presented as its mean value. The vertical arrows represent the 5% and 95% percentiles of the hazard score.

The classification system for hazard and risk posed by large unstable rock slopes in Norway is scenario-based, and focuses on the rate of displacement and the geological structures activated by sliding rock mass (Hermanns et al., 2013). The matrix combines a qualitative hazard score, based on a quantitative consequence score (loss of life). A simple estimation of 10 people in the potential run-out zone was made, however, by taking further consequences into account, one would assume a higher score. The hazard and risk evaluation resulted in a score of 5,4. For unstable rock slopes within a moderate risk class, periodic monitoring is suggested by Hermanns et al., 2013. However, fragmentation, and active disintegration of the area detected by GB-InSAR, indicates that the consequences of a failure may be smaller than the estimated worst-case scenario, since failure is more likely to occur in individual block or areas.

5 Summary and conclusions

The main goal of this thesis has been to interpret how brittle and ductile geological structures in the bedrock might have influenced on the evolution of morphological features, failures and displacement patterns in Oksfjellet. Further, satellite InSAR data have been analyzed and verified against field observations, and its contribution to the understanding of displacements at different temporal and spatial scales have been evaluated.

The Caledonian orogeny resulted in structures formed by ductile deformation, superimposed in primary bedding and lithological contacts. The dominant foliation is mostly parallel to bedding and display intrafolial and foliation-parallel thrust zones, indicating that it formed during Caledonian Nappe emplacement. Macroscale folds later deformed the main foliation as a result of emplacement of younger strata on top of older strata in an imbricated thrust stack.

In the unstable area at Oksfjellet, the location of exposed foliation surfaces, dipping 25 – 30° to the NW, coincides with the lithological contact between Caledonian thrust ramps and more flat-laying strata, and may thus be favorable oriented for reactivation forming a potential failure plane. The shear zone/thrust is associated with rusty mica schists, indicating that the decreased rock strength may have contributed to the failure. The main foliation is defined by large scale ductile folding, that may have resulted in decrease in slope stability due to shearing along foliation surfaces. The overall dip of the foliation surfaces in the unstable area is within the frictional angle range for mica schists and therefore favorable for reactivation.

The bedrock in Oksfjellet is truncated by post-Caledonian brittle structures, which intersects the ductile structures, observed as mostly NW-SE and NE-SW subvertical striking fractures in intact bedrock. The WNW-ESE trending back scarp is defined by a zigzag geometry made up of fractures striking NW-SE and NE-SW with an overall steep dip. These fractures are interpreted to have been re-activated due to gravitational and extensional down-faulting and opening of the unstable area, that may have been guided by a potential sliding surface that intersects both ductile and brittle structures at depth.

Similarly, deformations related the curved scarp, which is cut by alternations of NW-SE and NE-SW striking and steeply dipping fractures, may be related to re-activation of these fractures, due to down-faulting and possibly movement along a deep-seated detachment. Subsidiary scarps trending NW-SE might relate to reactivation of the shear zone/thrust. Surficial morphological elements are deposited on the lower slope of Oksfjellet by several slope processes, were rock falls are interpreted to be the pre-dominant process.

Displacements detected by InSAR correlate well to bedrock structures and morphological elements observed in the field, indicating that the data reflect real geological processes. GB-InSAR, focused on displacements at a scale of mm/day, detected fast moving objects such as e.g., assumed ice-rich debris through all campaigns. Displacement of a spatially larger area was detected in spring 2014 and 2015, indicating that the GB-InSAR campaigns at Oksfjellet have proved valuable for revealing seasonal changes. The lowermost displacements detected by GB-InSAR might correlate to antithetic back scarp parallel fractures, that could be considered as a lower limit of the unstable area. Satellite InSAR data was processed with long temporal baselines, in order to increase the ratio between deformation and noise, and with short spatial baseline, in order to reduce errors related to the DEM. Satellite InSAR data processed with a maximum temporal baseline of 720 days, revealed a distinct displacement pattern of subsidence, well-defined by the mapped geological structures bounding the unstable area. Satellite InSAR data, processed with a minimum threshold of 1460 days for temporal baseline, estimated displacement at a rate of less than 1 mm/year along the mapped curved scarp in the inner parts of Oksfjellet, that might relate to active down-faulting. This is close to the lower detection limit for long time series, but the consistency in several datasets indicates that the displacement is real. Movement related to this fault may have reactivated NW-SE and NE-SW striking fractures that controls the western boundary of the unstable area. Satellite InSAR time series from the unstable area revealed a consistent trend of 3 – 4 mm/year. The combined spatial pattern of the InSAR sensors proved valuable in order to the detect displacements, otherwise not illuminated by the sensors, or in areas that were inaccessible in the field. The combination of the sensors was beneficial to delimit the extent of deformations, which also verified against mapped structures. The fastest displacements were estimated by InSAR data in the middle of the unstable area (satellite InSAR) and in the upper slope (GB-InSAR) consistent with increased vertical movement in the upper part of the interpreted graben structure.

Kinematic analysis of fractures in intact bedrock and in the unstable area, show that block toppling and wedges are theoretical feasible mechanisms. Field observations indicating the presence of a deep-seated sliding surface are supported by displacement patterns detected by satellite InSAR that shows a homogeneous movement of the unstable area. The deep-seated sliding surface may exist along (1) moderately dipping foliation along the thrust, or (2) along the intersection between foliation/thrust and the main cross- fracture sets, producing a total movement vector down to the NNE. Interaction between these elements might have led to different stages of failure from the western part of Oksfjellet to the eastern part, where the western part is the most evolved.

Based on the large volume, the chaotic surface morphology, graben structure, segmented fault blocks and complex deformation mechanisms, the unstable rock slope at Oksfjellet is classified as a complex field. Oksfjellet show some similarities to deep-seated gravitational slope deformations, such as complexity of the interpreted movement pattern, the suggested failures at different stages, and its relation to pre-existing tectonic features.

The unstable rock slope at Oksfjellet has been influenced by several external factors that may have controlled the stability of the slope. Displacements could correlate to seasonal variations due to different processes, such as water pressure and frost weathering. Infiltration of water might have caused seasonal changes in the displacement pattern, by a reduction of shear strength along potential sliding surfaces or by adding weight and pressure on rock columns. The suggested presence of permafrost could cause a more complex interaction between water infiltration and ice temperature along a deep sliding surface.

The orientation of fractures and faults in the area, show a dominance of NW-SE and NE-SW striking and steeply dipping fractures, that coincides with regional mapped lineaments dominantly striking NNE-SSW to NE-SW and NW-SE. Hence, the failure at Oksfjellet is controlled by regional Mesozoic brittle structures.

Hazard evaluation of a worst case scenario-based failure, indicates that Oksfjellet is within moderate risk and periodic monitoring is suggested. However, fragmentation and active disintegration of the area indicates that the consequences of a failure will be smaller than the estimated worst-case scenario, since failure is more likely to occur in individual blocks or areas.

Appendix

Appendix 1 - GB- InSAR results

Cumulated displacement at Oksfjellet between 15 August – 23 August 2011.

Displacement: 0-18 mm.

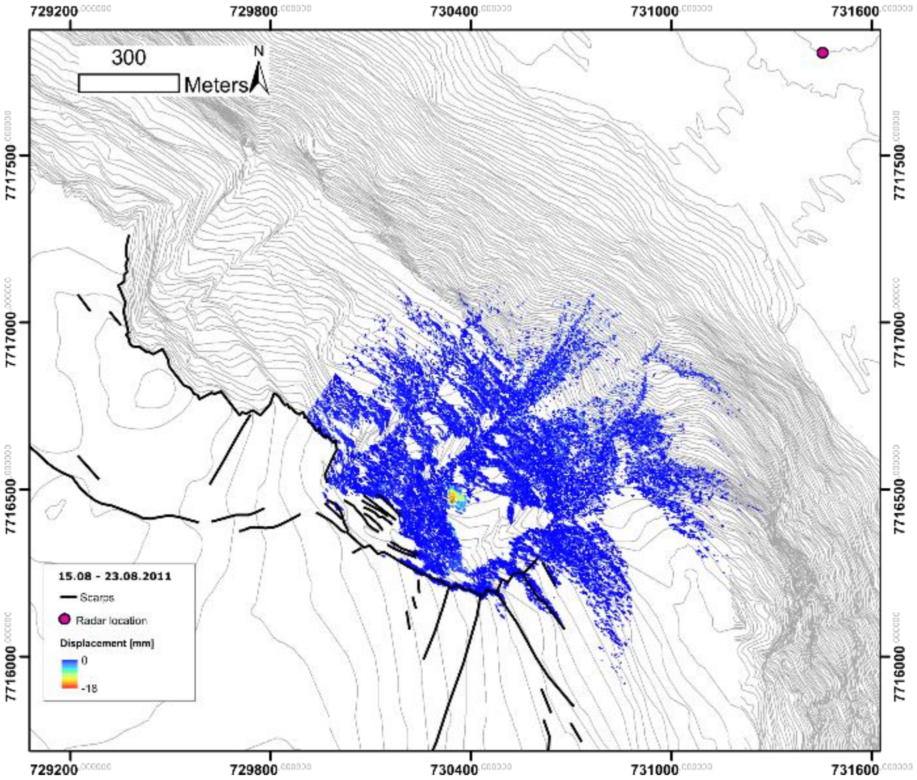

Cumulated displacement at Oksfjellet between 15 August – 23 August 2011.

Displacement: 0-50 mm.

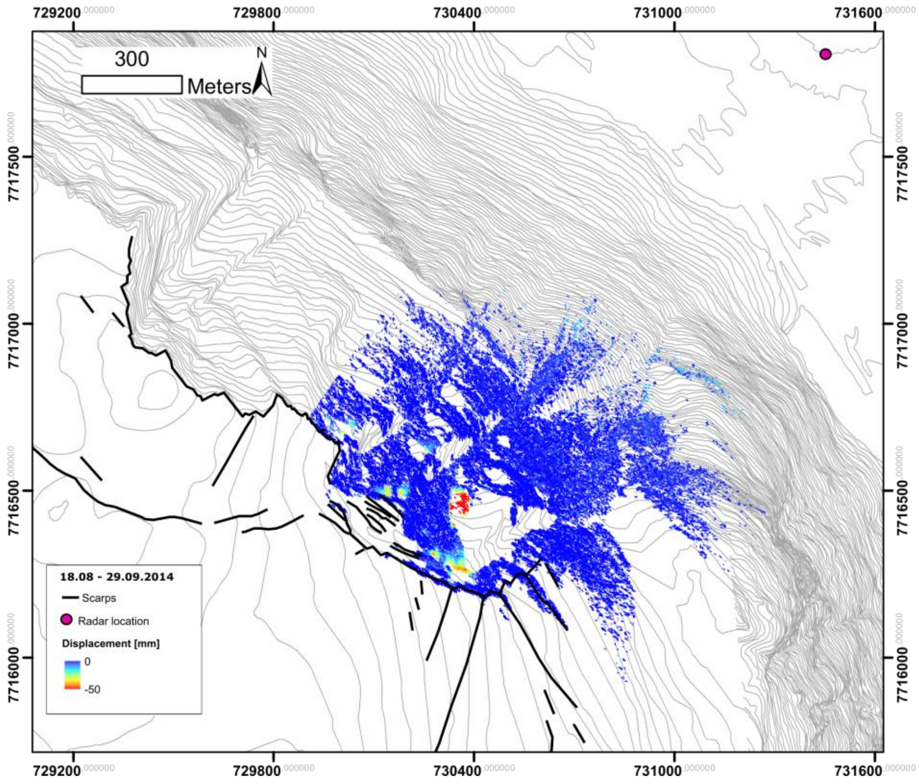

Appendix 2 - GB-InSAR processing parameters

Parameters	**Values**
Central frequency	17.2 GHz
Bandwidth	60 MHz
Length of Synthetic Aperture	3 m
Output power	22 dBm
Revisiting time	7.5 min
Antenna elevation	30°

Appendix 3 - Satellite InSAR processing parameters

RSAT-2 (720 d)

Number of SLC files	48
Time period	2009 – 2014
Multi-look factor in [azimuth, range]	2 x 4
Pixel size [m]	18,8 x 19,2
Number of interferograms generated	134
Manually selected interferograms	85
Maximum temporal baseline [days]	720
Maximum perpendicular baseline [m]	600
Reference point coordinates in range and azimuth	323 173
Reference point coordinates in UTM coordinates	33 W 728729 7717218 UTM
Coherence threshold for pixel selection	0,45
Percentage threshold for pixel selection	0,5
Algorithm	Mean velocity stacking

RSAT-2 (1460 d)

Number of SLC files	48
Time period	2009 – 2014
Multi-look factor in [azimuth, range]	2 x 4
Pixel size [m]	18,8 x 19,2
Number of interferograms generated	76
Manually selected interferograms	54
Maximum temporal baseline [days]	5000
Minimum temporal baseline [days]	1460
Maximum perpendicular baseline [m]	300
Reference point coordinates in range and azimuth	323 173
Reference point coordinates in UTM coordinates	33 W 728729 7717218 UTM
Coherence threshold for pixel selection	0,5
Percentage threshold for pixel selection	0,35
Algorithm	Mean velocity stacking

TSX (720 d)

Number of SLC files	72
Time period	2009 – 2015
Multi-look factor [azimuth, range]	5 x 5
Pixel size in m	9,9 x 9,4
Number of interferograms generated	277
Manually selected interferogram	128
Maximum temporal baseline [days]	720
Maximum perpendicular baseline [m]	40
Reference point coordinates in range and azimuth	738 510
Reference point coordinates in UTM coordinates	33W 728713 7717073 UTM
Coherence threshold for pixel selection	0,35
Percentage threshold for pixel selection	0,4
Algorithm	Mean velocity stacking & SBAS

TSX (1460 d)

Number of SLC files	72
Time period	2009 – 2015
Multi-look factor in [azimuth, range]	5 x 5
Pixel size [m]	9,9 x 9,4
Number of interferograms used	31
Manually selected interferograms	26
Maximum temporal baseline [days]	5000
Minimum temporal baseline [days]	1460
Maximum perpendicular baseline [m]	10
Reference point coordinates in range and azimuth	738 510
Reference point coordinates in UTM coordinates	33W 728713 7717073 UTM
Coherence threshold for pixel selection	0,4
Percentage threshold for pixel selection	0,45
Algorithm	Mean velocity stacking

References

Agliardi, F. et al., 2013. In situ and remote long term real-time monitoring of a large alpine rock slide. *Landslide Science and Practice*, 2 (Early Warning, Instrumentation and Monitoring), pp.415–422.

Agliardi, F., Crosta, G. & Zanchi, a., 2001. Structural constraints on deep-seated slope deformation kinematics. *Engineering Geology*, 59(1-2), pp.83–102.

Agliardi, F., Crosta, G.B. & Frattini, P., 2012. Slow rock-slope deformation. In J. J. Clague & D. Stead, eds. *Landslides*. Cambridge University Press, pp. 207–221.

Agliardi, F., Zanchi, A. & Crosta, G.B., 2009. Tectonic vs. gravitational morphostructures in the central Eastern Alps (Italy): Constraints on the recent evolution of the mountain range. *Tectonophysics*, 474(1-2), pp.250–270..

Ambrosi, C. & Crosta, G.B., 2006. Large sackung along major tectonic features in the Central Italian Alps. *Engineering Geology*, 83(1-3), pp.183–200.

Andersland, O.B. & Ladanyi, B., 2004. *Frozen Ground Engineering* 2nd ed., Wiley.

Andresen, A., 1988. Caledonian terranes of Northern Norway and their characteristics. *Trabajos de Geologia*, (17), pp.103–117.

Bakkhaug, I., 2015. Undersøkelse av ustabilt fjellparti ved Adjet, Storfjord, Troms. Betydningen av ulike kategorier av glideplan i berggrunnen og mekanismer for utglidning, Storfjord, Troms. *Master's thesis, University of Tromsø*.

Barla, G. et al., 2010. Monitoring of the beauregard landslide (Aosta Valley, Italy) using advanced and conventional technique. *Engineering Geology*, 116(3), pp.218–235.

Barton, N., 1973. Review of a new shear-strength criterion for rock joints. *Engineering Geology*, 7(4), pp.287–332.

Berardino, P. et al., 2002. A new algorithm for surface deformation monitoring based on small baseline differential SAR interferograms. *IEEE Transactions on Geoscience and Remote Sensing*.

Bergh, S.G. et al., 2007. The Lofoten-Vesterålen continental margin: A multiphase Mesozoic-Palaeogene rifted shelf as shown by offshore-onshore brittle fault-fracture analysis. *Norsk Geologisk Tidsskrift*, 87(1-2), pp.29–58.

Blikra, L.H. et al., 2006. Rock Slope Failures in Norwegian Fjord Areas: Examples, Spatial Distribution and Temporal Pattern. *Landslides from Massive Rock Slope Failure*, pp.475–496.

Blikra, L.H. & Christiansen, H.H., 2013. A field-based model of permafrost-controlled rockslide deformation in northern Norway. *Geomorphology*, 208, pp.34–49.

Blikra, L.H., Henderson, I. & Nordvik, T., 2009. Faren for fjellskred fra Nordnesfjellet i Lyngenfjorden, Troms. *NGU Rapport 2009.026*.

Blikra, L.H. & Nemec, W., 1998. Postglacial colluvium in western Norway: depositional processes, facies and palaeoclimatic record. *Sedimentology*, 45(5), pp.909–959.

Blindheim, O.T. & Øvstedal, E., 2002. Design principles and construction methods for water control in subsea road tunnels in rock. *Norwegian Tunneling Society*, 12, pp.43–49.

Braathen, A. et al., 2004. Rock-slope failures in Norway; type, geometry, deformation mechanisms and stability. *Norsk Geologisk Tidsskrift*, 84(1), pp.67–88.

Bunkholt, H. et al., 2011. NGU Rapport 2011.031 ROS Fjellskred i Troms: status og analyser etter feltarbeid 2010. *NGU Rapport 2010.031*.

Bunkholt, H. et al., 2013. Undersøkelser av ustabile fjellpartier i Troms – status og planer. *NGU Rapport 2013.021*.

Böhme, M. et al., 2011. Rock slope instabilities in Sogn and Fjordane County, Norway: a detailed structural and geomorphological analysis. *Geological Society, London, Special Publications*, 351(1), pp.97–111.

Christiansen, H.H. et al., 2010. The thermal state of permafrost in the nordic area during the international polar year 2007-2009. *Permafrost and Periglacial Processes*, 21(2), pp.156–181.

Colletta, B. et al., 1988. Longitudinal evolution of the Suez rift structure (Egypt). *Tectonophysics*, 153(1-4), pp.221–233.

Corfu, F., Andersen, T.B. & Gasser, D., 2014. The Scandinavian Caledonides: main features, conceptual advances and critical questions. *Geological Society, London, Special Publications*, 390(1), pp.9–43..

Corner, G.D., 1980. Preboreal deglaciation chronology and marine limits of the Lyngen-Storfjord area, Troms, North Norway. *Boreas*, 9(4), pp.239–249.

Corner, G.D., 1972. Rockslides in North Troms, Norway. *Tromsø Museum*, Unpublished.

Crosta, G.B. & Agliardi, F., 2003. Failure forecast for large rock slides by surface displacement measurements. *Canadian Geotechnical Journal*, 40(1), pp.176–191.

Dehls, J.F. et al., 2000. Neotectonic faulting in northern Norway; the Stuoragurra and Nordmannvikdalen postglacial faults. *Quaternary Science Reviews*, 19(14-15), pp.1447–1460.

Eriksen, H.Ø., 2013. Slope displacement patterns observed using satellite InSAR data in the Storfjord- Kåfjord-Lyngen region, Troms. *Master's thesis, University of Tromsø*

Faleide, J.I. et al., 2008. Structure and evolution of the continental margin off Norway and the Barents Sea. *Episodes*, 31(March), pp.82–91.

Ferretti, A., 2014. *Satellite InSAR Data Reservoir Monitoring from Space*, EAGE Publications bv.

Fossen, H. et al., 2006. En fjellkjede blir til. In I. B. Ramberg, I. Bryhni, & A. Nøtttvedt, eds. *Landet blir til*. Norsk geologisk forening.

Fossen, H., 2010. *Structural Geology*, Cambridge University Press.

Fossen, H. & Hurich, C. a., 2005. The Hardangerfjord Shear Zone in SW Norway and the North Sea: a large-scale low-angle shear zone in the Caledonian crust. *Journal of the Geological Society*, 162(4), pp.675–687.

Gabrielsen, R.H. et al., 2002. Tectonic lineaments of Norway. *Norsk Geologisk Tidsskrift*, 82(3), pp.153–174.

Gee, D.G. et al., 2008. From the early Paleozoic platforms of Baltica and Laurentia to the Caledonide orogen of Scandinavia and Greenland. *Episodes*, 31(1), pp.44–51.

Gibbs, a. D., 1984. Structural evolution of extensional basin margins. *Journal of the Geological Society*, 141(4), pp.609–620.

Glimsdal, S. & Harbitz, C.B., 2008. Flodbølger etter mulig fjellskred Nordnes , Lyngen kommune Beregning av mulige fjellskred og flodbølger. *NGI Rapport 20071677-1*,

Goddard, J. V. & Evans, J.P., 1995. Chemical changes and fluid-rock interaction in faults of crystalline thrust sheets, northwestern Wyoming, U.S.A. *Journal of Structural Geology*, 17(4), pp.533–547.

Goodman, R.E. & Bray, J.W., 1976. Toppling of Rock Slopes. *The proceedings of the Specialty Conference on Rock Engineering for Foundations and slopes*, pp.201–234.

Goscombe, B.D., Passchier, C.W. & Hand, M., 2004. Boudinage classification: End-member boudin types and modified boudin structures. *Journal of Structural Geology*, 26(4), pp.739–763.

Gruber, S. & Haeberli, W., 2007. Permafrost in steep bedrock slopes and its temperature-related destabilization following climate change. *Journal of Geophysical Research: Earth Surface*, 112(F2).

Haeberli, W., 1983. Permafrost-glacier Relationship in the Swiss Alps: Today and in the Past, *National Academy Press.*

Hansen, J.-A., 2009. Onshore-offshore tectonic relations on the Lofoten and Vesterålen Margin – Mesozoic to early Cenozoic structural evolution and morpological implications. Thesis, University of Tromsø.

Hansen, J.A. & Bergh, S.G., 2012. Origin and reactivation of fracture systems adjacent to the mid-norwegian continental margin on Hamarøya, North Norway: Use of digital geological mapping and morphotectonic lineament analysis. *Norsk Geologisk Tidsskrift*, 92(4), pp.391–403.

Hannus, M., 2012. Structural geometry and controlling factors for a rock slope failure area at HOMPEN/VÁRÁŠ, Signaldalen, Troms, North Norway. *Master's thesis, University of Tromsø*

Henderson, I.H.C. & Saintot, A., 2011. Regional spatial variations in rockslide distribution from structural geology ranking : an example from Storfjorden , western Norway. *Geological Society*, 351, pp.79–95.

Hermanns, R.L. et al., 2013. Hazard and risk classification for large unstable rock slopes in Norway. *Italian Journal of Engineering Geology and Environment*, 2013(TOPIC2), pp.245–254.

Hernes, I., 2014. Fjellskred ved Indre Nordnes, Nordnesfjellet, Lyngen, Troms — Berggrunnens indre struktur og bevegelsesmekanismer basert på strukturell analyse og overvakingsdata. *Master's thesis, University of Tromsø*

Herrera, G. et al., 2009. A landslide forecasting model using ground based sar data: The portalet case study. *Engineering Geology*, 105(3), pp.220–230.

Highland, L.M. & Bobrowsky, P., 2008. The Landslide Handbook — A Guide to Understanding Landslides. *Landslides*, p.129.

Hoek, E. et al., 2002. Hoek-Brown failure criterion – 2002 Edition. In *Proceedings of the Fifth North American Rock Mechanics Symposium*. Toronto, pp. 267–273.

Hoek, E. & Bray, J.W., 1981. *Rock Slope Engineering*, Taylor & Francis Group.

Hsü, K.J., 1975. Catastrophic debris stream (Sturtzstroms) generated by rockfall. *Bulletin of Geological Society of America*, 86(1), pp.129–140.

Hungr, O. & Evans, S.G., 2004. Entrainment of debris in rock avalanches: An analysis of a long run-out mechanism. *Bulletin of the Geological Society of America*, 116(9-10), pp.1240–1252.

Hungr, O., Leroueil, S. & Picarelli, L., 2014. The Varnes classification of landslide types, an update. *Landslides*, 11(2), pp.167–194.

Husby, E.D., 2011. Fjellskred i Nomedalstinden: en strukturstyrt masseutglidning på et underliggende storskala glideplan*. Master's thesis, University of Tromsø.*

Indrevær, K. et al., 2013. Post-Caledonian brittle fault zones on the hyperextended SW Barents Sea margin: New insights into onshore and offshore margin architecture. *Norsk Geologisk Tidsskrift*, 93(3-4), pp.167–188.

Jaboyedoff, M., Crosta, G.B. & Stead, D., 2011. Slope tectonics: a short introduction. *Slope Tectonics, Geological society, London*, (351), pp.1–10.

Kristensen, L., 2013a. Bakkebasert InSAR målinger for kartlegging av bevegelse på Jettan og Indre Nordnes, 2013 *Åknes rapport 07.2013*,

Kristensen, L., 2011. Ground based radar measurements at Gamanjunni 3 and Oksfjellet, Troms. *Åknes report 09.2011*.

Kristensen, L., 2013b. Radarkartlegging av potensielle løsneområder for steinskred på rv. 70 Oppdølsstranda - Slutrapport*. Åknes rapport 01.2013*,

Larsen, P.H., 1988. Relay structures in a Lower Permian basement- involved extension system, East Greenland. *Journal of Structural Geology*, 10(1), pp.3–8.

Larsen, Y. et al., 2005. A generic differential InSAR processing system, with applications to land subsidence and SWE retrieval. In *Proc. Advances in SAR Interferometry from ENVISAT and ERS missions (FRINGE 2005), ESA ESRIN, Frascati, Italy*. Frascati.

Lauknes, T.R. et al., 2010. Detailed rockslide mapping in northern Norway with small baseline and persistent scatterer interferometric SAR time series methods. *Remote Sensing of Environment*.

Lauknes, T.R., 2010. Rockslide Mapping in Norway by Means of Interferometric SAR Time Series Analysis. *Thesis, University of Tromsø*.

Lindahl, I., Stevens, B.P.J. & Zwaan, K.B., 2005. The geology of the Váddás area, Troms: a key to our understanding of the Upper Allochthon in the Caledonides of northern Norway. *Norges geologiske* *undersøkelse-Bulletin*, 445 (Lindahl 1974), pp.5–43.

Luzi, G., 2010. Ground based SAR interferometry: a novel tool for Geoscience. *InTech*.

Massonnet, D. & Feigl, K.L., 1998. Radar interferometry and its application to changes in the earth's surface. *Reviews of geophysics*, 36(4), pp.441–500.

Nopper, H., 2015. *Geomorphological study of the rock-slope failure at Adjet, Storfjord, Troms. Master's thesis, University of Tromsø*.

NVE, 2015a. *Steinsprangområde over Holmen i Kåfjorddalen, Geofaglig rapport fra Seksjon for fjellskred (SVF), 6. oktober 2015*,

NVE, 2015b. *Steinsprangområde over Holmen i Kåfjorddalen, Geofaglig rapport fra Seksjon for fjellskred (SVF), 15. september 2015*,

Olesen, O. et al., 1997. Basement structure of the contineltal margin in tpe Lofoten-Lopphavet area , orthern Norway : constraints from potential field data , on-land structural mapping and palaeomagnetic data. *Norsk Geologisk Tidsskrift*, 77, pp.15–30.

Olsen, L. et al., 2013. Quaternary glaciations and their variations in Norway and on the Norwegian continental shelf. *Quaternary Geology of Norway*, pp.27–78.

Osmundsen, P.T. et al., 2010. Active normal fault control on landscape and rock-slope failure in northern Norway. *Geology*, 37(2), pp.135–138.

Quenardel, J.M. & Zwaan, K.B., 2008. Berggrunnskart Manndalen 1633 I- M 1:50 000. *Norges geologiske undersøkelse*, Foreløpig utgave.

Rasmussen, E., 2011. Fjellskred Laksvatnfjellet, Balsfjord, Troms; indre struktur, morfologi og skredmekanismer. *Master's thesis, University of Tromsø*.

Rouyet, L. et al., 2014. Monitoring and characterization of Mannen/Børa rock slope (western Norway) using GB-InSAR and satellite InSAR. In *3rd Slope Tectonics Conference, Trondheim, Norway*.

Rouyet, L., 2013. Monitoring and characterization of rock slope instabilities in Norway using GB-InSAR. *Master Thesis*, University of Lausanne

Saintot, A., Henderson, I.H.C. & Derron, M.-H., 2011. Inheritance of ductile and brittle structures in the development of large rock slope instabilities: examples from western Norway. *Geological Society, London, Special Publications*, 351(2), pp.27–78.

Skrede, I., 2013. Jettan, Nordnesfjellet, Kåfjord, Troms-indre geomtri og struktur, kinematikk og styrande faktorar av eit ustabilt fjellparti, basert på strukturellanalyse, geomorfologi og overvakingsdata*, Master's thesis, University of Tromsø*.

Skrede, I., 2016. *Oksfjelletrapporten 2015 (in prep.)*, NVE rapport 2016

Skrede, I. & Kristensen, L., 2014. Radarkampanje Oksfjellet, Åknes Rapport 2014, (893), pp.1–19.

Stead, D. & Wolter, A., 2015. A critical review of rock slope failure mechanisms: The importance of structural geology. *Journal of Structural Geology*, 74, pp.1–23.

Twiss, R.J. & Moores, E.M., 2009. *Structural Geology*,

Varnes, D., 1978. Slope movement types and processes. In R. L. Schuster & R. J. Krizek, eds. *Landslides, analysis and control, special report 176*. Washington, DC: Transportation research board, National Academy of Sciences, pp. 11–33.

Vorren, T.O. & Mangerud, J., 2007. Istider kommer og går. In I. B. Ramberg, I. Bryhni, & A. Nøttvedt, eds. *Landet blir til*. pp. 532–555.

Wyllie, D.C. & Mah, C.W., 2005. *Rock Slope Engineering: Civil and Mining, 4th Edition* 4th ed.,

Zebker, H.A. & Villasenor, J., 1992. Decorrelation in interferometric radar echoes. *Geoscience and Remote Sensing*, 30(5), pp.950–959.